Artificial cilia - bridging the gap with nature

Sam Peerlinck^{a,*}, **Edoardo Milana**^{a,*}, **Elias De Smet**^{a}, **Michael De Volder**^{a,b}, **Dominiek Reynaerts**^{a}, **and Benjamin Gorissen**^{a}

^{a}Department of Mechanical Engineering, KU Leuven and Flanders Make, Leuven, Belgium; ^{b}Institute for Manufacturing, Department of Engineering, University of Cambridge, Cambridge, UK

Human ingenuity has found a multitude of ways to manipulate fluids across different applications. However, the fundamentals of fluid propulsion change when moving from the macro- to the microscale. Viscous forces dominate inertial forces rendering successful methods at the macroscale ineffective for microscale fluid propulsion. Nature however has found a solution; microscopic active organelles protruding from cells that feature intricate beating patterns: cilia. Cilia succeed in propelling fluids at small dimensions, hence they have served as a source of inspiration for microfluidic applications. Mimicking biological cilia however remains challenging due to their small size and the required kinematic complexity. Recent advances have pushed artificial cilia technology forward, yet discrepancies with natural cilia still exists. This work identifies this gap by analyzing artificial cilia technology and benchmarking them to natural cilia, to pinpoint the remaining design and manufacturing challenges that lay at the basis of the disparity with nature.

Artificial cilia | Low Reynolds fluid propulsion | Soft actuators | Biomimetics | Active Surfaces

1. Introduction

The modalities through which organisms and systems interact with the world change drastically with the length scale they operate at. Although the same physical laws apply at both the small and large scale, their effects can differ dramatically. In fluid dynamics this discrepancy originates from two major forces that scale differently with length. Inertial forces act on volume ($\sim L^3$), while viscous forces act on the surface ($\sim L^2$). The relative importance of both is captured by the Reynolds number $Re = LU/\nu$, where L is a characteristic length scale, U the fluid speed and ν the fluid's kinematic viscosity. For large organisms that typically work in high Reynolds numbers ($Re >> 1$), inertial forces dominate, meaning that fluid flows only die out slowly over time. However at very low Reynolds numbers ($Re << 1$), the time-dependency of Navier-Stokes equation is negligible, which means that viscous forces dominate and all movements die out instantly (6). Reciprocal motion, where the shape of the organism's body remains unchanged between forward and backwards stroke, has no net result in a low Reynolds environment as everything is reversible. Hence to propel fluids at the small scale, different solutions are required. Natural selection produced hair-like cell organelles, beating in a non-reciprocal manner to propel fluid at these microscales, called cilia and flagella. Flagella usually exhibit a very high aspect ratio and provide the ability for propulsion of unicellular organisms by beating in a whip-like or corkscrew pattern (7). Cilia are usually shorter and tend to appear in large carpets, where they emerged as an efficient mechanism for fluid propulsion at low Reynolds number conditions in and on diverse organisms: on the tentacles of ctenophores (1, 8) (Fig.1 A1), inside the tracheae of mammals (Fig.1 A2) (9–11), and on the membranes of eukaryotes like the paramecium (Fig.1 A3) (12), to give a few examples. The behavior of cilia and flagella has attracted research interest for centuries, accelerated in recent years by the potential application of biomimetic artificial ciliary systems in fields like microfluidics. Consequently, the nomenclature used in the remainder of this manuscript exlusively describes cilia, both natural - where a collective behavior of large carpets can be seen - and artificial cilia that attempt to approach their natural counterparts in various ways.

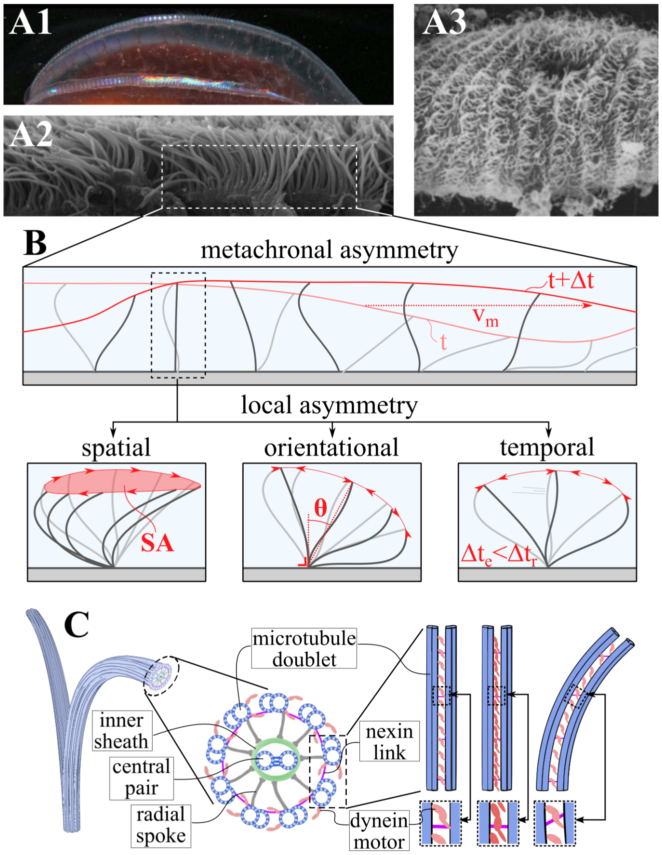

Fig. 1. Ciliated surfaces are nature's way to propel fluids at small scales, and can be found on the tentacles of ctenophores **A1**(1), inside the lung tract of mammals **A2**(2), or on the cell membranes of eukaryotes like the paramecium **A3**(3). **B**: To propel fluids, symmetry breaking strategies are deployed that can act on the global cilia level by introducing a phase shift between neighboring cilia, called metachronal asymmetry, or on the level of the individual cilium by following a different path between effective and return stroke, encapsulating a swept area 'SA' (spatial asymmetry), by tilting away from the surface normal with an angle 'θ' (orientational asymmetry) or by altering the speed between effective and return stroke, where Δt_e and Δt_r is the time to complete the effective and recovery stroke (temporal asymmetry). **C** Schematic of the cilia structure, showing the sliding mechanism in microtubule, where 'walking' dynein motor proteins instigate a relative motion between two microtubule doublets, based on (4) and (5). The relative sliding can be distinguished on the left and right inset figures, showing a changing nexin link orientation.

The orchestrated movement of these **natural cilia** has attracted attention from the scientific community, ever since their first observation by Antoni van Leeuwenhoek in 1675 (13). This continuing fascination by biologists (14) has led to accurate descriptions of the form and beat of cilia throughout the natural world (15–18), focusing on both individual and collective ciliary beat patterns. A remarkable variety in patterns is shown across different organisms, however all patterns need to break symmetry to instigate fluid flow at low Reynolds numbers, avoiding reciprocal motion. Four different asymmetries can be distinguished in ciliated systems, as schematically depicted on Fig.1 B, where three of them act on the level of a single cilium: spatial, orientational and temporal asymmetry. The fourth, metachronal asymmetry, acts on the level of the cilia array as a whole. A single cilium beats rhythmically and its motion can be divided into two phases, the effective (with the flow) and the recovery (against the flow) stroke (12, 15). Nonreciprocity occurs when the two strokes follow a different trajectory so that the tip of the cilium sweeps an enclosed area, SA (swept area) in Fig.1 B. This nonreciprocal motion particular to beating cilia is known as *spatial asymmetry* and can be attributed to their complex inner structure that is composed of microtubules and motor proteins (5). Depending on the organism, the microtubules are organised in a specific pattern where on Fig.1 C, we have depicted a 9+2 configuration. In this architecture 9 microtubule pairs, called doublets, encircle a central doublet. In between these outer doublets are dynein motor proteins that are able to instigate a relative local sliding between neighbouring doublets. When locally activating or inhibiting dynein activity between doublets on one side of the cilium, a force imbalance is generated across the cross-section of the axoneme, causing a the cilium to locally curve. This local dynein activation or inhibition, and induced curvature, progressively moves over the length of the cilium, thus generating a characteristic bending deformation pattern. Motion nonreciprocity and thus *spatial asymmetry* is the result of the targeted generation of a traveling wave of activation or inhibition of the motor proteins that goes from the base of the cilia to its tip (4, 19, 20). *Orientational asymmetry* refers to the global orientation of the cilium, characterized by the average angle the cilium makes with respect to the surface normal (θ in Fig.1 B at the bottom middle) (17). *Temporal asymmetry* occurs when effective and recovery stroke happen at different speeds, where usually the time to complete the effective stroke is smaller than the time to complete the recovery stroke ($\Delta t_e < \Delta t_r$, as shown in Fig.1 B). On a global level, *metachronal asymmetry* indicates a phase difference between neighbouring cilia, resulting in a traveling wave with wave speed V_m, that can move in the same direction as the fluid (symplectic) or in the opposite direction (antiplectic) (3). Usually, ciliary carpets combine these different types of asymmetry in complex beating patterns.

These biological observations are paralleled by **computational models** (see Fig.2 A1-A5), that are used to analyse the contributions of different forms of asymmetry on fluid flow and how these asymmetries are created in nature (21, 32–37). On the level of a single cilia, it has been shown that spatial asymmetry is essential to achieve low Reynolds fluid flow (6), where a bigger swept area results in higher fluid flow (38). In this regime, fluid flow is enhanced by orientational asymmetry, however orientational asymmetry alone does not suffice to propel fluids (38). Temporal asymmetry is irrelevant at $Re << 1$ (39), where the fluid flow is typically normalized by the time it takes a complete a full stroke, as displaced fluid scales linearly with the number of completed strokes (25). At high Reynolds number, any asymmetry enables fluid flow (40), orientational asymmetry influences the flow direction (38) and more spatial asymmetry leads to higher flow rates (32). Even fully symmetric motions are able to propel fluids in the direction of the cilium axis (41). Although asymmetries at the single cilium level are mostly the result of mechano-transduction inside the cilia (42), hydrodynamic interactions with the fluid have also shown to influence the deformations of the cilium that instigates the flow (43). On the level of the cilia array, even a small phase difference between neighboring cilia drastically increases flow speeds at low Reynolds numbers, where highest flows rates have been reported for antiplectic metachrony (25, 44). At high Reynolds numbers symplectic metachrony led to the highest absolute flowrates while flow reversal was observed when switching from symplectic to antiplectic wave propagation at certain actuation frequencies (40) without changing the bending direction of the cilia. Although these investigations provided insights in the *effect* of metachronal asymmetry, they did not explain where this collective behavior originates. In contrast with the single cilium, where mostly internal mechanisms coordinate deformation patterns, interactions between cilia via the viscous fluid dictate the coordination throughout the array. These fluid-structure interactions were studied by Taylor in 1951 (45) who reported emerging lateral waves of flexible sheets in a high viscous fluid flow and the synchronisation of such waves in neighboring sheets. Computational hydrodynamic models corroborated these results using highly simplified models of ciliary carpets, where cilia are represented by arrays of rotating (46–48) or translating (49) beads, where metachronal waves spontaneously emerged. More realistic beating patterns were simulated by Hines et al. (50) by mimicking the microtubular structure of natural cilia arranged in two-dimensional arrays, again leading to emerging waves (51, 52). These results are corroborated by computational cilia with more complex individual beating patterns, grouped together in two-dimensional arrays (53–55) and three-dimensional 5x5 carpets of cilia (56) and even hundreds of cilia(24). To allow synchronisation and wave emergence, all previous simulations include mechanism to adapt the phase difference between cilia (47, 55). Consequently a similar mechanism needs to present in nature, better known as the 'geometric clutch hypothesis' (57), which postulates that an internal mechanism in the axoneme, controlled by external viscous fluid forces, is able to alter the transmission of the internal stimuli that instigates the cilium's deformation. This seems to lie at the base of the non-equilibrium state of cilia phase-locking and -unlocking in which metachronal waves emerge. Besides the hypothesis that viscous fluid interactions enable this spontaneous coordination, it has also been postulated and simulated that the elastic connection between basal bodies of adjacent cilia play an important role

E-mail: benjamin.gorissen@kuleuven.be

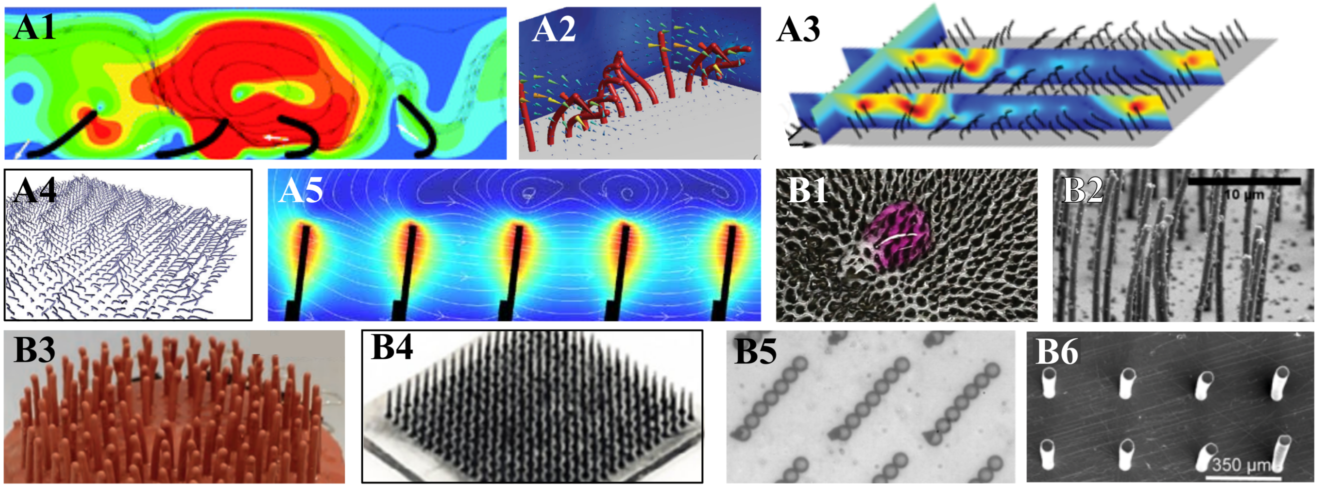

Fig. 2. Natural cilia have been analysed using numerical techniques that study the the influence of asymmetries on fluid flow **A1**(21), particle trapping capabilities **A2**(22), the emergence of synchronisation **A3**(23), mixing capabilities **A4**(24) and metachronal effects **A5**(25). In parallel, artificial ciliated surfaces have been developed that: show droplet manipulation **B1**(26), are magnetically actuated **B2**(27), are manufactured using dip molding **B3**(28), are able to propel particles **B4**(29), are self-assembled **B5**(30), are used to make micropumps and climbing robots **B6**(31).

in the intra-cilia connection (58). Further, it has been found that the theoretical optimal motion of a single computational cilia coincides with natural ciliary motion when optimising for efficiency (59). On a carpet level, fluid propulsion efficiency optimisation led to disjoint conclusions with optimal beating patterns that are either similar (60) or dissimilar (61) to nature.

In addition to biological observations and computational models, experimental research (see Fig.2 B1-6) has created **artificial ciliary systems**. Some are directed towards validating the theory behind cilia-mediated fluid flow, both on the individual cilium (62, 63) and collective system level (64). To corroborate earlier findings from biology or computational models, these experimental setups attempt to recreate the Stoke's flow natural cilia operate at, mostly by working with similar Reynolds number which enables relaxation of the constraints on absolute cilia size. In contrast, the main focus of artificial cilia research is directed towards the development of microscopic devices (65), where by definition absolute size does matter. Research groups have created crawling robots employing the coordinated motion of artificial cilia arrays actuated by a magnetic field (31, 44, 66), or surfaces of artificial cilia that are able to manipulate particles or droplets, resulting in self-cleaning properties (67, 68). The most obvious biomimetic application of artificial ciliary systems however, is their use in microfluidics, for mixing (69, 70) and/or pumping (71). Here the constraint of their use in microfluidic channels often dictates the low Reynolds conditions they operate at. Regardless of whether these artificial ciliary systems are directed towards researching fluid-flow or target microscopic applications, they need to be compatible with microfabrication techniques, while displaying large deformations that continuously and gradually change over the length of the cilia. Whereas the first requirements is needed to ensure low Reynolds flow conditions, comparable fluid-instigating performances to natural cilia demand the second requirement. Because of these requirements, artificial cilia are being shaped using soft actuator technology where low stiffness materials (72) are used to create actuators with complex deformation modes (73). In this paper, we analyse literature spanning observations and analyses in multiple domains of cilia research, in an attempt to gather insights in the state-of-the-art of artificial cilia. Rather than from an applied technology point-of-view, which has already been provided by Islam et al (65), this manuscript critically analyses literature in a fundamental way, along two axes. In a first, purely technological axis, we focus on the technology behind artificial cilia, how they are actuated, fabricated, and how closely their morphology resembles natural cilia, both on the individual and collective level. The second axis discusses the biomimicking properties of artificial cilia by benchmarking them against natural cilia, using key metrics that unveil the behavioral (dis)similarity between the two. Both axes will be combined in a concluding section where we will address pressing challenges in future research working towards creating artificial ciliary systems that approach the capabilities and semblance of their natural counterparts.

2. Actuation technologies

The development of artificial cilia that mimic biological cilia involves several fundamental challenges. (i) Biological cilia have features across different length-scales, with individual cilia having diameters in the sub-micrometer range and lengths in the 10's of micrometers, and with carpets that measure 100's of micrometers to even multiple millimeters in length (74). (ii) Across these different length-scales, intricate motion patterns can be distinguished with nonreciprocity at the local cilium level and globally at the cilia carpet level (75). (iii) These motion patterns are able to adapt to the fluidic environment they perceive (76). In an attempt to fulfill these challenges, different actuation principles were proposed in the past decades to drive the needed large deformations. We will use these actuation principles to discern trends in artificial cilia development. Figure 3 gives an overview of key developments in time with their associate length scale, where we make

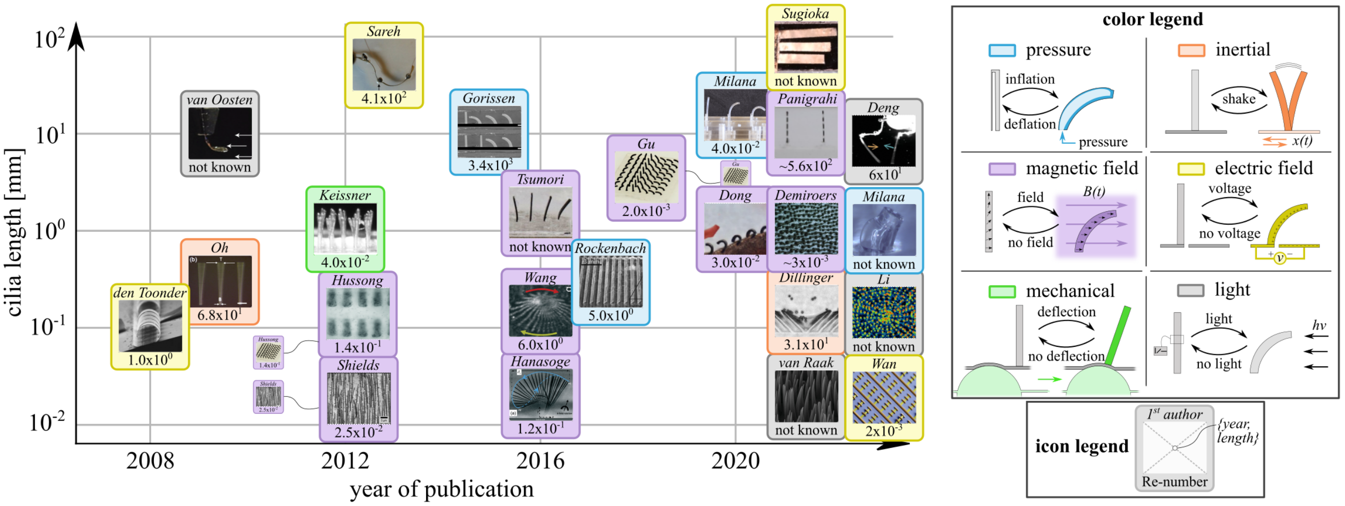

Fig. 3. Timeline overview of the advances in artificial cilia. Cilia length is expressed in the vertical axis, while the year of publication in the horizontal axis. The color code represents the actuation technologies, as depicted in more details in the color legend on the right hand side. Each icon resembles a breakthrough in the field, where above the inset figure we report the first author of the publication and below the Reynolds number of the experiment in the same publication. When the Reynolds number is not directly reported but it can be calculated from data in the paper, we add the symbol "~". If no relevant data on Reynolds number was included, we indicated it with "not known". The raw data of this plot, as well as the references, are reported in Table S1.

a distinction between different driving technologies that are schematically depicted on the right. Each symbol represents a significant development in the area; above the inset figure, we list the publication's first author, and below that, the experiment's Reynolds number. Throughout the remainder of the manuscript, we will employ the same colour coding for the different driving technologies.

A. Electric field actuation. By employing the electrostatic attraction between oppositely charged surfaces or repulsion between likely charged surfaces, conductive slender objects, cilia, can be bent towards or away from a ground electrode that typically coincides with the substrate on witch the cilia are implanted. Den Toonder *et al.* (77) employ this mechanism to create artificial cilia systems that consist of an array of microcantilevers ($L = 100$ µm) that curl when an electric field is applied. The microbeams are 1 µm thick polymide structures with a 20 nm coating of chromium as electrode. An indium-tin-oxide electrode is patterned on the glass substrate and covered with a layer of dielectric silicon oxide-nitride with a thickness of 1 µm. These cilia are able to induce net flows up to 500 µm/s in silicone oil. However the developed cilia exhibit no path asymmetry and net flow is only observed at high Reynolds numbers that are possible due to the high actuation frequency of up to 200 Hz. In an alternative approach, the voltage mediated migration of ions through a porous structure is used to create a bending deformation, instigated by an excess of ions that lead to swelling and a lack of ions that lead to shrinking. When applied in soft materials, electro-active polymers have been used to create artificial cilia, where spatial asymmetry was achieved by patterning mulitple electrodes along the cilia length. As such, Sareh *et al.* (62) developed a three-segments 64 mm long artificial cilium, where each segment is directly controlled and consists of an ionic polymer metal composite (IPMC) containing a Nafion 115 membrane. The artificial cilium's tip sweeps a large area, comparable (if normalized) with the one of the algae *Volvox*. However, no fluid propulsion testing was done. Another electrical actuation mechanism is induced charge electro-osmosis (ICEO). Sugioka *et al.* (78) demonstrated the metachronal motion of three ICEO cilia with different lengths, when an AC electric field is applied. The metachrony is induced by a delayed response time of the cilia with the shortest length. At a smaller scale, Wang *et al.* (79) used electrochemical actuators to create cilia metasurfaces that can be directly controlled. Those actuators (50 µm in length, 5 µm in width and 10 nm thick) are realized through a lithographic process and consist of a platinum cantilever covered on a side with a passive layer of titanium. Actuation in a neutral phosphate-buffered saline (PBS) solution occures by imposing a potential of 1 V, which induces an oxidation reaction of the platinum film with the PBS, such that it expands and causes the whole structure to bend. Oppositely, a decrease in voltage to -0.2 V triggers the reduction reaction that restores the actuator to its original state. The authors demonstrated a pumping speed of 60 µm/s at an actuation speed of 40 Hz, corresponding to a Reynolds number of approximately $2 \cdot 10^{-3}$. Recently, Ren *et al.* (80) fabricated arrays of independently controlled polypyrrole bending actuators on deformable 3D substrates. These arrays exhibit various forms of metachronal asymmetries and succeed in substantial fluid propulsion in various configurations at intermediate Reynolds numbers. The absence of a spatial asymmetry does seem to limit their low-Reynolds capabilities.

B. Light-driven actuation. Artificial cilia can be fabricated out of Liquid Crystal Elastomers (LCEs), a rubbery material composed of a crosslinked polymeric chain of liquid crystal units (mesogens). Since the polymeric chain follows the order of the mesogens, a global deformation of the material appears when the orientation of the mesogens changes locally. This change in orientation corresponds to a phase change of the liquid crystal from an ordered to a disordered configuration, as a response to an external stimulus such as light. Van Oosten *et al.* (81) shaped 10 mm long artificial cilia with spatial asymmetry through an inkjet printing technology combined with self-organizing LCE structures. The spatial symmetry is broken due to the bi-segment configuration of the cilium, where each segment bends in response to a different wave length of the light source. Further, van Raak *et al.* (82) developed micro-sized ciliary carpets made of a photoresponsive LCE. The bending motion is programmed by applying an electric field with a variable intensity across the length of the pillars, so that the mesogens follow a splay alignment. The cilia exhibit an oscillating movement as a response to an on-off stimulus of a UV light source. Given their symmetric movement, those cilia are not foreseen to be used for fluid propulsion but rather micro object transport or self-cleaning surfaces. Cilia-inspired micropillars have been developed by Li *et al.* (83) using a photosensitive LCE. The micropillars exhibit a complex combination of a bending and twisting deformation caused by the interplay between light direction, mesogen orientation and the variation of the geometrical axis during deformation. This interplay induces a nonreciprocal motion of the single pillar. Moreover, multiple pillars impose a travelling-wave trigger across the cilia surface, caused by shadow casting of neighbouring cilia. Despite showing self-regulated nonreciprocal motion at a sub-mm scale (the pillars dimensions are 150 µm in length and 30 µm in width), the authors do not report on fluid propulsion capabilities. A recent and novel approach to LCE-based actuator technology showed a self-regulating behavior and was fabricated by Deng *et al.* (84). They proposed a piecewise self-oscillationg LCE filament, excited by two lasers beams. The laser spot causes local bending, generating a self-imposed shadow initiating an oscillating motion. Because of the double bending, a nonreciprocal periodical beat is generated. Two adjacent LCE strips showed a phase locking behavior when submerged in water and their respective initial beating frequencies differed. The mutual interaction between the structures, light field and surrounding fluid yielded behavior resembling natural cilia. This particular behavior diverges from the general trend in light-driven actuation, as the self-oscillating principle enables the actuators to function in a non-equilibrium state instead of being externally coordinated. Gelebart and colleagues (85) developed a photoresponsive fiber array consisting of high aspect ratio LCE pillars of 70 µm diameter. By directing a UV light-source, a 3D spatially asymmetric beat is created. Repeating this pattern resulted in an induced fluid flow in low Reynolds conditions, indicated by the propulsion of solid particles on the surface of a paraffin oil bath. In a similar manner, Liu *et al.* (86) fabricated light tracking and light guiding fiber array that exhibits a substantial bending angle when exposed to different wavelengths of light. By manipulating the direction of the light source, a cilia-like beat can be generated, and the fibers' bending angle are shown to not be greatly influenced by being submerged in water. No fluid propulsion tests were conducted in this work.

C. Magnetic field actuation. Ferromagnetic materials have the tendency to align themselves with external magnetic fields. By incorporating magnetic dipoles in flexible materials that have a changing dipole orientation throughout, an external magnetic field can be used to impose non-uniform deformations in a flexible material. And even when a single dipole orientation is chosen throughout, rigid body motions can be induced where cilia are rotating around the attachment point with the substrate. Evans *et al.* (27) manufactured an array of 25 µm long microrods with diameters ranging between 0.2-1 µm, made of PDMS-ferrofluid composite material. When a rotating magnetic field is applied, the rods describe a tilted conical swept area. As opposed to the planar spatial asymmetry described earlier, these conically beating cilia induce flow in low Reynolds fluid conditions on the basis of asymmetric boundary conditions. During the recovery stroke of the cilium, of which the trajectory is closer to the surface from which the structure protrudes, the affected fluid encounters a higher resistance (attributed to the no slip condition of the stationary surface) than during the effective stroke. The same authors (87) showed that a flow is generated on top of the cilia with an average velocity varying across the distance between the cilia and the measurement plane, varying between -2 and 8 µm/s. Artificial cilia with similar conical rotations have been developed by Vilfan *et al.* (30), using an array of superparamagnetic beads held together by the same field used for actuation. An average flow velocity up to 4 µm/s was demonstrated. Conical beating cilia have also been developed by Wang *et al.* using a different out-of-the-cleanroom fabrication process (88–91). The developed rod-like cilia with lengths ranging between 30 and 300 µm, generate fluid flow velocities up to 120 µm/s at the largest lengths. These artificial cilia have actuation frequencies up to 40 Hz. Alternatively, Hussong *et al.* (92) developed a different morphology of magnetic cilia, more similar to the cantilever structures of electrostatic cilia (77), with a length of 70 µm and a width of 20 µm. The material is a composite of superparamagnetic nanoparticles embedded in a polymeric matrix and instead of a conical beat, the cilia tip sweeps an area in a plane. Motion asymmetry is achieved by to the interplay between the cilium stiffness and the applied magnetic torque. However, there is no control over the cilia motion and no metachronal effect is observed. Flow measurement showed a maximum average flow velocity of 130 µm/s at 10 Hz. Hanasoge *et al.* (93) made 200 µm long artificial cilia with the same configuration using thin NiFe films. Those cilia have a significant swept area and are able to generate fluid speeds up to 1350 µm/s. In another work they show the programming of a metachronal wave in arrays of cilia with varying lengths (94), where a variation in length corresponds to a variation of the bending stiffness, which is the parameter that determines at what magnetic angle the recovery stroke takes place. However no experiment was conducted that relates the metachronal phase shift to the fluid flow. Tsumori *et al.* (95) made an array of 2 mm long magnetic cilia that exhibit metachronal asymmetry. These cilia consist of PDMS with embedded chainlike clusters of ferromagnetic particles (iron powder). Each cilium is made at a different step so that it can be magnetized along a different orientation compared to its neighbour. When a rotating magnetic field is applied, the cilia moves with a phase shift proportional to the angle between the magnetization direction of the neighbouring cilia. In a follow-up study (96), the same authors use their cilia with a slightly larger length (3 mm) to propel fluid in a channel filled with silicone oil to ensure low Reynolds conditions. They tested antiplectic and symplectic configurations at 30° and 45° phase shift, finding a maximum average flow velocity of 60 µm/s at 0.5 Hz. In a similar approach, Gu *et al.* (97) developed a magnetic ciliary array ($L = 4$ mm) with pre-programmed metachronal waves, where here the magnetization is done in one step by wrapping the cilia carpet around a curved support. The degree of curvature of the support defines the phase shift of the metachronal wave. The rod-like cilia are composed of silicone rubber (Ecoflex 00-30) mixed with NdFeB microparticles. Fluid flow tests at low Reynolds are conducted only for antiplectic waves between 0° and 40°, showing a maximum average flow velocity in proximity of the cilia of about 100 µm/s for an actuation period of 12 s and a phase shift of 40°. The same materials were used by Dong et al. (44) to make a ciliary array with metachronal motion patterns. After fabrication, each cilium ($L = 1$ mm) is inserted into a template jig to induce different orientations for subsequent magnetization. The cilia are afterwards manually glued to a substrate and, when actuated, a metachronal wave occurs according to the defined magnetization profile. The study characterizes the generated fluid flow in function of different metachronal configurations, reporting higher flows for the antiplectic wave, consistently with (25). Where the previous studies use either a changing magnetisation or geometry throughout the cilia length, metachronal waves can also be induced through non-uniform magnetic fields. Zhang et al (98) used an array of external rod-shaped magnets where neighbouring magnets have opposite magnetic dipole orientations. This magnetic array translates under the ciliary surfaces similarly to a conveyor belt, inducing a phase shift across neighboring cilia. The advantage of this method is that it does not require additional fabrication steps to magnetize single cilia, facilitating the production of densely packed ciliary carpets (cilia are 350 µm in length). More recently, Demirors *et al.* (99) created a soft magnetic ciliary carpet composed of a mix of silicone rubber (Ecoflex 00-20) and NdFeB particles, using a self-assembly process based on the Rosensweig instability. The length of the cilia varies between 0.6-2 mm and they follow a cone-like trajectory when activated by a rotating magnetic fields. The authors demonstrated not only fluid propulsion but also the transport of solid objects that are larger and heavier than the cilia. At a larger scale ($L = 10$ mm), Panigrahi *et al.* (100) developed an analogue fabrication technique to make multi-segment magnetic cilia, in the perspective of programming the bending motion of each cilium in the array. Miao *et al.* (101) used the geometry of pine needles as inspiration for creating a dense carpet of bending pillars, exhibiting a varying degree of spatial asymmetry and capable of transporting solid particles and droplets. Besides these technologies employing actuation by magnetic field for biomimetic ciliary propulsion, it is worth mentioning that microscopic artificial swimmers have been created (102) that rely on the same principles. Here, two transverse magnetic fields are used: one for aligning a linear chain of colloidal magnetic particles linked by DNA and attached to a red blood cell to act as an artificial flagellum, and a second oscillating magnetic field to induce a cyclic beating of that chain. This results in a beating pattern that propels the structure, relying on similar fluidic principles as the mentioned artificial ciliary carpets.

D. Pressure-driven actuation. Large deformations in soft materials can be created through inflation with fluids (gases or liquids), where an elevated fluid pressure is used to deform a surrounding polymer materials. These inflatable voids can be situated at the base, leaving the protruding cilia to tilt as a rigid body. This concept was materialized by Rockenback *et al.* (103), where a series of pneumatic membranes sequentially inflate to create a wave-like base deformation. Regarding this work, it should be noted that instead of rod like-cilia, plate-like cilia are positioned on top of the membranes, that mimic the propulsion system of biological ctenophores. Each plate thus stands on a thin membrane which can be pressurized or depressurized. The variation of pressure deflects the membranes and consequently changes their curvatures, tilting the attached plate-like cilia. The plates are made out of PDMS using soft lithography, by means of two moulds, one to make the plates and one to form the pneumatic connections. The fabricated plate measures 500 µm high and 50 µm thick, standing on a membrane which is 175 µm thick and 600 µm wide. In order to create additional orientational asymmetry, the plates in resting position are tilted 45° with respect to the surface normal. Experiments were conducted in DI water at a Reynolds number of 5, showing the ability to create both spatial and metachronal asymmetry, including shifting between symplectic and antiplectic waves at various frequencies and duty cycles. This ciliary system gives reliable results for frequencies up to 5 Hz where the net flow is always moving in the same direction when metachronal asymmetry is changed. Besides rigid cilia deformations that are instigated via base deformations, inflatable voids in the protruding cilia itself can also be used to create bending deformations. Gorissen *et al.* (104) designed and fabricated a soft fluidic bending microactuator which when pressureizd, approaches the reciprocal motion of natural cilia. The artificial cilium consist of a PDMS cylinder with a length of 8 mm and a diameter of 1 mm, which has an inner cylindrical void with a diameter of 0.6 mm that is placed eccentrically with respect to the outer structure. Due to this eccentricity, the structure bends when the inner void is pressurized, generating the effective stroke of the artificial cilium. In this single void configuration, the cilium tip follows a symmetric trajectory during deflation, without spatial asymmetry. In a follow-up research (40), an array of six of these microactuators, equispaced at 8 mm, forms the artificial ciliary system, where each cilium is individually actuated through a block pressure waveform of 2 bar. By individually addressing the cilia, this setup was used to study the influence of metachronal phase difference and actuation frequency on high Reynolds fluid flow. Below 11 Hz and for all applied phase differences, a flow directed in the opposite direction of the effective strokes of the cilia is observed, which leads to the conclusion that metachrony is not as relevant as for biological cilia. However, above 11 Hz, the change in the orientational asymmetry induces a flow reversal, instigated by inertial effects. On a smaller scale, the same research group focused on downsizing of similar actuators to sub-mm dimensions (450 µm in length) by fabricating micromoulds through a soft lithography process. The pneumatic microactuator can bend up to 30° when pressurized at 1 bar (105). To create more spatial asymmetry, Milana *et al.* (25, 63) introduced a second eccentric bending channel in the same cilia, enabling programmable spatial asymmetry on top of programmable metachronal, orientational and temporal asymmetry. To assess the role of the asymmetries, the cilia propulsion was tested in glycerol to experience low Reynolds number flow conditions. This setup was used to corroborate theoretical results, identifying multiple-vortex structures in the flow to reduce overall fluid velocities and confirming that antiplectic waves are the most efficient at propelling fluid at low Reynolds. One of the major drawbacks of this system is large amount of needed fluidic valves, where twelve valves are needed to instigate the deformations of six cilia. In an attempt to limit the amount of fluidic valves, the same research group harnessed nonlinearities in a new design of bistable inflatable cilia to create both spatial asymmetry and metachronal asymmetry with only one pressure supply line, at a larger scale (106). However, no fluid propulsion tests were carried out. Becker *et al.* (28) used a dip molding process to create large-scale and high aspect ratio inflatable bending actuators, featuring the possibility of a metachronal asymmetry. However, these cilia only have a single internal void, excluding the possibility of creating a non-reciprocal motion.

E. Mechanism driven actuation. Where for fluidic cilia, pressures on internal voids are used to impose deformations, artificial cilia can also be more directly manipulated by imposing contact forces on flexible structures. Again we can make the distinction between base-induced actuation, and the case where forces are directly transmitted to the protruding members. In the latter case, Nonake *et al.* (107) created rigid cilia out of wire, where a conical movement of these wires by means of stepper motor rotations, imposed a conical swept area that can be set by titling the motors away from the surface normal. Flow speeds of up to $8mm/min$ were registered for a cilia length of $6mm$ and a Reynolds number of $4.6\text{x}10^{-4}$. On a larger scale, Miller *et al.* (108) actuated flexible beams by means of a wire connected to a camshaft to impose a certain bending profile, showing fluid flow from the base to the tip of the cilium. Regarding base-induced actuation, Keissner and Brucker (109) imposed undulatory base deformations by pulling a ball chain under a series of flexible membranes with implanted cilia. The moving ball chain thus produces a travelling wave (metachronal asymmetry) of the artificial cilia with an orbital tip trajectory. The body of the cilium doesn't deform and stays straight during the motion. The artificial cilia are cylindrical PDMS micropillars, 1 mm long and 0.1 mm in diameter, manufactured through a micromoulding process based on chemical deep etching of silicon to make the micromould. When placed in a microchannel, fluid flow capabilities are evaluated through PIV measurements, where the actuation is performed at three different beating frequencies, 1 Hz, 2 Hz and 3 Hz. In all cases, a flow directed in the same direction of ball chain with flow speeds proportional to the driving frequency is observed. As no orientational asymmetry is present, flow reversal occurs when the speed of the ball-chain is reversed.

F. Inertial actuation. In a last method, cilia deformations are imposed by introducing high frequency vibrations to the cilia carpet as a whole. Whereas in contact force actuated cilia deformations are directly imposed to the cilia, here the dynamic behaviour of the carpet as a whole determines the actual output deformations. Typically, vibrating cilia beat at very high frequencies, often even higher than biological cilia where motion asymmetries are hard to implement. Vibrating cilia were reported by Oh *et al.* (41), who made PDMS micropillars with micromoulding fabrication method similar to the one used by Keissner and Brucker (109). These cilia are 400 µm long, with a rectangular cross-section of 10 µm x 75 µm, equispaced at 200 µm apart. A PZT piezo-electric microstage with an excitation amplitude of 20 µm is used to actuate the cilia array at a frequency of 65 Hz, which equals the resonance frequency of the cilia. Fluid flow experiments show the presence of rotational flows and a propulsive flow parallel to cilia length. The flow velocities are found to increase with increasing excitation amplitude. This system has been optimized in a subsequent work done by Lee *et al.* (110) where the impact of cilia spacing on the mixing performances is studied, with individual cilia measuring 800 µm x 45 µm x 10 µm. For large interciliary distances (>400 µm), small localized vortices above the cilia tip impede macro-mixing, while below a spacing of 300 µm, a large single vortex drastically improves mixing efficiency. Brucker and Keissner (111) developed vibrating cilia where the base is actuated using a magnetically driven piston. 36 micropillars of PDMS with a diameter of 50 µm and a length of 500 µm were patterned in a “V” structure on top of a PDMS membrane that is agitated by the driving piston. The motion of the piston is in the same direction of the cilia axis, generating vertical displacements of the membrane with an oscillation frequency of 50 Hz and an amplitude of 300 µm. The vertical movement of the piston induces a curvature of the supporting membrane, tilting the cilia radially outward and inducing lateral effective and recovery strokes. As such, fluid flow can be created. Another solution consists of exploiting acoustic waves as reported by Orbay *et al.* (112), who bonded a piezo-actuator to a supporting structure with integrated microchannel and cilia. To fabricate the cilia, a solution of photo-curable polyethylene glycol (PEG) polymer is injected in the microchannel and exposed to UV light using a mask with a patterned array of holes. Cylindrical flexible micropillars (170 µm in length and 30 µm in diameter) are thus formed. Acoustic excitations generated by a piezo transducer with a frequency of 4.6 kHz induce an oscillation of the artificial cilia with a maximum displacement of 55 µm, which was used to mix a solution of DI water and fluorescein. Dillinger *et al.* (113) developed ultra-sound activated ciliary bands, composed of two cilia arrays (L = 0.1 mm) that face each other. They used this technique to transport fluid and to propel a microrobot. According to the reciprocal orientation of the cilia array, the actuated band can attract or repel surrounding fluid, when actuated at very high frequencies (kHz range). The acoustic actuation induces a small-amplitude oscillation of the cilia that, despite the symmetric motion, can produce a net fluid displacement due to the high inertia caused by the ultrafast motion. Interestingly, the authors reported that they did not observe any net fluid displacement at lower frequencies (less than 100 Hz).

All the presented technologies are able to actuate artificial cilia, with varying degrees and types of asymmetry and collective behavior, as summarized in table S2 in SI. For further reference, we direct readers interested in advanced materials and actuation technologies for artificial cilia to the review by Zhang *et al.* (114). There are however some general observations that can be made and that are fundamental for the future of artificial cilia research. A *first* important observation is the locality of actuation. Optical and magnetic field actuation are generally globally imposed, where the cilia array as a whole experiences the same driving force. This global actuation approach drastically simplifies the control strategy, as asymmetries are physically encoded in the mechanical structures, either through the implantation direction, or through a varying magnetization across the cilia length. Inertial actuation also acts globally, where the mechanism of propulsion is not based on spatial asymmetries but rather on high driving frequencies, which cause the Reynolds number to be high in the proximity of the cilia. Localized actuation on the other hand enables a higher degree of control of the collective behavior, as the beat of neighboring cilia can be tuned to create tailored metachronal patterns. This approach can be seen in some pressure-driven and electrically actuated cilia, but necessitates either a multitude of peripherals or a way of multiplexing control signals, which is an uphill task when large cilia arrays are envisioned. *Secondly*, the amount and degree of tethering is vastly different between technologies. For actuation by contact force or inertial effects, there is a rigid connection between the cilia and the peripheral equipment. For actuation by pressure or electric fields a physical connection to an energy source is still needed, however this can be done through flexible routing. Actuation by light or magnetic field by contrast allows to break all contact. A *third* observation is the presence of bulky peripheral systems in general. Actuation by magnetic field requires big magnets or coils, a multitude of valves is needed to control pressure-driven cilia and light-driven cilia are actuated using light sources and optics. This seems to be a general fundamental problem in current artificial cilia arrays, and further research is needed to move the presented technologies to stand-alone systems.

Overall, the trend in artificial cilia technologies seems to be towards higher aspect ratio, more densely packed and more elastic actuators in forced external fields in a strive towards better performing microfluidic propulsion systems. This evolution diverges from the most fundamental principle of the behavior of natural ciliary carpets. These natural systems exhibit no central coordination. On the contrary, the beating patterns emerging in ciliary carpets are the result of spontaneous phase-locking and -unlocking of the structures under the influence of external and self-imposed stimuli, only supplied by an uncoordinated energy input. This non-equilibrium state has only sparsely been replicated in an artificial cilia technology (84) and this void in the state-of-the-art lies at the basis of the gap between artificial and natural cilia.

3. Fabrication technologies

Different production processes have been developed to fabricate artificial cilia. Although some techniques are more suited for a certain actuation technology, we have identified four basic processes that are regularly used for producing artificial cilia across the actuation spectrum. In this section we will elaborate on these techniques and give details on their specific implementation. Next we will qualitatively compare the fitness of different production processes to shape carpets of artificial cilia. The comparison is based on three characteristic metrics that are crucial for the overall fluid-driving performance, but are highly constrained by the production method. As a benchmark, naturally occurring cilia have been evaluated using the same three metrics.

A. Micromoulding. Micromoulding is regularly used to fabricate cilia carpets, as schematically shown on Fig. 4A. The process starts with the fabrication of the mould, defining the negative shape of the cilia. Typically, this mould is filled with a liquid prepolymer, that undergoes a cross-linking reaction inside. The actual geometry of the cilia thus depends on the mould dimensions. This process is heavily applied in conventional soft robotics (115), albeit on a larger scale. In literature, the moulds are fabricated through either conventional (micro)machining (104), lithography (105, 116), 3D printing (97), or by using materials that feature elongated pores (27). As cilia are high aspect-ratio structures, their release from the mould is particularly challenging. Alternatively, dissolving moulds has been used in literature to eliminate mechanically loading the cilia after curing (27). After demoulding, the geometrically defined cilia structures often need to follow a post-processing step, depending on the actuation principle. Compatibility with fluidic actuation is achieved through defining inflatable voids (117) within the structure of the cilia, whereas the compatibility with magnetic actuation is enabled by embedding ferromagnetic particles in the pre-polymerized blend that are subsequently magnetized in the preferred directions (118).

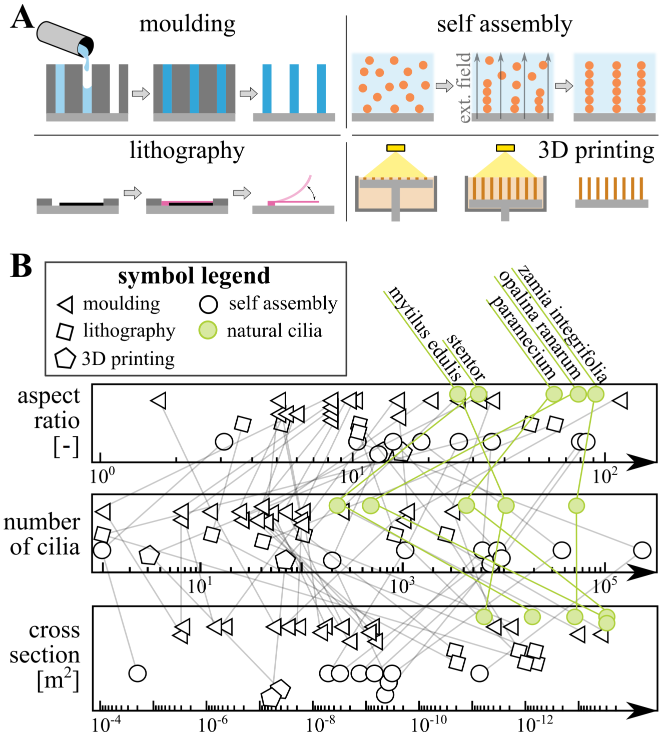

Fig. 4. Comparison of different fabrication technologies for artificial cilia, that are schematically depicted in **A**. These fabrication technologies are benchmarked against natural cilia in **B** along three axes: aspect ratio [-], number of cilia, and cross section of different artificial cilia [m^2]. The general trend for natural cilia is to lean towards the right side in each of the axes, however artificial cilia generally lack in at least one of the axes. The methodology that was used to populate this figure is detailed in SI (section S1C), along with enlarged versions of this figure. Raw data and references are reported in Table S5.

B. Lithography. Using lithographic processes, highly accurate cilia carpets can be made that are compatible with magnetic actuation (93), electric actuation (77, 79), and fluidic actuation (119). Here it should be noted that while some moulded cilia use lithographically produced moulds (40, 105), here lithography is used to directly shape the cilia, increasing the overall accuracy. Whereas moulded cilia are typically cast in an upright position, sharing a common support layer, cilia that are fabricated by means of lithography typically show a planar architecture (79) (see Fig. 4A).

C. Self-assembly. In addition to using processes that directly define the shape of the cilia, self-assembly processes use stochastic principles to produce carpets of cilia, without precise control on material deposition or removal. Magnetic or electrostatic fields, or a combination of both have been employed as the driving forces of these stochastic principles. A static magnetic field has been combined with solvent casting on multiple occasions in literature to autonomously grow a carpet of cilia with susceptibility for magnetic field actuation. (86, 99, 120, 121). To do so, magnetic and polymeric particles are first mixed into a solvent. A static magnetic field then is applied while the solvent is evaporated. After the solvent has fully evaporated, pillars consisting of magnetic and polymeric particles have grown vertically upwards from the bottom of the container which serves as a substrate. A post-processing step may be necessary to transform these pillars into mechanically stable cilia. Alternatively, a static magnetic field can be applied to support a process where strands of cilia are pulled from a film of liquid polymer. Wang *et al.* (90) proved that the presence of a magnetic field improves the shape of the pulled cilia, since magnetic particles were mixed into the polymer film beforehand. Sugioka *et al.* (78) utilize an electrostatic field to have a single cilium grow from a graphite rod. To this end, the rod is first placed in deionized water where an electrostatic field is induced using two parallel plate electrodes. The cilium, a mesh of interconnected carbon fibers, is formed under these conditions through the induced-charge electro-osmosis process (ICEO), without further external manipulations. Wang *et al.* (88) combine a magnetic and electrostatic field into a hybrid process in which a carpet of cilia is created from ferromagnetic beads and latex nanoparticles that are suspended in a liquid. The beads form chains and connect to a rigid surface by applying an external magnetic field, while electrostatic attraction between the beads and latex nanoparticles causes the latex to attach to the beads and enclose the chains completely. A subsequent heating step ensures that the latex particles form a continuous coating, without tears or other imperfections.

D. 3D printing. Recent studies have shown that 3D printing is a suitable method for cilia fabrication as well. Examples exist of cilia that have been produced by means of stereolithography (SLA), in which photopolymer resin is selectively exposed to UV light in a layer-wise fashion to construct multiple cilia simultaneously. The resulting array of cilia can be made compatible with magnetic actuation, when magnetic particles are introduced in the printing resin (122, 123).

Fabrication processes impose constraints to downsizing of artificial cilia without loss of functionality. There is thus an intricate entanglement between fabrication capabilities and the ability to instigate fluid flow at small scales. In order to assess this entanglement, we benchmark different production processes in literature to the geometrical characteristics of natural cilia. This benchmarking is done using three metrics. First, we take into account the actual size of the cilium, where we use the cross-sectional area as a defining metric, to capture both plate-like and rod-like cilia. This cilia size directly influences the Reynolds number at which they operate. The number of cilia in the carpet is employed as a second metric which represents the capabilities of the manufacturing process to work across different length-scales and reflects the pumping ability of a carpet; usually the larger the carpet, the more fluid can be displaced. Lastly, we employ the aspect ratio of the produced cilia (L/x, where L is the length of the cilia and x the diameter of circular cilia or the width of rectangular ones) to assess the inherent capabilities of the production process to create slender objects, disregarding the actual size. The aspect ratio is an important feature of these structures, as it influences its bending resistance and ultimately how well viscous forces transfer onto the elastic structure of the cilium. Figure 4B displays the data of different artificial and natural cilia for each of the three metrics on separate 1D plots with logarithmic scales. Straight lines between the different 1D plots connect data from a single literature reference. According to these metrics, natural cilia (marked in green colored circles) have aspect ratio's of about 15-75. They have a broad range of carpet sizes, with the number of cilia being highly depending on the size of the organism, ranging from a few 100's 1000's for eukaryotes to 10k's for large invertebrates. This is a direct consequence of the size of the cilia that doesn't scale with the size of the organism, as hydrodynamic interactions need to be preserved. The cross-sectional area of natural cilia are in the order of $1\text{x}10^{-13} - 1\text{x}10^{-14} m^2$. As a conclusion for natural cilia, we see that they combine high aspect ratios, with large carpet sizes and a small cross sectional area. When comparing this to the different fabrication technologies that are used to shape artificial cilia (triangles for moulding, squares for lithography, pentagons for 3D printing and circles for self assembly, on Fig. 4 B), the following conclusions can be made. *First*, there are artificial cilia that have larger aspect ratios than natural cilia. Evans *et al.* (27), Liu *et al.* (86) and Sun *et al.* (121) produced cilia with the largest aspect ratios that even surpass some of the highest ones of cilia found in nature. And while artificial cilia have been produced with aspect ratios similar to their natural counterpart (87, 95, 96, 99, 124, 125), most are too wide for their length. *Secondly*, the number of cilia that occur in natural organisms is matched by several artificial cilia carpets. The carpet size observed in Zamia Integrifolia is surpassed by the ones obtained by Wang *et al.* (88) and nearly contested by the carpets seen in Liu *et al.* (86). In addition, the carpets produced by Jaakko *et al.* (120) and Sun *et al.* (121) contained a similar amount of cilia as is observed on Mytilus Edulis. *Third*, even the natural cilia with the smallest cross sections reported here (Paramecium and Opalina Ranarum) are almost bested by the cilia produced by Evans *et al.* (27) and Islam *et al.* (125). The cilia found in the works of Hanasoge *et al.* (93, 94, 124, 126), Shields *et al.* (87) and Wang *et al.* (88) are close runner-ups. However, the majority of artificial cilia is still orders of magnitude larger in cross-section than the ones found in nature. *Fourth*, the individual comparisons for each of the three proposed metrics show that some artificial cilia can compete with their natural counterparts or even surpass them in certain aspects. Additionally, there does not seem to be a trend indicating an optimal fabrication process for creating life-like artificial cilia. Moulding, lithography and self-assembly procedures each provided actuators that can rival natural cilia in one or two of the metric categories. However, ideal cilia carpets should perform well for all of the metrics simultaneously, which is currently not the case for artificial cilia.

4. Assessing cilia functionality

The previous paragraph shows limitations of production processes to create large high aspect-ratio cilia carpets with small ciliary dimensions. However it does not assess the capabilities of these artificial cilia to induce fluid flow. As detailed in the introduction, fluid flow at low Reynolds numbers is highly depending on symmetry breaking and on the hydrodynamic interactions between cilia. These characteristics do not only depend on the geometry of the cilia, which is defined through the fabrication process, but also on the actuation technology and the mode of actuation. We have identified two metrics that enable us to assess the flow inducing capabilities of artificial cilia and benchmark them against natural cilia. More details and calculations of these metrics can be found in SI.

In first instance we assess the ability of a single cilium to generate fluid flow at low Reynolds numbers. These conditions require a certain complexity in the cilium's beating pattern, where it is necessary for the effective stroke and recovery stroke to follow a different path. This form of asymmetry, called spatial asymmetry, can be quantified by the area the tip of cilium encloses when completing a full stroke, and is called the swept area (SA), as is schematically depicted in red on the inset figure of Fig.1 B. From literature (34), it is known that the SA is directly proportional to the flow induced during one full stroke. Considering artificial cilia with a planar beating pattern, we non-dimensionalize swept area by dividing it with the theoretical maximum swept area a cilia of length (L), being a semi-circle with area ($0.5\pi L^2$), to discern flow producing capabilities from size. On Fig.5 A we have plotted this metric against the length of the cilia, and this for both natural (17, 18, 62, 127, 128) and artificial cilia, where we made a distinction between the different actuation technologies. As we only compare the planar dimensionless SA, a number of conically beating cilia were excluded from this overview. An overview of the data points can be found in SI, along with the methods used for calculating the SA's. From this plot (Fig.5 A) we can draw the following conclusions. *First*, it is apparent that for artificial cilia the largest swept areas are found in cilia actuated by magnetic field, with an absolute maximum of 47%, developed by Dong *et al.* (44). The combination of programming the magnetic dipole vector throughout the length of the cilia with a time and spatially varying magnetic field leads to high SA's. This makes it possible to alter the curvature of the cilia throughout the length of the cilia, resembling natural cilia, as will be discussed later on. *Second*, the smallest artificial cilia do not display any spatial asymmetry. Techniques that are used on a large scale to create spatial asymmetry are hard to apply on a small scale without losing functionality. Whereas the smallest cilia are made using lithographic techniques, spatial asymmetry inducing properties are not yet accessible at these small scales. *Third*, a large discrepancy exists with natural cilia, which display a large variety for spatial asymmetries at one or two orders smaller in size than typical artificial cilia. This large discrepancy can be explained by the underlying mechanism that natural cilia employ to create spatial asymmetry, discussed earlier in the introduction. The sliding-mode mechanism resulting from the travelling wave of activation/inhibition of motor proteins along the length of the cilium is very different from techniques used in artificial cilia, however the main principle of creating traveling waves of local bending deformation is being mimicked. For magnetic cilia (44, 97) this is done by altering the magnetization along the length, and creating a traveling wave by changing the external magnetic field. For pressure driven cilia (25), the 2-channel approach can be thought of as a rough discretization in 2 segments with a similar bottom-to-tip actuation pattern, which is analogue to the 3-segmented approach applied by Sareh *et al* (62).

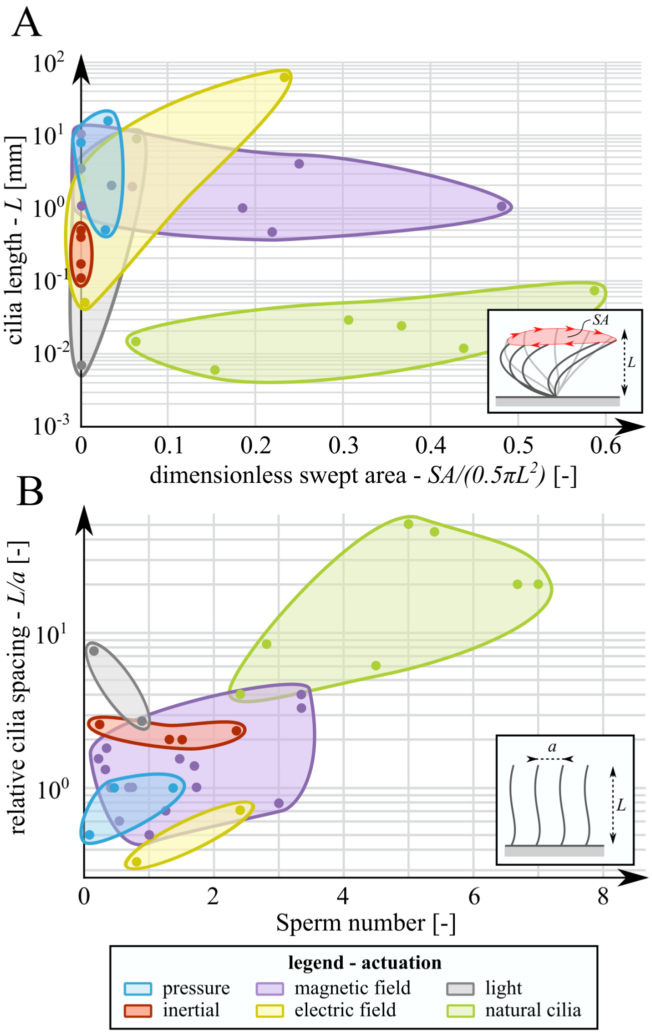

Fig. 5. **A**: A comparison between artificial and natural cilia in terms of size and beat complexity, considering only 2D planar beating motions. Natural cilia tends to exhibit larger spatial asymmetry, at smaller size. **B**: A comparison between artificial and natural cilia in terms of Sperm number and cilia proximity. Natural cilia tend to show a higher Sperm number, meaning that the effects of viscous forces are more easily transferred from the fluid onto the cilia structure, and are packed more closely. This indicates that a higher mutual influence through the fluid is to be expected and self-coordinated metachronal asymmetry can emerge. Data points are detailed in SI.

In a second metric we asses the ability of cilia carpets to create metachronal beating patterns. In nature it is apparent that this global synchronisation emerges without high-level coordination (24). Key to this emerging behaviour is the existence of slip in nature's sliding mode mechanism, where the actual sliding between microtubule pairs is not rigidly coupled to the activation of the motor proteins. As a result, the local bending deformation is not only influenced by internal forces from the motor proteins, but also by the hydrodynamic forces that are imposed by the surrounding fluid. Enabled by the surrounding fluid, a local interaction between neighbouring cilia that forms the basis of global motion coordination (24) thus exists. For this coupling mechanism to happen, the bending stiffness of the cilia needs to be within certain bounds. If the cilium is too stiff, the hydrodynamic forces are not able to influence its deformation. If the cilium is too flexible, it cannot instigate fluid flow and influence neighboring cilia. This interplay between bending rigidity and viscous hydrodynamic forces is captured by the non-dimensional Sperm number introduced by Lagomarsino (43) and applied to cilia by Eloy *et al* (59), representing the ratio of viscous forces to elastic forces, with expression:

$$Sp = L\left(\frac{8\pi^2\mu f}{ln(L/r)EI}\right)^{0.25},$$

where f is a single cilium's beating frequency, μ the dynamic viscosity of the surrounding fluid, E the Young's modulus, I the second moment of inertia, r the radius and L the length of the cilium. A second factor that heavily influences motion orchestration between cilia is their inter-ciliary distance a. Due to dissipation in the viscous fluid, fluid flows die out rapidly with distance, hence cilia in closely packed carpets exhibit a stronger coupling with their neighbours. In the end this leads to a global motion behavior were traveling waves can be seen over the surface of the cilia carpet. This phenomenon is self regulating and stable, meaning that out-of-sync cilia passively experience flow conditions that push them to the right timing (24). In Fig.5 B we have plotted both key factors that determine the ability of cilia to sustain spontaneous orchestration, being Sperm number and relative cilia spacing L/a. We have done this both for artificial and natural cilia (17, 62, 127, 129–133), and added a section in SI detailing the calculation of the used Sperm numbers. Not all artificial cilia described in section 2 could be taken into account, as data needed for calculating the Sperm number were not always reported, or the cilia were not actuated in a liquid.

From this plot (Fig. 5 B), we can draw the following conclusions. *First* There is a big discrepancy between artificial and natural cilia in terms of relative cilia spacing, where natural cilia are in general more densely packed than artificial cilia. Nature is thus at an advantage to use hydrodynamic coupling between cilia as a mechanism for motion orchestration. *Second*, in terms of Sperm number, there exist some magnetic cilia that attain the values of natural cilia, however it is apparent that most artificial cilia are too stiff for the fluidic environment they operate in. *Third*, When looking at artificial cilia, there is a large spread in characteristics with magnetic cilia spanning the entire range, depending on the soft materials and the production processes used. For cilia actuated by inertial effects, there are some fundamental limitations in attainable sperm number, as the vibration frequency is also directly linked to the bending rigidity EI. *Fourth*, Although artificial cilia exist with comparable Sperm number and relative cilia spacing to natural cilia, it should be noticed that this Sperm number only takes the passive mechanics into account. The 'geometric-clutch mechanism' theorized for natural cilia (134) that opens up the possibility of spontaneous motion synchronization is not present in current collective artificial ciliary systems. Metachrony is still induced by specifically tuning the physical properties of the single cilium to display a pre-programmed motion to the global actuation field. Natural ciliary motions are dictated by the interplay between inner molecular motors and the hydrodynamic forces generated by the neighboring cilia. In that sense, each cilium can be thought as a self-sensing actuator that adjust its own beat to the viscous forces that act against it, basically functioning in a state of non-equilibrium. This local adaptive behavior cannot be mimicked using force fields actuation, where the cilia move in unison or with a pre-programmed pattern. This seems to be the most fundamental difference between current artificial cilia and their natural counterparts, and filling this gap will be challenging. If actively beating artificial ciliary carpets are to showcase emerging metachronal waves, this coupling has to be broken.

A first step in creating this emergent self-coordination has already been taken, and consists of creating an external feedback loop to control the fluid-influenced behavior of beating flexible flaplets (135), but this still requires extensive peripherals. Moving forward, to create integrated and more independent ciliary carpets which achieve spontaneous synchronization, we need a new design of artificial cilia, where part of the control is outsourced to the cilium itself, namely the onset of the actuation that should be triggered when the cilium reaches a certain geometrical configuration while the external source is limited to periodically supply energy. This has been shown to be effective by using the self-oscillating behavior of light-sensitive actuators in a carefully designed experimental setting (84), but has still to be proven in a larger and less tightly controlled environment and remains reliant on the transfer of viscous fluid forces on the elastic structures. However, the principle of non-equilibrium that these actuators function in can serve as great inspiration for implementation in other soft robotic technologies. Harnessing local and distributed physical properties is a way of embodying control schemes and energy flows within the system, an approach to embodied intelligence that is a great object of interest in soft robotics (136). On a larger scale this philosophy was implemented to create locomotion using a soft robot that consists of locally controlled segments (137). However new architectures need to be developed that can be down-scaled to cilia dimensions.

5. Conclusion and outlook

Artificial cilia mimic nature's solution of fluid propulsion at the small scales, that is tailored to the fundamentals of low Reynolds fluid flow. Where large scale industrial pumps clearly exceed the capabilities of nature's large scale solutions (eg. heart or lungs), the verdict on natural vs. artificial cilia is not that clear at the microscale. This paper attempts to provide a broader perspective on how these artificial cilia compare to their natural counterparts by means of several metrics derived from both their fundamental flow inducing capabilities and the fabrication techniques behind the physical embodiments of the artificial cilia. This novel approach unveils new insights in the state-of-the-art of artificial cilia research and identifies the discrepancies between artificial and natural ciliary systems and potentially interesting research trajectories to close the gap between them.

Three major conclusions can be drawn from this analysis. *Firstly*, natural cilia are often of smaller size while exhibiting a similar or more complex beating pattern, captured by their dimensionless swept area. This influences the amount of fluid moved per beat cycle for an individual cilium. *Secondly*, artificial cilia carpet sizes are generally underwhelming compared to natural systems, despite the large influence this has on collective fluid propulsion. *Thirdly*, in natural cilia, the collective optimization of flow inducing capability stems from the ability to influence the beat of neighboring cilia such that intricate and non-coordinated metachronal patterns emerge. This is currently absent in artificial cilia, as is shown by both the discrepancy in cilia proximity or carpet density and higher Sperm numbers in natural cilia and seems to be the most fundamental difference between current artificial cilia and their natural counterparts, and filling this gap will be challenging. Regardless of whether future research in artificial cilia will result in the practical implementation of these principles in microfluidic applications or the further unveiling of the specific physics behind these principles, it seems that the road towards closing the gap between artificial and natural ciliary systems leads past the interface between microscopic fluid dynamics and fundamental soft matter research and will provide ample opportunity for novel and exciting research.

Acknowledgments

Funding: Research was supported by the Fund for Scientific Research-Flanders (FWO). **Author contributions:** All authors contributed and revised the manuscript. **Competing interests:** The authors declare no conflict of interest. **Data and materials availability:** All data used to generate the figures is available upon reasonable request.

References

1. Victoria Welch, Jean Pol Vigneron, Virginie Lousse, and Andrew Parker. Optical properties of the iridescent organ of the comb-jellyfish beroë cucumis (ctenophora). *Physical Review E*, 73(4):041916, 2006.
2. David Gudis, Ke Qing Zhao, and Noam A. Cohen. Acquired cilia dysfunction in chronic rhinosinusitis. *American Journal of Rhinology and Allergy*, 26:1–6, 1 2012. .
3. Sidney L. Tamm. Ciliary motion in paramecium: A Scanning Electron Microscope Study. *J. Cell Biol.*, 55(1):250–255, oct 1972.
4. Jianfeng Lin and Daniela Nicastro. Asymmetric distribution and spatial switching of dynein activity generates ciliary motility. *Science*, 360(6387), 2018.
5. Charles B Lindemann and Kathleen A Lesich. Flagellar and ciliary beating: the proven and the possible. *J. Cell Sci.*, 123(4):519–528, feb 2010.
6. E. M. Purcell. Life at low Reynolds number. *Am. J. Phys.*, 45:3–11, 1977.
7. Michael A. Sleigh. Flagellar beat patterns and their possible evolution. *BioSystems*, 14: 423–431, 1981.
8. Sidney L. Tamm. Cilia and the life of ctenophores. *Invertebrate Biology*, 133(1):1–46, 2014.
9. J. Gray. The mechanism of ciliary movement. *Proc. R. Soc. B Biol. Sci.*, 93(650):104–121, feb 1922.
10. Christopher Brennen and Howert Winet. Fluid Mechanics of Propulsion By Cilia and Flagella. *Annu. Rev. Fluid Mech.*, 9(Lehninger 1971):339–398, jan 1977.
11. Zhi-Guo Zhou and Zhi-Wen Liu. Biomimetic Cilia Based on MEMS Technology. *J. Bionic Eng.*, 5:358–365, 2008. .
12. Eric Lauga and Thomas R Powers. The hydrodynamics of swimming microorganisms. *Reports Prog. Phys.*, 72(9):096601, sep 2009.
13. Oliver T. Thatcher (ed). *The library of original sources*, volume 6. New york, Chicago University Research Extension, 1907.
14. Denis H. Lynn. *The Ciliated Protozoa*, volume 3rd edition. Springer, 2008.
15. Shoji A Baba. Regular steps in bending cilia during the effective stroke. *Nature*, 282(5740): 717–720, 1979.
16. J. Gray. The mechanism of ciliary movement. *Proceedings of the Royal Society B*, 93(650): 104–121, 1922.
17. M. A. Sleigh. The form of beat in cilia of stentor and opalina. *Experimental Biology*, 37(1), 1960.
18. Edward Aiello and MichaelA. Sleigh. The metachronal wave of lateral cilia of mytilu edulis. *The Journal of Cell Biology*.
19. Jacobo Wais-Steider and Peter Satir. Effect of vanadate on gill cilia: Switching mechanism in ciliary beat. *Journal of Supramolecular Structure*, 11(3):339–347, 1979.
20. S L Tamm and S Tamm. Alternate patterns of doublet microtubule sliding in atp-disintegrated macrocilia of the ctenophore beroë. *Journal of Cell Biology*, 99(4).
21. S. N. SN Khaderi, CB Craus, J Hussong, N Schorr, J. M J den Toonder, and P. R. Onck. Magnetically-actuated artificial cilia for microfluidic propulsion. *Lab Chip*, pages 2002–2010, 2011.
22. Yang Ding and Eva Kanso. Selective particle capture by asynchronously beating cilia. *Physics of Fluids*, 27:121902, 12 2015.
23. Yang Ding, Janna C. Nawroth, Margaret J. McFall-Ngai, and Eva Kanso. Mixing and transport by ciliary carpets: A numerical study. *J. Fluid Mech.*, 743:124–140, 2014.
24. Jens Elgeti and Gerhard Gompper. Emergence of metachronal waves in cilia arrays. *Proc. Natl. Acad. Sci. U. S. A.*, 110(12):4470–5, mar 2013.
25. Edoardo Milana, Rongjing Zhang, Maria Rosaria Vetrano, Sam Peerlinck, Michael De Volder, Patrick R Onck, Dominiek Reynaerts, and Benjamin Gorissen. Metachronal patterns in artificial cilia for low reynolds number fluid propulsion. *Science advances*, 6(49):eabd2508, 2020.
26. Ahmet F. Demirors, Sumeyye Aykut, Sophia Ganzeboom, Yuki A. Meier, and Erik Poloni. Programmable droplet manipulation and wetting with soft magnetic carpets. *Proceedings of the National Academy of Sciences of the United States of America*, 118, 11 2021.
27. B. A. Evans, A. R. Shields, R. Lloyd Carroll, S. Washburn, M. R. Falvo, R. Superfine, Chapel Hill, Chapel Hill, North Carolina, West Virginia, V Uni, West Virginia, Chapel Hill, Chapel Hill, and North Carolina. Magnetically Actuated Nanorod Arrays as Biomimetic Cilia. *Nano Lett.*, 7(5):1428–1434, 2007.
28. Kaitlyn P Becker, Yufeng Chen, Robert J Wood, K P Becker, Y Chen, R J Wood John A Paulson, and R J Wood. Mechanically programmable dip molding of high aspect ratio soft actuator arrays. 2020. .
29. Shuang Ben, Jinjia Yao, Yuzhen Ning, Zhihong Zhao, Jinlong Zha, Dongliang Tian, Kesong Liu, and Lei Jiang. A bioinspired magnetic responsive cilia array surface for microspheres underwater directional transport. *Science China Chemistry*, 63(3):347–353, 2020.
30. Mojca Vilfan, Anton Potocnik, Blaz Kavcic, Natan Osterman, Igor Poberaj, Andrej Vilfan, and Dusan Babic. Self-assembled artificial cilia. *Proc. Natl. Acad. Sci. U. S. A.*, 107(5): 1844–1847, feb 2010.
31. Shuaizhong Zhang, Zhiwei Cui, Ye Wang, and Jaap Den Toonder. Metachronal -cilia for on-chip integrated pumps and climbing robots. *ACS Applied Materials and Interfaces*, 13: 20845–20857, 5 2021.
32. Alexander Alexeev, J M Yeomans, and Anna C Balazs. Designing synthetic, pumping cilia that switch the flow direction in microchannels. *Langmuir*, 24(21):12102–12106, 2008.
33. Hassan Masoud and Alexander Alexeev. Harnessing synthetic cilia to regulate motion of microparticles. *Soft Matter*, 7:8702–8708, 2011.
34. S N Khaderi, M G H M Baltussen, P D Anderson, D Ioan, J M J Den Toonder, and P R Onck. Nature-inspired microfluidic propulsion using magnetic actuation. *Phys. Rev. E - Stat. Nonlinear, Soft Matter Phys.*, 79(4), 2009.
35. S N Khaderi, J M J den Toonder, and P R Onck. Microfluidic propulsion by the metachronal beating of magnetic artificial cilia: a numerical analysis. *J. Fluid Mech.*, 688:44—–65 M3 – 10.1017/jfm.2011.355, 2011.
36. Mojca Vilfan, Gašper Kokot, Andrej Vilfan, Natan Osterman, Blaž Kavčič, Igor Poberaj, and Dušan Babič. Analysis of fluid flow around a beating artificial cilium. *Beilstein J. Nanotechnol.*, 3:163–171, feb 2012. .
37. Rongjing Zhang, Jaap den Toonder, and Patrick R Onck. Transport and mixing by metachronal waves in nonreciprocal soft robotic pneumatic artificial cilia at low reynolds numbers. *Physics of Fluids*, 33(9):092009, 2021.
38. S N Khaderi, M G H M Baltussen, P D Anderson, J M J Den Toonder, and P R Onck. Breaking of symmetry in microfluidic propulsion driven by artificial cilia. *Phys. Rev. E - Stat. Nonlinear, Soft Matter Phys.*, 82(2), 2010.
39. S. N. Khaderi, J. M J Den Toonder, and P. R. Onck. Magnetically actuated artificial cilia: The effect of fluid inertia. *Langmuir*, 28(20):7921–7937, 2012.
40. Benjamin Gorissen, Michaël de Volder, and Dominiek Reynaerts. Pneumatically-actuated artificial cilia array for biomimetic fluid propulsion. *Lab Chip*, 15(22):4348–4355, 2015.
41. Kieseok Oh, Jae-Hyun Chung, Santosh Devasia, and James J. Riley. Bio-mimetic silicone cilia for microfluidic manipulation. *Lab Chip*, 9(11):1561, 2009.
42. Rita R. Ferreira, Hajime Fukui, Renee Chow, Andrey Vilfan, and Julien Vermot. The cilium as a force sensor-myth versus reality. *Journal of Cell Science*, 132, 2019.
43. M. C. Lagomarsino, F. Capuani, and C. P. Lowe. A simulation study of the dynamics of a driven filament in an Aristotelian fluid. *J. Theor. Biol.*, 224(2):215–224, sep 2003.
44. Xiaoguang Dong, Guo Zhan Lum, Wenqi Hu, Rongjing Zhang, Ziyu Ren, Patrick R Onck, and Metin Sitti. Bioinspired cilia arrays with programmable nonreciprocal motion and metachronal coordination. *Science advances*, 6(45):eabc9323, 2020.
45. Geoffrey Ingram Taylor. Analysis of the swimming of microscopic organisms. *Proceedings of the Royal Society A*, 209(1099):447–460, 1951.
46. Andrej Vilfan and Frank Jülicher. Hydrodynamic flow patterns and synchronization of beating cilia. *Phys. Rev. Lett.*, 96(5):1–4, 2006.
47. Thomas Niedermayer, Bruno Eckhardt, and Peter Lenz. Synchronization, phase locking, and metachronal wave formation in ciliary chains. *Chaos*, 18(3), 2008.
48. Nariya Uchida and Ramin Golestanian. Synchronization and collective dynamics in a carpet of microfluidic rotors.
49. C. Wollin and H. Stark. Metachronal waves in a chain of rowers with hydrodynamic interactions. *The European Physical Journal E*, 34(42), 2011.
50. M. Hines and J. Blum, J. Thee-dimensional mechanics of eukaryotic flagella. *Biophysical Journal*, 41:67–79, 1983.
51. Boris Guirao and Jean-François Joanny. Spontaneous creation of macroscopic flow and metachronal waves in an array of cilia. *Biophysical Journal*, 92:1900–1917, 2007.
52. Xingzhou Yang, Robert H. Dillon, and Lisa J. Fauci. An integrative computational model of multiciliary beating. *Bulletin of Mathematical Biology*, 70:1192–1215, 2008.
53. Shay Gueron and Nadav Liron. Ciliary motion modeling, and dynamic multicilia interactions. *Biophys. J.*, 63(4):1045–1058, 1992.
54. Shay Gueron, Konstantin Levit-Gurevich, Nadav Liron, and Jacob J. Blum. Cilia internal mechanism and metachronal coordination as the result of hydrodynamical coupling. *Proceedings of the National Academy of Sciences of the United States of America*, 94:6001–6006, 1997.
55. Shay Gueron and Konstantin Levit-Gurevich. Energetic considerations of ciliary beating

and the advantage of metachronal coordination. *Proc. Natl. Acad. Sci. U. S. A.*, 96(22): 12240–12245, 1999.

56. Shay Gueron and Konstantin Levit-Gurevich. A three-dimensional model for ciliary motion based on the internal 9+2 structure. *Proceedings of the The Royal Society of London B*, 268: 599–607, 2001.
57. Charles B. Lindemann. The geometric clutch as a working hypothesis for future research on cilia and flagella. *Annals of the New York Academy of Sciences*, 1101:477–493, 2007.
58. Yujie Liu, Rory Claydon, Marco Polin, and Douglas R. Brumley. Transitions in synchronizations states of model cilia through basal-connection coupling. *Journal of the Royal Society Interface*, 15(147), 2018.
59. Christophe Eloy and Eric Lauga. Kinematics of the most efficient cilium. *Phys. Rev. Lett.*, 109(3), 2012.
60. Natan Osterman and Andrej Vilfan. Finding the ciliary beating pattern with optimal efficiency. *Proc. Natl. Acad. Sci. U. S. A.*, 108(38):15727–32, 2011.
61. Hanliang Guo, Janna Nawroth, Yang Ding, and Eva Kanso. Cilia beating patterns are not hydrodynamically optimal. *Phys. Fluids*, 26(9):1–12, 2014.
62. Sina Sareh, Jonathan Rossiter, Andrew Conn, Knut Drescher, and Raymond E Goldstein. Swimming like algae: biomimetic soft artificial cilia. *J. R. Soc. Interface*, 10(78):20120666–, 2012.
63. Edoardo Milana, Benjamin Gorissen, Sam Peerlinck, Michael De Volder, and Dominiek Reynaerts. Artificial Soft Cilia with Asymmetric Beating Patterns for Biomimetic Low-Reynolds-Number Fluid Propulsion. *Adv. Funct. Mater.*, 1900462:1–8, 2019.
64. Edoardo Milana, Bert Van Raemdonck, Kevin Cornelis, Enrique Dehaerne, Jef De Clerck, Yarno De Groof, Toon De Vil, Benjamin Gorissen, and Dominiek Reynaerts. EELWORM : a bioinspired multimodal amphibious soft robot. 2020.
65. Tanveer ul Islam, Ye Wang, Ishu Aggarwal, Zhiwei Cui, Hossein Eslami Amirabadi, Hemanshul Garg, Roel Kooi, Bhavana Venkataramanachar, Tongsheng Wang, Shuaizhong Zhang, et al. Microscopic artificial cilia-a review. *Lab on a Chip*, 2022.
66. Haojian Lu, Mei Zhang, Yuanyuan Yang, Qiang Huang, Toshio Fukuda, Zuankai Wang, and Shen Yajing. A bioinspired multilegged soft millirobot that functions in both dry and wet conditions. *Nature Communications*, 9(3944), 2018.
67. Anna C Balazs, Amitabh Bhattacharya, Anurag Tripathi, and Henry Shum. Designing bioinspired artificial cilia to regulate particle-surface interactions, 2014.
68. Shuaizhong Zhang, Ye Wang, Patrick R. Onck, and Jaap M.J. den Toonder. Removal of microparticles by ciliated surfaces - an experimental study. *Advanced Functional Materials*, 29(6), 2019.
69. Jaap den Toonder, Femke Bos, Dick Broer, Laura Filippini, Murray Gillies, Judith de Goede, Titie Mol, Mireille Reijme, Wim Talen, Hans Wilderbeek, Vinayak Khatavkar, and Patrick Anderson. Artificial cilia for active micro-fluidic mixing. *Lab Chip*, 8:533–541, 2008.
70. Yu-An Wu, Bivas Panigrahi, Yueh-Hsun Lu, and Chia-Yuan Chen. An Integrated Artificial Cilia Based Microfluidic Device for Micropumping and Micromixing Applications. *Micromachines*, 8(9):260, 2017.
71. Jaap M.J. den Toonder and Patrick R. Onck. Microfluidic manipulation with artificial/bioinspired cilia. *Trends in Biotechnology*, 31(2), 2013.
72. Daniela Rus and Michael T. Tolley. Design, fabrication and control of soft robots. *Nature*, 521 (7553):467–475, may 2015.
73. Benjamin Gorissen, Dominiek Reynaerts, Satoshi Konishi, Kazuhiro Yoshida, Joon-Wan Kim, and Michael De Volder. Elastic Inflatable Actuators for Soft Robotic Applications. *Adv. Mater.*, page 1604977, sep 2017.
74. William Gilpin, Matthew Storm Bull, and Manu Prakash. The multiscale physics of cilia and flagella. *Nature Reviews Physics*, 2(2):74–88, 2020.
75. Béla Párducz. Ciliary movement and coordination in ciliates. *International review of cytology*, 21:91–128, 1967.
76. Charles B Lindemann and Kathleen A Lesich. The geometric clutch at 20: stripping gears or gaining traction? *Reproduction*, 150(2):R45–R53, 2015.
77. Jaap den Toonder, Femke Bos, Dick Broer, Laura Filippini, Murray Gillies, Judith de Goede, Titie Mol, Mireille Reijme, Wim Talen, Hans Wilderbeek, Vinayak Khatavkar, and Patrick Anderson. Artificial cilia for active micro-fluidic mixing. *Lab Chip*, 8(4):533–41, 2008.
78. Hideyuki Sugioka and Hiroki Yoshijima. Metachronal motion of artificial cilia using induced charge electro-osmosis. *Colloids and Surfaces A: Physicochemical and Engineering Aspects*, 626:127023, 2021.
79. Wei Wang, Qingkun Liu, Ivan Tanasijevic, Michael F Reynolds, Alejandro J Cortese, Marc Z Miskin, Michael C Cao, David A Muller, Alyosha C Molnar, Eric Lauga, et al. Cilia metasurfaces for electronically programmable microfluidic manipulation. *Nature*, 605(7911):681–686, 2022.
80. Ziyu Ren, Mingchao Zhang, Shanyuan Song, Zemin Liu, Chong Hong, Tianlu Wang, Xiaoguang Dong, Wenqi Hu, and Metin Sitti. Soft-robotic ciliated epidermis for reconfigurable coordinated fluid manipulation. *Science Advances*, 8(34), 2022.
81. Casper L van Oosten, Cees W M Bastiaansen, and Dirk J Broer. Printed artificial cilia from liquid-crystal network actuators modularly driven by light. *Nat. Mater.*, 8(8):677–682, 2009.
82. Roel J. H. van Raak, Simon J. A. Houben, Albertus P. H. J. Schenning, and Dirk J. Broer. Patterned and collective motion of densely packed tapered multiresponsive liquid crystal cilia. *Advanced Materials Technologies*, n/a(n/a):2101619, 2022.
83. Shucong Li, Michael M Lerch, James T Waters, Bolei Deng, Reese S Martens, Yuxing Yao, Do Yoon Kim, Katia Bertoldi, Alison Grinthal, Anna C Balazs, et al. Self-regulated non-reciprocal motions in single-material microstructures. *Nature*, 605(7908):76–83, 2022.
84. Zixuan Deng, Hang Zhang, Arri Priimagi, and Hao Zeng. Light-fueled nonreciprocal self-oscillators for fluidic transportation and coupling. *Advanced Materials*, 2022.
85. Anne Helene Gelebart, Matthew Mc Bride, Albertus P. H..J. Schenning, Christopher N. Bowman, and Dirk J. Broer. Photoresponsive fiber array: Toward mimicking the collective motion of cilia for transport applications. *Advanced Functional Materials*, 26(29):5322–5327, 2016.
86. Li Liu, Marc del Pozo, Fateme Mohseninejad, Michael G. Debije, Dirk J. Broer, and Albert P.H.J. Schenning. Light tracking and light buiding fiber arrays by adjusting the location of photoresponsive azobenzene in liquid crystal networks. *Advanced Optical Materials*, 8(18), 2020.
87. a R Shields, B L Fiser, B a Evans, M R Falvo, S Washburn, and R Superfine. Biomimetic cilia arrays generate simultaneous pumping and mixing regimes. *Proc. Natl. Acad. Sci. U. S. A.*, 107(36):15670–15675, 2010.
88. Ye Wang, Yang Gao, Hans Wyss, Patrick Anderson, and Jaap den Toonder. Out of the cleanroom, self-assembled magnetic artificial cilia. *Lab Chip*, 13(17):3360–6, 2013.
89. Ye Wang, Yang Gao, Hans M Wyss, Patrick D Anderson, and Jaap M J den Toonder. Artificial cilia fabricated using magnetic fiber drawing generate substantial fluid flow. *Microfluid. Nanofluidics*, 18(2):167–174, 2014.
90. Ye Wang, Jaap den Toonder, Ruth Cardinaels, and Patrick Anderson. A continuous roll-pulling approach for the fabrication of magnetic artificial cilia with microfluidic pumping capability. *Lab Chip*, 16(12):2277–2286, 2016.
91. Shuaizhong Zhang, Ye Wang, Reinoud Lavrijsen, Patrick R. Onck, and Jaap M.J. den Toonder. Versatile microfluidic flow generated by moulded magnetic artificial cilia. *Sensors Actuators, B Chem.*, 263:614–624, jun 2018.
92. J. Hussong, N. Schorr, J. Belardi, O. Prucker, J. Rühe, and J. Westerweel. Experimental investigation of the flow induced by artificial cilia. *Lab Chip*, 11(12):2017–2022, 2011.
93. Srinivas Hanasoge, Peter J. Hesketh, and Alexander Alexeev. Microfluidic pumping using artificial magnetic cilia. *Microsystems Nanoeng.*, 4(1):11, dec 2018.
94. Srinivas Hanasoge, Peter J. Hesketh, and Alexander Alexeev. Metachronal motion of artificial magnetic cilia. *Soft Matter*, 14(19):3689–3693, may 2018.
95. Fujio Tsumori, Ryuma Marume, Akinori Saijou, Kentaro Kudo, Toshiko Osada, and Hideshi Miura. Metachronal wave of artificial cilia array actuated by applied magnetic field. In *Jpn. J. Appl. Phys.*, volume 55, 2016. .
96. Hayato Shinoda and Fujio Tsumori. Development of Micro Pump Using Magnetic Artificial Cilia with Metachronal Wave. *Proc. IEEE Int. Conf. Micro Electro Mech. Syst.*, 2020-Janua: 497–500, 2020.
97. Hongri Gu, Quentin Boehler, Haoyang Cui, Eleonora Secchi, Giovanni Savorana, Carmela De Marco, Simone Gervasoni, Quentin Peyron, Tian Yun Huang, Salvador Pane, Ann M. Hirt, Daniel Ahmed, and Bradley J. Nelson. Magnetic cilia carpets with programmable metachronal waves. *Nat. Commun.*, 11(1):1–10, 2020.
98. Shuaizhong Zhang, Zhiwei Cui, Ye Wang, and Jaap M. J. den Toonder. Metachronal actuation of microscopic magnetic artificial cilia generates strong microfluidic pumping. *Lab Chip*, 20: 3569–3581, 2020.
99. Ahmet F Demirörs, Sümeyye Aykut, Sophia Ganzeboom, Yuki A Meier, Robert Hardeman, Joost de Graaf, Arnold JTM Mathijssen, Erik Poloni, Julia A Carpenter, Caner Ünlü, et al. Amphibious transport of fluids and solids by soft magnetic carpets. *Advanced Science*, 8(21): 2102510, 2021.
100. Bivas Panigrahi, Vignesh Sahadevan, and Chia-Yuan Chen. Shape-programmable artificial cilia for microfluidics. *iScience*, 24(12):103367, 2021.
101. Jiaqi Miao, Siqi Sun, Tieshan Zhang, Gen Li, Hao Ren, and Yajing Shen. Natural cilia and pine needles combinedly inspired asymmetric pillar actuators for all-space liquid transport and self-regulated robotic locomotion. *ACS Applied Materials Interfaces*, 14(44):50296–50307, 2022.
102. Rémi Dreyfus, Jean Baudry, Marcus L. Roper, Marc Fermigier, Howard A. Stone, and Jérôme Bibette. Microscopic artificial swimmers. *Nature*, 437(7060):862–865, 2005. ISSN 14764687. .
103. A Rockenbach, V Mikulich, Ch Br, U Schnakenberg, Ch Brücker, and U Schnakenberg. Fluid transport via pneumatically actuated waves on a ciliated wall. *J. Micromechanics Microengineering*, 25(12):125009, dec 2015.
104. Benjamin Gorissen, Wannes Vincentie, Farid Al-Bender, Dominiek Reynaerts, and Michaël De Volder. Modeling and bonding-free fabrication of flexible fluidic microactuators with a bending motion. *J. Micromech. Microeng*, 23:45012–10, 2013.
105. Edoardo Milana, Benjamin Gorissen, Eline De Borre, Frederik Ceyssens, Dominiek Reynaerts, and Michael De Volder. Out-of-plane soft lithography for soft pneumatic microactuator arrays. *Soft Robotics*, 0(0), 2022.
106. Edoardo Milana, Bert Van Raemdonck, Andrea Serrano Casla, Michael De Volder, Dominiek Reynaerts, and Benjamin Gorissen. Morphological control of cilia-inspired asymmetric movements using nonlinear soft inflatable actuators. *Frontiers in Robotics and AI*, 8, 2021.
107. Shigenori Nonaka, Satoko Yoshiba, Daisuke Watanabe, Shingo Ikeuchi, Tomonobu Goto, Wallace F Marshall, and Hiroshi Hamada. De novo formation of left–right asymmetry by posterior tilt of nodal cilia. *PLoS biology*, 3(8):e268, 2005.
108. CE Miller and H Goldfarb. An in vitro investigation of ciliated activity. *Transactions of the Society of Rheology*, 9(1):135–144, 1965.
109. Armin Keißner and Christoph Brücker. Directional fluid transport along artificial ciliary surfaces with base-layer actuation of counter-rotating orbital beating patterns. *Soft Matter*, 8(19):5342, 2012.
110. Tae-Rin Lee, Kieseok Oh, Jae-Hyun Chung, Yoon-Suk Chang, Jae-Boong Choi, Genki Yagawa, and Young-Jin Kim. Resonant behavior and microfluidic manipulation of silicone cilia due to an added mass effect. *Soft Matter*, 7(9):4325, 2011.
111. Christoph Brücker and Armin Keissner. Streaming and mixing induced by a bundle of ciliary vibrating micro-pillars. *Exp. Fluids*, 49(1):57–65, 2010.
112. Sinem Orbay, Adem Ozcelik, Hunter Bachman, and Tony Jun Huang. Acoustic actuation of in situ fabricated artificial cilia. *J. Micromechanics Microengineering*, 28(2):025012, 2018.
113. Cornel Dillinger, Nitesh Nama, and Daniel Ahmed. Ultrasound-activated ciliary bands for microrobotic systems inspired by starfish. *Nature communications*, 12(1):1–11, 2021.
114. Xiaoxuan Zhang, Jiahui Guo, Xiao Fu, Dagan Zhang, and Yuanjin Zhao. Tailoring flexible arrays for artificial cilia actuators. *Advanced Intelligent Systems*, 3:2000225, 10 2021. ISSN 2640-4567. .
115. Meng Li, Aniket Pal, Amirreza Aghakhani, Abdon Pena-Francesch, and Metin Sitti. Soft actuators for real-world applications. *Nature Reviews Materials*, pages 1–15, 2021.
116. Shuaizhong Zhang, Rongjing Zhang, Ye Wang, Patrick R Onck, and Jaap MJ den Toonder. Controlled multidirectional particle transportation by magnetic artificial cilia. *ACS nano*, 14

(8):10313–10323, 2020.

117. B Gorissen, R Donose, D Reynaerts, and M De Volder. Flexible pneumatic micro-actuators: Analysis and production. In *Procedia Eng.*, volume 25, pages 681–684, 2011. .
118. Guo Zhan Lum, Zhou Ye, Xiaoguang Dong, Hamid Marvi, Onder Erin, Wenqi Hu, and Metin Sitti. Shape-programmable magnetic soft matter. *Proceedings of the National Academy of Sciences*, 113(41):E6007–E6015, 2016.
119. Benjamin Gorissen, Chris Van Hoof, Dominiek Reynaerts, and Michael De Volder. SU8 etch mask for patterning PDMS and its application to flexible fluidic microactuators. *Microsystems Nanoeng.*, 2(May):16045, 2016.
120. Jaakko V. I. Timonen, Christoffer Johans, Kyösti Kontturi, Andreas Walther, Olli Ikkala, and Robin H. A. Ras. A facile template-free approach to magnetodriven, multifunctional artificial cilia. *ACS Applied Materials & Interfaces*, 2(8):2226–2230, 2010.
121. Wenjie Sun, Huiming Wang, and Jinxiong Zhou. Actuation and instability of interconnected dielectric elastomer balloons. *Appl. Phys. A Mater. Sci. Process.*, 119(2):443–449, may 2015.
122. Hayato Shinoda, Seiji Azukizawa, Kazuki Maeda, and Fujio Tsumori. Bio-mimic motion of 3d-printed gel structures dispersed with magnetic particles. *Journal of the Elechtrochemical Society*, 166(9), 2019.
123. Seiji Azukizawa, Hayato Shinoda, Kazuki Tokumaru, and Fujio Tsumori. 3d printing system of magnetic anisotropy for artificial cilia. *Journal of Photopolymer Science and Technology*, 31(1):139–144, 2018. .
124. Srinivas Hanasoge, Matthew Ballard, Peter J Hesketh, and Alexander Alexeev. Asymmetric motion of magnetically actuated artificial cilia. *Lab Chip*, 17, 2017.
125. Tanveer ul Islam, Yves Bellouard, and Jaap M. J. den Toonder. Highly motile nanoscale magnetic artificial cilia. *Proceedings of the National Academy of Sciences*, 118(35):e2104930118, 2021.
126. Srinivas Hanasoge, Peter J. Hesketh, and Alexander Alexeev. Metachronal actuation of microscale magnetic artificial cilia. *ACS Applied Materials & Interfaces*, 12(41):46963–46971, 2020.
127. John Blake. Hydrodynamic calculations on the movements of cilia and flagella. ii. opalina. *Journal of theoretical Biology*, 52:67–82, 1975.
128. J. Sanderson, M. and A. Sleigh, M. Ciliary activity of cultured rabbit tracheal epithelium: Beat pattern and metachrony. *Journal of Cell Science*, 47:331–347, 1981.
129. Asma Yaghi and B Dolovich, Myrna. Airway epithelial cell cilia and obstructive lung disease. *Cells*, 5(40), 2016.
130. R. Fulford, G. and R. Blake J. Muco-ciliary transport in the lung. *Journal of theoretical Biology*, 121:381–402.
131. Knut Norstog. Fine structure of the spermatozoid of zamia with special reference to the flagellar apparatus. *American Journal of Botany*, 54(7):831–840, 1967.
132. A. Sleigh, M. *The Biology of cilia and Flagella*. Pergamon Press, 1962.
133. Knut Drescher, E. Goldstein, Raymond, and Idan Tuval. Fidelity of adaptive phototaxis. *PNAS*, 107(25):11171–11176, 2010.
134. Charles B Lindemann. Experimental evidence for the geometric clutch hypothesis. *Current topics in developmental biology*, 95:1–31, 2011.
135. Mohamed Elshalakani and Christoph Brucker. Simulation of self-coordination in a row of beating flexible flaplets for micro-swimmer applications: Model and experiment study. *Journal of Fluids and Structures*, 94(102923), 2020.
136. Cameron A Aubin, Benjamin Gorissen, Edoardo Milana, Philip R Buskohl, Nathan Lazarus, Geoffrey A Slipher, Christoph Keplinger, Josh Bongard, Fumiya Iida, Jennifer A Lewis, et al. Towards enduring autonomous robots via embodied energy. *Nature*, 602(7897):393–402, 2022.
137. Giorgio Oliveri, Lucas C van Laake, Cesare Carissimo, Clara Miette, and Johannes TB Overvelde. Continuous learning of emergent behavior in robotic matter. *Proceedings of the National Academy of Sciences*, 118(21):e2017015118, 2021.

Supplementary Materials

Artificial cilia - bridging the gap with nature

Sam Peerlinck*,Edoardo Milana*, Elias De Smet, Michael De Volder, Dominiek Reynaerts, and Benjamin Gorissen

E-mail: benjamin.gorissen@kuleuven.be

This PDF file includes:

Figs. S1 to S6
Tables S1 to S5
References for SI reference citations

S1. Additional information

This sections details the methods used to create the figures in the main text. The raw data that has been used to populate the figures in the main text are tabulated in section S2.

A. Comparison Size versus Swept Area.

Figure S1 is a larger copy of figure 5A in the main text, displaying both cilium length and dimensionless swept area (SA), for different natural and artificial cilia. The numerical values of the data points are provided in table S3. For data points indicated with an asterisk (*) in the table, the dimensionless SA are not directly reported in the manuscripts. For these data points, we estimated the SA based on figures and diagrams in the manuscripts. Figure S2 gives an overview of the specific figures that were used for these estimations. To reduce errors in the estimation, we first tracked the trajectory formed by the cilia tips using image analysis software. This created the boundary of the SA, and the area contained within this boundary is used to calculate the SA. This image-based SA is then nondimensionalized with the cilium length, also derived from the figure, using the following equation:

$$SA_{dimensionless} = \frac{SA_{figure}}{0.5\pi L_{figure}^2}.$$

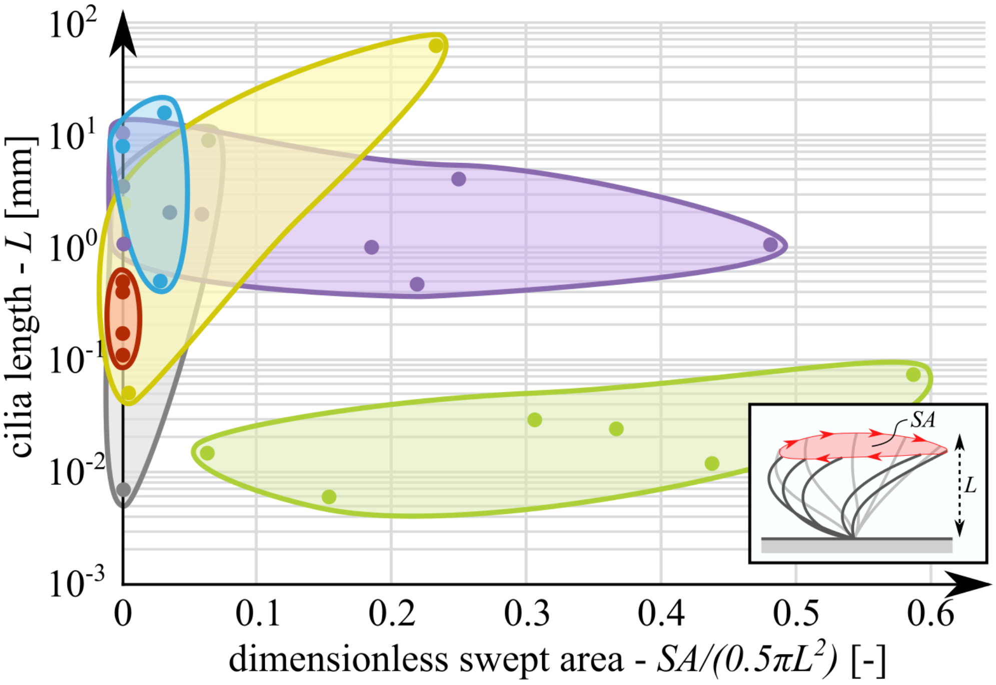

Fig. S1. A comparison between artificial and naturally occurring cilia in terms of size and beat complexity. Here only 2D planar beating motions are considered. Natural cilia beat tends to exhibit larger spatial asymmetry, at smaller size.

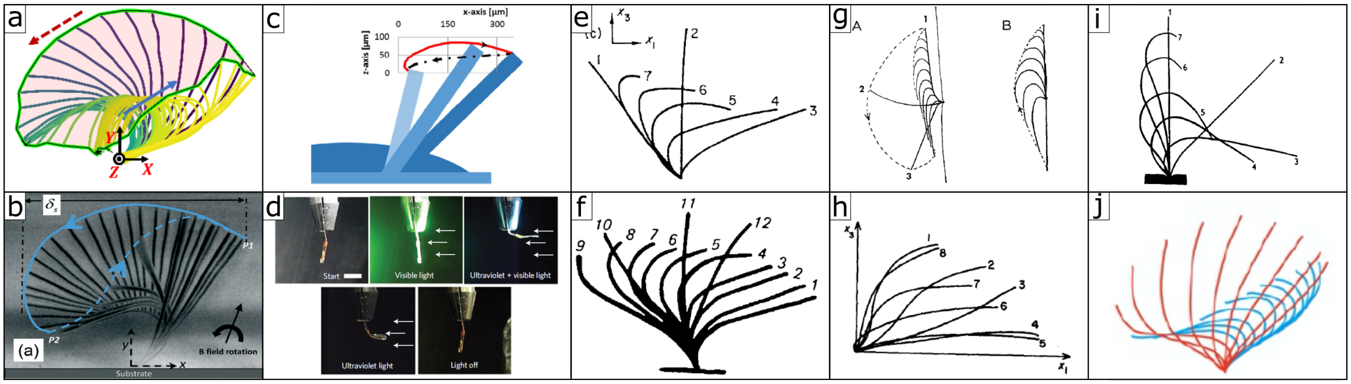

Fig. S2. Figures used for estimation of dimensionless swept area: a(1), b(2), c(3), d(4), e(5), f(6), g(7), h (8), i(9) and j(10).

B. Comparison Sperm number versus proximity.

Figure S3 is a larger copy of figure 5B in the main text displaying the cilia proximity (length divided by interciliary distance) on the logaritmic y-axis and the dimensionless Sperm number on the x-axis. The numerical values of the data points are enumerated in table S4. Although some references report a Sperm number, the same procedure for calculating the Sperm number is used for every data point to be consistent. For reference these are the reported Sperm numbers: Hanasoge (11): 3.2, Milana (12): 1.7, Orbay(13): 1.5 and Eloy(14) for Paramecium: 4.6. For the calculation of the Sperm number, the formulation according to Eloy and Lauga (14) was used:

$$Sp = L\left(\frac{\omega \xi_{\perp}}{B}\right)^{1/4} \qquad [1]$$

with: $\xi_{\perp} = \frac{4\pi\mu}{ln(L/r)}$, $B = EI$, the structure's bending resistance and $\omega = 2\pi f$ the angular frequency. This yields the following expression:

$$Sp = L\left(\frac{8\pi^2 \mu f}{ln(L/r)EI}\right)^{1/4}, \qquad [2]$$

where f is a single cilium's beating frequency, μ the dynamic viscosity of the surrounding fluid, E the Young's modulus, I the second moment of inertia, r the radius and L the length of the cilium. These variables are derived from the information in the corresponding references to the best of our ability and displayed in table S4. The bending resistance of the artificial cilia is derived from the material and geometry of the circular or rectangular cross-section of the structures. To enable a fair comparison, the Sperm number of the natural cilia data points is estimated following the same principles as the artificial cilia. The difficulty here is to estimate the passive bending resistance of natural cilia. That is done according to the following reasoning:

All the considered natural cilia are constituted of a 9 + 2 axoneme and the microtubule doublets are the most important factor in the passive bending resistance of the structure (15). By estimating a generalized elasticity modulus (E) for this axoneme microstructure, assuming this remains fairly constant over different cilia sizes and calculating the moment of inertia (I) for the respective cilia cross-sections, the bending stiffness ($B = EI$) of each natural cilium is estimated. Hines and Blum (15) analyzed the kinematics and structure of the sliding filaments inside *Paramecium* cilia, and thus calculated the bending resistance of around 25 $pN\mu m^2$. Using this, we derived the generalized elasticity modulus to be $E = 153500 pN/\mu m^2$, using the reported radius of the *Paramecium* cilium (r = 0.12 µm) to divide the bending resistance by the second moment of inertia (I $= \pi r^4/4$). This generalized elasticity modulus is then used for all the data points representing natural cilia.

Finally, the inter-ciliary distance, or spacing between cilia a is either directly used from the references, or estimated based on images and/or mentioned carpet density. This yields the cilia proximity, a dimensionless metric based on the ratio of the cilium length and this inter-ciliary distance. The higher this ratio, the closer neighbouring cilia are packed together.

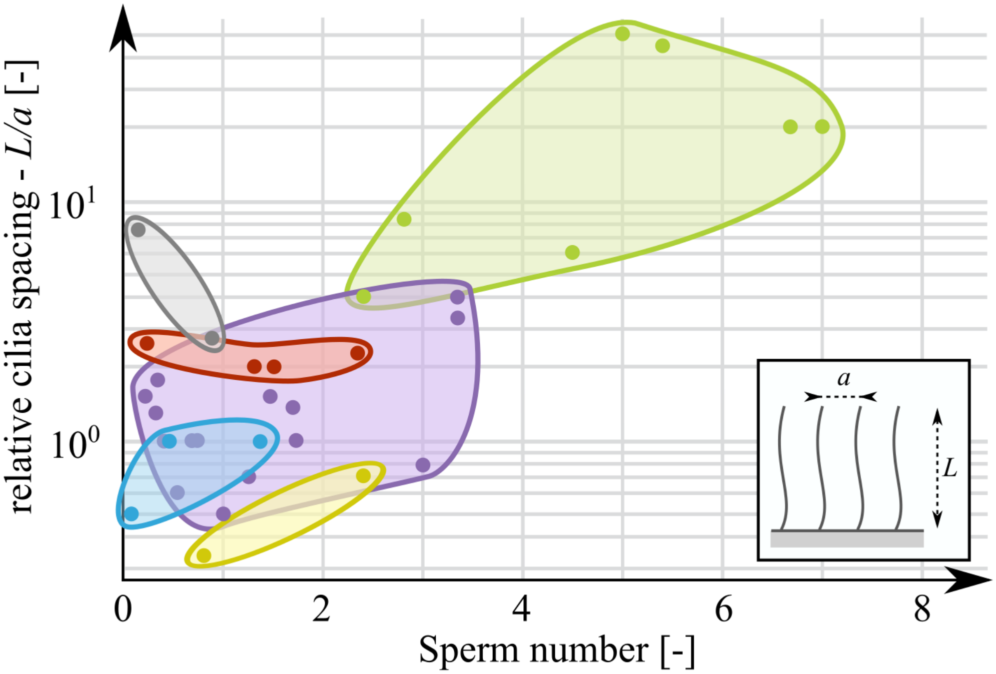

Fig. S3. A comparison between artificial and naturally occurring cilia in terms of Sperm number and cilia proximity. Natural cilia tend to show a higher Sperm number, meaning that the effects of viscous forces are more easily transferred from the fluid onto the cilia structure, and are packed more closely. This indicates that a higher mutual influence through the fluid is to be expected and self-coordinated metachronal asymmetry can emerge.

C. Determination of production technique metrics.

Figures S4, S5 and S6 show the same data as figure 4B in the main text, but are made more legible to facilitate extracting data on specific references. Furthermore, table S5 shows the data points of artificial and natural cilia which were compared in terms of aspect ratio, number of cilia on a carpet and cross sectional area on the aforementioned figures. To determine these three metrics, a distinction was made first between cilia with a rectangular or a circular cross section. For the former a width and thickness has been defined, whereas a diameter has been identified for the latter. The table below gives a summary of the formulas used to determine the aspect ratio and cross sectional area, where L, W, T and D are the length, width, thickness and diameter of cilia, respectively.

	Aspect Ratio	Cross Section
Rectangular	L/W	$W.T$
Circular	L/D	$\pi D^2/4$

Data concerning the number of cilia on the carpets was obtained directly from the text and figures presented in all but five literature resources. It was necessary to estimate the number of cilia produced in these references in order to complete the data. This was done in the following ways:

1. Islam *et al.* (16) present densities of the cilia carpets they produced, but not the total amount of cilia on the carpet. The cilia densities of the carpets that were investigated the most are 10^4 and 10^5 cilia per square centimeter. The publications SI reports a piece of cilia carpet being submerged vertically in an ethanol container with a depth of 500 µm. Based on this, the size of the cilia carpet is assumed here to be at least 500x500 µm or 2.510^7 m^2, which was multiplied by the aforementioned cilia densities to obtain the estimated number of cilia.

2. The amount of cilia on carpets produced by Liu *et al.* (17) was approximated using figure 1(a) and 1(e) of the publication. These figures show close-up side views of the cilia carpets and include a scale bar of 500µm as a reference. The spacing between cilia positioned roughly in line with each other can be observed from these figures. On average, cilia are deemed to be 200µm apart from each other in figure 1(a) and 375 µm in figure 1(e). Assuming the same spacing between cilia occurs in the horizontal direction perpendicular to the observed one, the densities of cilia on the carpet are estimated to be $(1/200)^2$ µm^2 and $(1/375)^2$ µm^2. Additionally, the overall size of the carpet is believed to be 7x2 cm^2, as this value is the size of a PTFE mold, reported in section 4: 'Experimental Section', subsection: 'Characterization'. The total number of cilia on the carpet was again calculated as the product of the carpet size and the cilia density.

3. Sun *et al.* (18) report cilia densities of 660 and 730 cilia per square centimeter and mention using a 35mm wide paper beaker during production of the cilia carpet. The carpet size was calculated as the surface of circle with a diameter of 35mm and the total number of cilia on the carpet was obtained by multiplying this value by the reported cilia densities.

4. Jaakko *et al.* (19) construct their cilia carpet on a 35 mm wide substrate plate, which was assumed to be circular for deriving its surface. Figure 5 of the publication shows a close-up of a small patch of cilia with a density estimated here to be nine per square millimeter. The total number of cilia was obtained analogous to the previous cases.

5. Wang *et al.* (20) fabricated their cilia on 10mm wide circular cover slips and observed a surface coverage of 1.5% (up to 2.9%), counting the area covered by a single bead each time. Therefore, the total area covered by the beads is taken here to be 1.5% of the surface of the cover slips. Dividing this area by the area a single bead takes up results in the total number of cilia on the carpet, since the cilia in this publication are pillars of single beads stacked on top of each other. Wang *et al.* reported the beads to be spherical with a diameter of 2.7µm, which was used as an input to calculate the circular surface they take up on the cover slips.

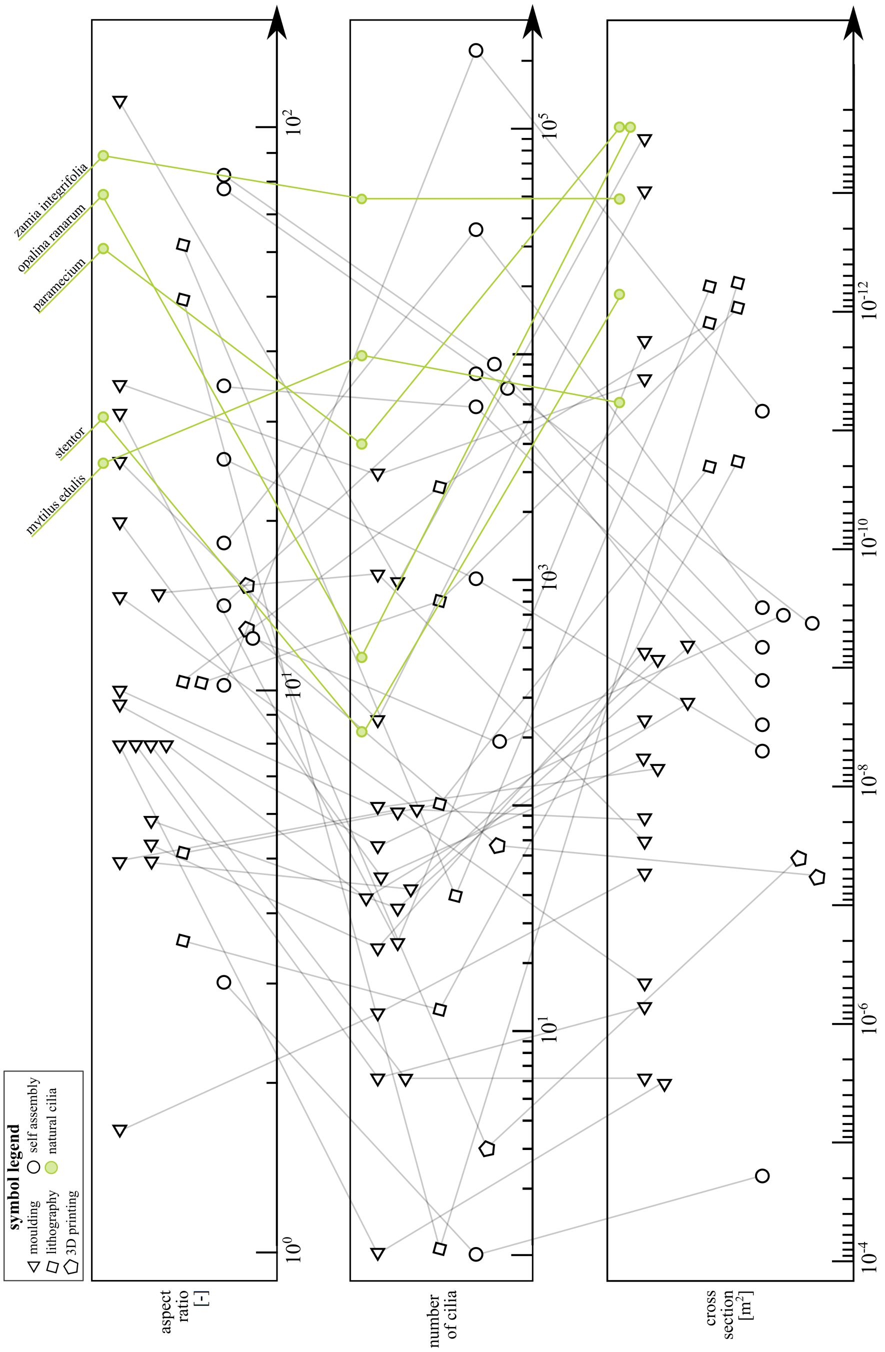

Fig. S4. Production techniques comparison, all data points

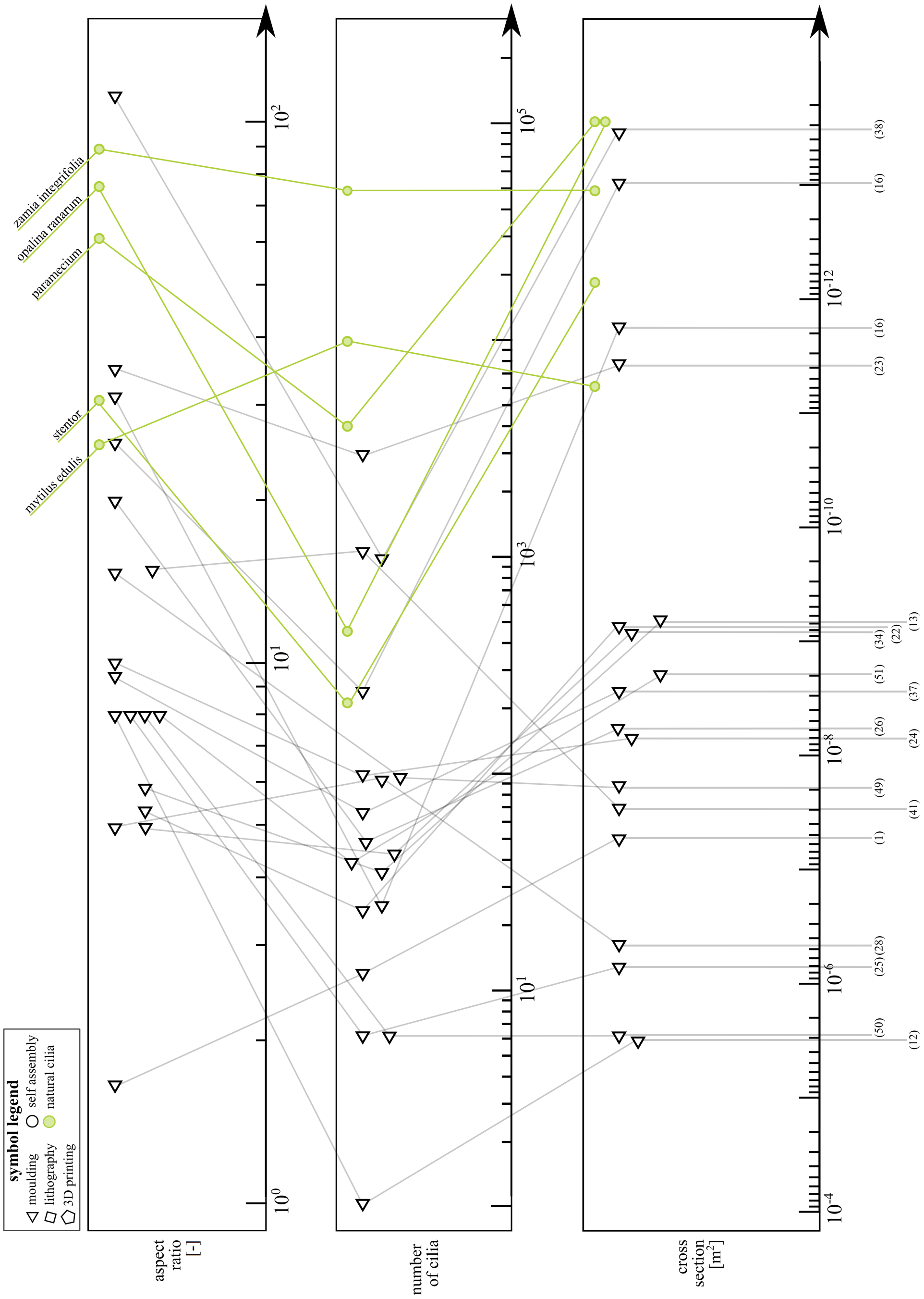

Fig. S5. Production techniques comparison, all data points

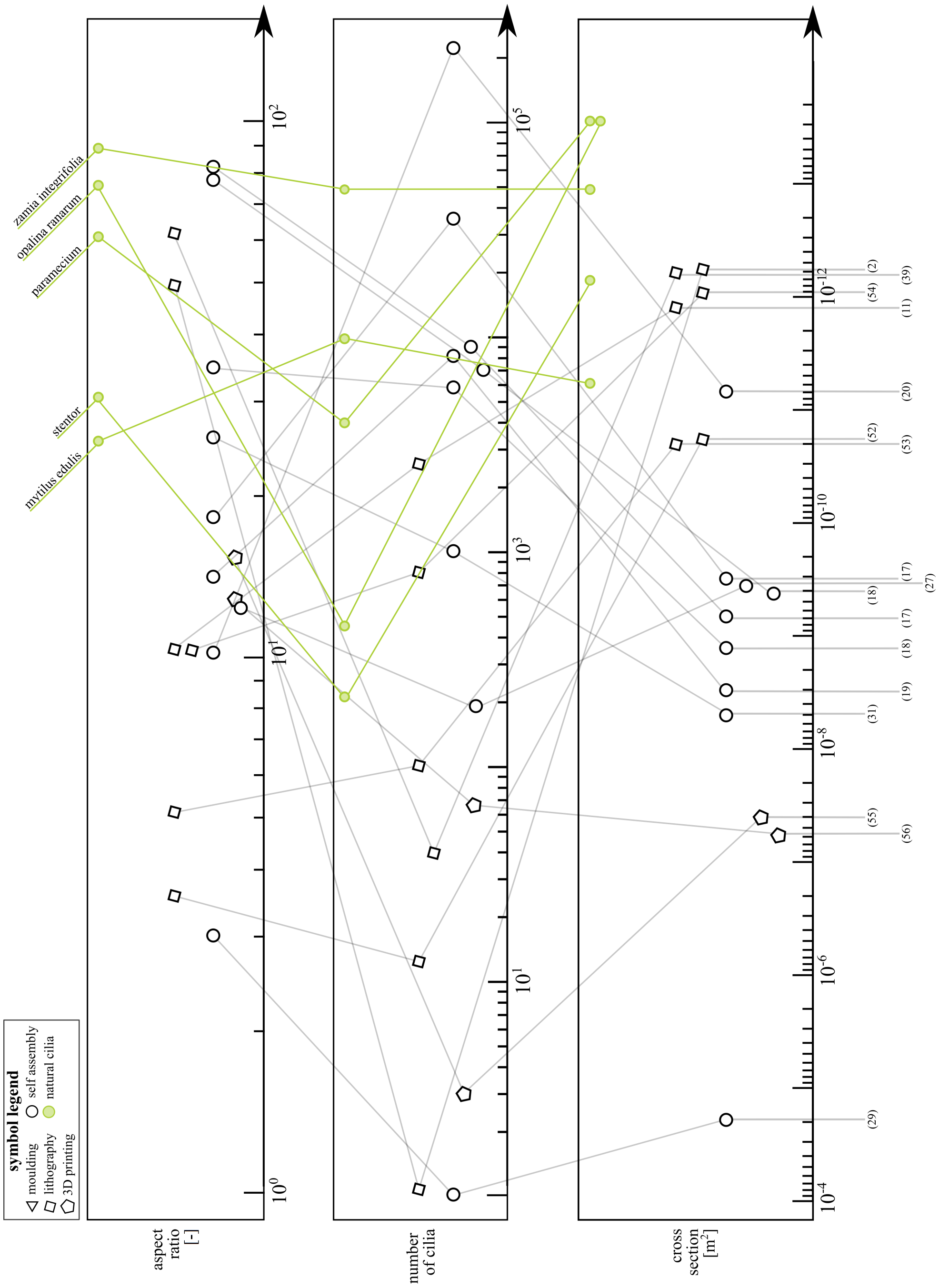

Fig. S6. Production techniques comparison, all data points

S2. Data used for analysis

This section tabulates the data points used to compose the figures in the main text and in SI.

Table S1. Datapoints of the plot displayed in Fig. 3 of the main text. Artificial cilia are classified according to the publication year, cilia length (mm) and Reynolds number. For publication where no fluid propulsion experiments are reported the Reynolds number is not available (n/a).

Author	Year of Publication	Cilia Length (mm)	Reynolds Number
den Toonder (21)	2008	0.1	1
Oh (22)	2009	0.4	68
van Oosten (4)	2009	10	n/a
Shields (23)	2010	0.025	0.025
Hussong (24)	2011	0.070	0.14
Keissner (25)	2012	1	0.040
Sareh (10)	2013	64	410
Gorissen (26)	2015	10	3480
Tsumori (27)	2016	2	n/a
Wang (28)	2016	0.3	6
Hanasoge (2)	2016	0.2	0.12
Rockenbach (3)	2017	0.5	5
Gu (29)	2020	4	0.002
Milana (12)	2020	14	0.04
Dong (1)	2020	1	0.03
Sugioka (30)	2021	16-30	n/a
Panigrahi (31)	2021	10	∼560
Demiroers (32)	2021	0.6-2	∼0.003
Dillinger (33)	2021	0.1	31
van Raak (34)	2021	0.01	n/a
Li (35)	2022	0.15	n/a
Wang (36)	2022	0.05	0.002
Milana (37)	2022	0.45	n/a
Deng (38)	2022	9	60

Table S2. Overview of actuation technologies per reference, indicating presence and type of spatial and metachronal asymmetry, and type of coordination and tethering.

Actuation	Author	Year	Spatial	Metachronal	Coordination	Tethering
Electrical	Den Toonder (39)	2008	-	variable	local	flexible
Electrical	Sareh (10)	2012	yes	-	local	flexible
Electrical	Sugioka (30)	2021	-	fixed	local	flexible
Electrical	Wang (36)	2022	yes	variable	local	flexible
Electrical	Ren (40)	2022	-	variable	local	flexible
Optical	Van Oosten (4)	2009	yes	-	global	contactless
Optical	van Raak (34)	2022	-	-	global	contactless
Optical	Li (35)	2022	planar	emerging	self	contactless
Optical	Deng (38)	2022	planar	emerging	self	contactless
Optical	Gelebart (41)	2016	conical	-	global	contactless
Optical	Liu (17)	2020	conical	-	global	contactless
Magnetic	Evans (42)	2007	conical	-	global	contactless
Magnetic	Shields (23)	2010	conical	-	global	contactless
Magnetic	Vilfan (43)	2010	conical	-	global	contactless
Magnetic	Wang (20)	2013	conical	-	global	contactless
Magnetic	Wang (44)	2014	conical	-	global	contactless
Magnetic	Wang (28)	2016	conical	-	global	contactless
Magnetic	Zhang (45)	2018	conical	-	global	contactless
Magnetic	Hussong (24)	2011	planar	-	global	contactless
Magnetic	Hanasoge (46)	2018	planar	-	global	contactless
Magnetic	Hanasoge (11)	2018	planar	fixed	global	contactless
Magnetic	Tsumori (27)	2016	planar	-	global	contactless
Magnetic	Shinoda (47)	2020	planar	fixed	global	contactless
Magnetic	Gu (29)	2020	planar	fixed	global	contactless
Magnetic	Dong (1)	2020	planar	fixed	global	contactless
Magnetic	Zhang (48)	2020	conical	fixed	global	contactless
Magnetic	Demirors (49)	2020	-	fixed	global	contactless
Magnetic	Panigrahi (31)	2021	planar	fixed	global	contactless
Magnetic	Miao (50)	2022	planar	-	global	contactless
Pressure	Rockenbach (3)	2015	planar	variable	local	elastic
Pressure	Gorissen (51)	2013	-	-	local	elastic
Pressure	Gorissen (26)	2015	-	variable	local	elastic
Pressure	Milana (37)	2022	-	-	local	elastic
Pressure	Milana (12)	2019	planar	-	local	elastic
Pressure	Milana (52)	2020	planar	variable	local	elastic
Pressure	Milana (53)	2021	planar	fixed	global	elastic
Pressure	Becker (54)	2020	-	fixed	local	elastic
Mechanical	Nonaka (55)	2005	conical	variable	local	rigid
Mechanical	Miller (56)	1965	planar	-	local	rigid
Mechanical	Keissner (25)	2012	conical	variable	local	rigid
Inertial	Oh (22)	2009	-	-	global	rigid
Inertial	Lee (57)	2011	-	-	global	rigid
Inertial	Brucker (58)	2010	-	-	global	rigid
Inertial	Orbay (13)	2018	-	-	global	rigid
Inertial	Dillinger (33)	2021	-	-	global	contactless

Table S3. Datapoints for comparison cilium length and nondimensional planar swept area, used to populate figure 5A in the main text.

Actuation	Author	Length (µm)	Swept area absolute (µm²)	Swept area nondimensional
Electric field	Den Toonder (21)	100	0	0%
Electric field	Sareh (10)	64,000	1.5 10^9	23%
Electric field	Wang (36)	50	39	1%
Electric field	Ren (40)	1500	0	0%
Magnetic field	Dong (1)	1,000	7.5 10^5	47%*
Magnetic field	Hanasoge (2)	480	7.9 10^4	22%*
Magnetic field	Tsumori (27)	2,000	3.7 10^5	6%
Magnetic field	Panigrahi (31)	10,000	0	0%
Magnetic field	Miao (50)	3000	3.6 10^6	25%
Pressure	Gorissen (26)	8,000	0	0%
Pressure	Milana (12)	16,000	1.2 10^7	3%
Pressure	Rockenbach (3)	500	1.05 10^4	3%*
Inertial	Brucker (58)	500	0	0%
Inertial	Oh (22)	400	0	0%
Inertial	Orbay (13)	170	0	0%
Inertial	Dillinger (33)	100	0	0%
Light	Van Oosten (4)	10,000	6.3 10^6	4%*
Light	Van Raak (34)	50	0	0%
Light	Deng (38)	9000	8.6 10^6	7%
Natural	Paramecium (5)	12	99	44%*
Natural	Rabbit trachea (6)	6	8.6	15%*
Natural	Mytilus Edulis (7)	75	5.2 10^3	59%*
Natural	Opalina Ranarum (8)	15	22	6%*
Natural	Stentor (9)	30	4.3 10^2	31%*
Natural	Volvox (10)	25	3.6 10^2	37%*

*Swept area not clearly reported in reference but calculated from figures as explained in text.

Table S4. Data points for comparison cilia proximity and Sperm number, used to populate figure 5B in the main text.

Actuation	Author	Length (L) (µm)	Radius (r) (µm)	Frequency (Hz)	Viscosity (mPa.s)	Youngs Modulus	Moment of Inertia (m^4)	Bending stiffness (Nm^2)	Spacing (a) (µm)	Proximity (L/a)	Sperm Number
Electric field	Den Toonder (21)	100	0.5	200	9.3	4 GPa	1.67 10^{-24}	6.67 10^{-15}	300	0.3	0.8
Electric field	Sareh (10)	64000	250	0.5	0.89	180 MPa	5.21 10^{-14}	9.38 10^{-6}	single	single	0.3
Electric field	Wang (36)	50	0.005	40	1	150 GPa	4.17 10^{-31}	6.25 10^{-20}	0	0.7	2.4
Magnetic field	Dong (1)	1000	50	2.5	876	0,144 MPa	4.58 10^{-17}	6.6E 10^{-12}	1000	1.0	137
Magnetic field	Evans (42)	22.5	0.125	15	1	2.6 MPa	1.92 10^{-28}	4.99 10^{-22}	7	3.2	3.3
Magnetic field	Gu (29)	4000	400	0.083	1150	0.185 MPa	2.01 10^{-14}	3.72 10^{-9}	4000	1.0	0.7
Magnetic field	Hanasoge (2)	480	0.03	24	4	200 GPa	1.8 10^{-28}	3.6 10^{-17}	single	single	5.8
Magnetic field	Hanasoge (11)	200	0.03	24	1	200 GPa	3.6 10^{-28}	7.2 10^{-17}	single	single	1.5
Magnetic field	Hanasoge (46)	600	0.03	4	1	200 GPa	1.8 10^{-28}	3.6 10^{-17}	150	4.0	3.3
Magnetic field	Hussong (24)	70	0.45	20	1	2.5 MPa	1.22 10^{-24}	3.0 10^{-18}	100	0.7	1.3
Magnetic field	Shields (23)	25	0.35	34	1	2.5 MPa	1.18 10^{-26}	2.9 10^{-20}	18	1.4	1.7
Magnetic field	Shinoda (47)	3000	100	0.5	970	0.144 MPa	1.33 10^{-15}	1,9 10^{-10}	2113	1,4	1,5
Magnetic field	Tsumori (27)	2000	150	20	1	2.5 MPa	3.98 10^{-16}	9.9 10^{-10}	1100	1.8	0.3
Magnetic field	Vilfan (43)	45	2.2	1	1	2.5 MPa	1.84 10^{-23}	4.6 10^{-17}	30	1.5	0.2
Magnetic field	Wang (20)	30	1.5	10	1	10 MPa	3.98 10^{-24}	4.0 10^{-17}	23	1.3	0.3
Magnetic field	Wang (44)	300	15	15	2.5	2.5 MPa	3.98 10^{-20}	9.9 10^{-14}	500	0.6	0.5
Magnetic field	Wang (28)	250	10	20	10	2.5 MPa	7.85 10^{-21}	2.0 10^{-14}	550	0.5	1.0
Magnetic field	Zhang (45)	350	25	40	0.89	2.5 MPa	3.07 10^{-19}	7.67 10^{-13}	350	1.0	0.4
Magnetic field	Zhang (59)	350	25	100	1400	2.5 MPa	3.07 10^{-19}	7.67 10^{-13}	450	0.8	3.0
Magnetic field	Panigrahi (31)	10000	130	1	1	2.5 MPa	3.26 10^{-16}	8.1 10^{-10}	10000	1.0	0.7
Contact	Keissner (25)	1000	50	3	11.1	2.5 MPa	4.91 10^{-18}	1.2 10^{-7}	500	2.0	0.5
Pressure	Gorissen (26)	8000	500	35	1	2.5 MPa	4.91 10^{-14}	1.2 10^{-7}	8000	1.0	0.4
Pressure	Milana (12)	16000	1000	0.5	1000	2.5 MPa	1.1 10^{-13}	2.75 10^{-7}	single	single	1.4
Pressure	Milana (52)	16000	1000	0.5	1000	2.5 MPa	1.1 10^{-13}	2.75 10^{-7}	16000	1.0	1.4
Pressure	Rockenbach (3)	500	50	9.8	1	2.5 MPa	2.08 10^{-16}	5.2 10^{-10}	1000	0.5	0.1
Inertial	Brucker (58)	500	25	50	10	1.6 MPa	3.07 10^{-19}	4.9 10^{-13}	250	2.0	1.1
Inertial	Oh (22)	400	5	65	1	1 MPa	6.25 10^{-21}	6.25 10^{-15}	200	2.0	1.5
Inertial	Orbay (13)	170	15	4600	1	0.1 MPa	3.98 10^{-20}	4.0 10^{-15}	75	2.3	2.4
Inertial	Dillinger (33)	100	20	100	1	1 MPa	1.13 10^{-19}	1.13 10^{-13}	40	2.5	0.3
Light	Van Oosten (4)	2000	100	1	1	1 GPa	1.33 10^{-18}	1.33 10^{-9}	300	6.7	0.1
Light	Deng (38)	9000	50	2.7	1	4.9 MPa	8.33 10^{-17}	4.08 10^{-10}	5000	1.8	0.9
Natural	Paramecium (5)	12	0.12	31.8	0.89			2.5 10^{-23}	2	6.0	4.5
Natural	Rabbit Trachea (6)	6	0.2	16	1000	0.15 MPa	1.26 10^{-27}	1.9 10^{-22}	0.3	20.0	7.1
Natural	Opalina Ranarum (8)	15	0.1	10	1	0.15 MPa	7.85 10^{-29}	1.2 10^{-23}	0.3	50.0	5.1
Natural	Stentor (9)	30	0.5	33	1	0.15 MPa	4.91 10^{-26}	7.54 10^{-21}	3.5	8.6	2.9
Natural	Mytilu Edulis (7)	80	1.5	25	1	0.15 MPa	3.98 10^{-24}	6.1 10^{-19}	20	4.0	2.4
Natural	Zamia Integrifolia (60, 61)	35	0.1	30	0.0181	0.15 MPa	7.85 10^{-29}	1.2 10^{-23}	0.8	43.8	5.5
Natural	Volvox (10)	25	0.15	25	0.89	0.15 MPa	3.98 10^{-28}	6.1 10^{-23}	1.3	20.0	6.8

Table S5. Data points for comparing aspect ratio, number of cilia, and cross section; used to populated figure 4B in the main text.

Author	Length (m)	Width (m)	Thickness (m)	Diameter (m)	Aspect Ratio	Number of Cilia	Cross Section (m²)
Artificial cilia							
Molding							
Brücker (58)	5.70 10^{-4}			6.0 10^{-5}	9.500 10^{0}	6.7 10^{1}	2.827 10^{-9}
Dai 2018 (62)	2.35 10^{-3}			1.6 10^{-4}	1.469 10^{1}	1.0 10^{2}	2.011 10^{-8}
Dong (1)	1.00 10^{-3}	6.0 10^{-4}	1.0 10^{-4}		1.667 10^{0}	1.2 10^{1}	6.000 10^{-8}
Evans (42)	2.25 10^{-5}			2.0 10^{-7}	1.125 10^{2}	1.0 10^{3}	3.142 10^{-14}
Gorissen (26)	8.00 10^{-3}			1.0 10^{-3}	8.000 10^{0}	6.0 10^{0}	7.854 10^{-7}
Gu (29)	4.00 10^{-3}			8.0 10^{-4}	5.000 10^{0}	1.0 10^{2}	5.026 10^{-7}
Islam (16)	4.70 10^{-5}			1.5 10^{-6}	3.133 10^{1}	2.5 10^{1}	1.767 10^{-12}
Islam (16)	9.00 10^{-6}			3.5 10^{-7}	2.571 10^{1}	2.5 10^{2}	9.621 10^{-14}
Keissner (25)	1.00 10^{-3}			1.0 10^{-4}	1.000 10^{1}	1.0 10^{2}	7.854 10^{-9}
Li (35)	1.50 10^{-4}	3.0 10^{-5}	3.0 10^{-5}		5.000 10^{0}	4.4 10^{1}	9.000 10^{-10}
Milana (12)	1.60 10^{-2}			2.0 10^{-3}	8.000 10^{0}	1.0 10^{0}	3.142 10^{-6}
Milana (63)	1.60 10^{-2}			2.0 10^{-3}	8.000 10^{0}	6.0 10^{0}	3.142 10^{-6}
Oh (22)	4.00 10^{-4}	7.5 10^{-5}	1.0 10^{-5}		5.333 10^{0}	2.4 10^{1}	7.500 10^{-10}
Orbay (13)	1.70 10^{-4}			3.0 10^{-5}	5.667 10^{0}	3.2 10^{1}	7.068 10^{-10}
Shields (23)	2.50 10^{-5}			7.0 10^{-7}	3.571 10^{1}	3.0 10^{3}	3.848 10^{-13}
Shinoda (47)	3.00 10^{-3}			2.0 10^{-4}	1.500 10^{1}	1.2 10^{3}	3.142 10^{-8}
Tsumori (27)	2.00 10^{-3}			1.0 10^{-4}	2.000 10^{1}	4.8 10^{1}	7.854 10^{-9}
Wu (64)	4.00 10^{-4}			5.0 10^{-5}	8.000 10^{0}	4.0 10^{1}	1.963 10^{-9}
Lithography							
Belardi (65)	7.00 10^{-5}	2.0 10^{-5}	9.0 10^{-7}		3.500 10^{0}	1.2 10^{1}	1.800 10^{-11}
Den Toonder (39)	1.00 10^{-4}	2.0 10^{-5}	1.0 10^{-6}		5.000 10^{0}	1.0 10^{2}	2.040 10^{-11}
Hanasoge (2)	4.80 10^{-4}	1.0 10^{-5}	5.6 10^{-8}		4.800 10^{1}	1.0 10^{0}	5.600 10^{-13}
Hanasoge (11)	2.00 10^{-4}	2.0 10^{-5}	6.0 10^{-8}		1.000 10^{1}	2.6 10^{3}	1.200 10^{-12}
Hanasoge (46)	6.00 10^{-4}	1.0 10^{-5}	6.0 10^{-8}		6.000 10^{1}	3.8 10^{1}	6.000 10^{-13}
Hanasoge (66)	1.50 10^{-4}	1.5 10^{-5}	6.0 10^{-8}		1.000 10^{1}	8.0 10^{2}	9.000 10^{-13}
Self assembly							
Demirörs (32)	2.00 10^{-3}			8.0 10^{-5}	2.500 10^{1}	1.0 10^{3}	5.026 10^{-9}
Jaakko (19)	7.81 10^{-4}			5.5 10^{-5}	1.420 10^{1}	8.7 10^{3}	2.376 10^{-9}
Liu (17)	3.75 10^{-4}			2.0 10^{-5}	1.875 10^{1}	3.5 10^{4}	3.142 10^{-10}
Liu (17)	2.50 10^{-3}			3.0 10^{-5}	8.333 10^{1}	1.0 10^{4}	7.068 10^{-10}
Sugioka (30)	1.50 10^{-2}			5.0 10^{-3}	3.000 10^{0}	1.0 10^{0}	1.963 10^{-5}
Sun (18)	1.73 10^{-3}			2.2 10^{-5}	7.864 10^{1}	7.0 10^{3}	3.801 10^{-10}
Sun (18)	1.34 10^{-3}			3.9 10^{-5}	3.436 10^{1}	5.8 10^{3}	1.195 10^{-9}
Wang (20)	3.27 10^{-5}			3.0 10^{-6}	1.090 10^{1}	2.1 10^{5}	7.068 10^{-12}
Wang (28)	2.50 10^{-4}			2.0 10^{-5}	1.250 10^{1}	1.9 10^{2}	3.142 10^{-10}
3D printing							
Azukizawa (67)	3.00 10^{-3}	2.0 10^{-4}	2.0 10^{-4}		1.500 10^{1}	3.0 10^{0}	4.000 10^{-8}
Shinoda (68)	3.00 10^{-3}	2.4 10^{-4}	2.4 10^{-4}		1.250 10^{1}	6.4 10^{1}	5.760 10^{-8}
Natural cilia							
Mytilus Edulis (7)	7.50 10^{-5}			3.0 10^{-6}	2.500 10^{1}	1.0 10^{4}	7.068 10^{-12}
Opalina Ranarum (8)	1.50 10^{-5}			2.0 10^{-7}	7.500 10^{1}	4.5 10^{2}	3.142 10^{-14}
Paramecium (5)	1.20 10^{-5}			2.0 10^{-7}	6.000 10^{1}	4.0 10^{3}	3.142 10^{-14}
Stentor (9)	3.00 10^{-5}			1.0 10^{-6}	3.000 10^{1}	2.1 10^{2}	7.854 10^{-13}
Zamia Integrifolia (60)	3.50 10^{-5}			4.0 10^{-7}	8.750 10^{1}	5.0 10^{4}	1.257 10^{-13}

References

1. Xiaoguang Dong, Guo Zhan Lum, Wenqi Hu, Rongjing Zhang, Ziyu Ren, Patrick R Onck, and Metin Sitti. Bioinspired cilia arrays with programmable nonreciprocal motion and metachronal coordination. *Science advances*, 6(45):eabc9323, 2020.
2. Srinivas Hanasoge, Matthew Ballard, Peter J Hesketh, and Alexander Alexeev. Asymmetric motion of magnetically actuated artificial cilia. *Lab Chip*, 17, 2017. .
3. A Rockenbach, V Mikulich, Ch Br, U Schnakenberg, Ch Brücker, and U Schnakenberg. Fluid transport via pneumatically actuated waves on a ciliated wall. *J. Micromechanics Microengineering*, 25(12):125009, dec 2015.
4. Casper L van Oosten, Cees W M Bastiaansen, and Dirk J Broer. Printed artificial cilia from liquid-crystal network actuators modularly driven by light. *Nat. Mater.*, 8(8):677–682, 2009. .
5. John Blake. Hydrodynamic calculations on the movements of cilia and flagella. i. paramecium. *Journal of theoretical Biology*, 45:183–203, 1974.
6. J. Sanderson, M. and A. Sleigh, M. Ciliary activity of cultured rabbit tracheal epithelium: Beat pattern and metachrony. *Journal of Cell Science*, 47:331–347, 1981.
7. Edward Aiello and MichaelA. Sleigh. The metachronal wave of lateral cilia of mytilu edulis. *The Journal of Cell Biology*.
8. John Blake. Hydrodynamic calculations on the movements of cilia and flagella. ii. opalina. *Journal of theoretical Biology*, 52:67–82, 1975.
9. M. A. Sleigh. The form of beat in cilia of stentor and opalina. *Experimental Biology*, 37(1), 1960.
10. Sina Sareh, Jonathan Rossiter, Andrew Conn, Knut Drescher, and Raymond E Goldstein. Swimming like algae: biomimetic soft artificial cilia. *J. R. Soc. Interface*, 10(78):20120666–, 2012. .
11. Srinivas Hanasoge, Peter J. Hesketh, and Alexander Alexeev. Metachronal motion of artificial magnetic cilia. *Soft Matter*, 14(19):3689–3693, may 2018. .
12. Edoardo Milana, Benjamin Gorissen, Sam Peerlinck, Michael De Volder, and Dominiek Reynaerts. Artificial Soft Cilia with Asymmetric Beating Patterns for Biomimetic Low-Reynolds-Number Fluid Propulsion. *Adv. Funct. Mater.*, 1900462: 1–8, 2019.
13. Sinem Orbay, Adem Ozcelik, Hunter Bachman, and Tony Jun Huang. Acoustic actuation of in situ fabricated artificial cilia. *J. Micromechanics Microengineering*, 28(2):025012, 2018. .
14. Christophe Eloy and Eric Lauga. Kinematics of the most efficient cilium. *Phys. Rev. Lett.*, 109(3), 2012. .
15. M. Hines and J. Blum, J. Thee-dimensional mechanics of eukaryotic flagella. *Biophysical Journal*, 41:67–79, 1983.
16. Tanveer ul Islam, Yves Bellouard, and Jaap M. J. den Toonder. Highly motile nanoscale magnetic artificial cilia. *Proceedings of the National Academy of Sciences*, 118(35), 2021. .
17. Li Liu, Marc del Pozo, Fateme Mohseninejad, Michael G. Debije, Dirk J. Broer, and Albert P.H.J. Schenning. Light tracking and light buiding fiber arrays by adjusting the location of photoresponsive azobenzene in liquid crystal networks. *Advanced Optical Materials*, 8(18), 2020.
18. Wenjie Sun, Huiming Wang, and Jinxiong Zhou. Actuation and instability of interconnected dielectric elastomer balloons. *Appl. Phys. A Mater. Sci. Process.*, 119(2):443–449, may 2015. .
19. Jaakko V. I. Timonen, Christoffer Johans, Kyösti Kontturi, Andreas Walther, Olli Ikkala, and Robin H. A. Ras. A facile template-free approach to magnetodriven, multifunctional artificial cilia. *ACS Applied Materials & Interfaces*, 2(8): 2226–2230, 2010.
20. Ye Wang, Yang Gao, Hans Wyss, Patrick Anderson, and Jaap den Toonder. Out of the cleanroom, self-assembled magnetic artificial cilia. *Lab Chip*, 13(17):3360–6, 2013. .
21. Jaap den Toonder, Femke Bos, Dick Broer, Laura Filippini, Murray Gillies, Judith de Goede, Titie Mol, Mireille Reijme, Wim Talen, Hans Wilderbeek, Vinayak Khatavkar, and Patrick Anderson. Artificial cilia for active micro-fluidic mixing. *Lab Chip*, 8(4):533–41, 2008. .
22. Kieseok Oh, Jae-Hyun Chung, Santosh Devasia, and James J. Riley. Bio-mimetic silicone cilia for microfluidic manipulation. *Lab Chip*, 9(11):1561, 2009. .
23. a R Shields, B L Fiser, B a Evans, M R Falvo, S Washburn, and R Superfine. Biomimetic cilia arrays generate simultaneous pumping and mixing regimes. *Proc. Natl. Acad. Sci. U. S. A.*, 107(36):15670–15675, 2010. .
24. J. Hussong, N. Schorr, J. Belardi, O. Prucker, J. Rühe, and J. Westerweel. Experimental investigation of the flow induced by artificial cilia. *Lab Chip*, 11(12):2017–2022, 2011. .
25. Armin Keißner and Christoph Brücker. Directional fluid transport along artificial ciliary surfaces with base-layer actuation of counter-rotating orbital beating patterns. *Soft Matter*, 8(19):5342, 2012. .
26. Benjamin Gorissen, Michaël de Volder, and Dominiek Reynaerts. Pneumatically-actuated artificial cilia array for biomimetic fluid propulsion. *Lab Chip*, 15(22):4348–4355, 2015.
27. Fujio Tsumori, Ryuma Marume, Akinori Saijou, Kentaro Kudo, Toshiko Osada, and Hideshi Miura. Metachronal wave of artificial cilia array actuated by applied magnetic field. In *Jpn. J. Appl. Phys.*, volume 55, 2016. .
28. Ye Wang, Jaap den Toonder, Ruth Cardinaels, and Patrick Anderson. A continuous roll-pulling approach for the fabrication of magnetic artificial cilia with microfluidic pumping capability. *Lab Chip*, 16(12):2277–2286, 2016. .
29. Hongri Gu, Quentin Boehler, Haoyang Cui, Eleonora Secchi, Giovanni Savorana, Carmela De Marco, Simone Gervasoni, Quentin Peyron, Tian Yun Huang, Salvador Pane, Ann M. Hirt, Daniel Ahmed, and Bradley J. Nelson. Magnetic cilia carpets with programmable metachronal waves. *Nat. Commun.*, 11(1):1–10, 2020. .

30. Hideyuki Sugioka and Hiroki Yoshijima. Metachronal motion of artificial cilia using induced charge electro-osmosis. *Colloids and Surfaces A: Physicochemical and Engineering Aspects*, 626:127023, 2021.
31. Bivas Panigrahi, Vignesh Sahadevan, and Chia-Yuan Chen. Shape-programmable artificial cilia for microfluidics. *iScience*, 24(12):103367, 2021.
32. Ahmet F Demirörs, Sümeyye Aykut, Sophia Ganzeboom, Yuki A Meier, Robert Hardeman, Joost de Graaf, Arnold JTM Mathijssen, Erik Poloni, Julia A Carpenter, Caner Ünlü, et al. Amphibious transport of fluids and solids by soft magnetic carpets. *Advanced Science*, 8(21):2102510, 2021.
33. Cornel Dillinger, Nitesh Nama, and Daniel Ahmed. Ultrasound-activated ciliary bands for microrobotic systems inspired by starfish. *Nature communications*, 12(1):1–11, 2021.
34. Roel J. H. van Raak, Simon J. A. Houben, Albertus P. H. J. Schenning, and Dirk J. Broer. Patterned and collective motion of densely packed tapered multiresponsive liquid crystal cilia. *Advanced Materials Technologies*, page 2101619, 2022.
35. Shucong Li, Michael M Lerch, James T Waters, Bolei Deng, Reese S Martens, Yuxing Yao, Do Yoon Kim, Katia Bertoldi, Alison Grinthal, Anna C Balazs, et al. Self-regulated non-reciprocal motions in single-material microstructures. *Nature*, 605(7908):76–83, 2022.
36. Wei Wang, Qingkun Liu, Ivan Tanasijevic, Michael F Reynolds, Alejandro J Cortese, Marc Z Miskin, Michael C Cao, David A Muller, Alyosha C Molnar, Eric Lauga, et al. Cilia metasurfaces for electronically programmable microfluidic manipulation. *Nature*, 605(7911):681–686, 2022.
37. Edoardo Milana, Benjamin Gorissen, Eline De Borre, Frederik Ceyssens, Dominiek Reynaerts, and Michael De Volder. Out-of-plane soft lithography for soft pneumatic microactuator arrays. *Soft Robotics*, 0(0), 2022. .
38. Zixuan Deng, Hang Zhang, Arri Priimagi, and Hao Zeng. Light-fueled nonreciprocal self-oscillators for fluidic transportation and coupling. *Advanced Materials*, 2022.
39. Jaap den Toonder, Femke Bos, Dick Broer, Laura Filippini, Murray Gillies, Judith de Goede, Titie Mol, Mireille Reijme, Wim Talen, Hans Wilderbeek, Vinayak Khatavkar, and Patrick Anderson. Artificial cilia for active micro-fluidic mixing. *Lab Chip*, 8:533–541, 2008. .
40. Ziyu Ren, Mingchao Zhang, Shanyuan Song, Zemin Liu, Chong Hong, Tianlu Wang, Xiaoguang Dong, Wenqi Hu, and Metin Sitti. Soft-robotic ciliated epidermis for reconfigurable coordinated fluid manipulation. *Science Advances*, 8(34), 2022.
41. Anne Helene Gelebart, Matthew Mc Bride, Albertus P. H..J. Schenning, Christopher N. Bowman, and Dirk J. Broer. Photoresponsive fiber array: Toward mimicking the collective motion of cilia for transport applications. *Advanced Functional Materials*, 26(29):5322–5327, 2016.
42. B. A. Evans, A. R. Shields, R. Lloyd Carroll, S. Washburn, M. R. Falvo, R. Superfine, Chapel Hill, Chapel Hill, North Carolina, West Virginia, V Uni, West Virginia, Chapel Hill, Chapel Hill, and North Carolina. Magnetically Actuated Nanorod Arrays as Biomimetic Cilia. *Nano Lett.*, 7(5):1428–1434, 2007. .
43. Mojca Vilfan, Anton Potocnik, Blaz Kavcic, Natan Osterman, Igor Poberaj, Andrej Vilfan, and Dusan Babic. Self-assembled artificial cilia. *Proc. Natl. Acad. Sci. U. S. A.*, 107(5):1844–1847, feb 2010. .
44. Aihui Wang, Mingcong Deng, Shuichi Wakimoto, and Toshihiro Kawashima. Characteristics analysis and modeling of a miniature pneumatic curling rubber actuator. *Int. J. Innov. Comput. Inf. Control*, 10(3):1029–1039, 2014.
45. Shuaizhong Zhang, Ye Wang, Reinoud Lavrijsen, Patrick R. Onck, and Jaap M.J. den Toonder. Versatile microfluidic flow generated by moulded magnetic artificial cilia. *Sensors Actuators, B Chem.*, 263:614–624, jun 2018. .
46. Srinivas Hanasoge, Peter J. Hesketh, and Alexander Alexeev. Microfluidic pumping using artificial magnetic cilia. *Microsystems Nanoeng.*, 4(1):11, dec 2018. .
47. Hayato Shinoda and Fujio Tsumori. Development of Micro Pump Using Magnetic Artificial Cilia with Metachronal Wave. *Proc. IEEE Int. Conf. Micro Electro Mech. Syst.*, 2020-Janua:497–500, 2020. .
48. Shuaizhong Zhang, Zhiwei Cui, Ye Wang, and Jaap M. J. den Toonder. Metachronal actuation of microscopic magnetic artificial cilia generates strong microfluidic pumping. *Lab Chip*, 20:3569–3581, 2020. .
49. Ahmet F. Demirors, Sumeyye Aykut, Sophia Ganzeboom, Yuki A. Meier, and Erik Poloni. Programmable droplet manipulation and wetting with soft magnetic carpets. *Proceedings of the National Academy of Sciences of the United States of America*, 118, 11 2021. ISSN 10916490. .
50. Jiaqi Miao, Siqi Sun, Tieshan Zhang, Gen Li, Hao Ren, and Yajing Shen. Natural cilia and pine needles combinedly inspired asymmetric pillar actuators for all-space liquid transport and self-regulated robotic locomotion. *ACS Applied Materials Interfaces*, 14(44):50296–50307, 2022.
51. Benjamin Gorissen, Wannes Vincentie, Farid Al-Bender, Dominiek Reynaerts, and Michaël De Volder. Modeling and bonding-free fabrication of flexible fluidic microactuators with a bending motion. *J. Micromech. Microeng*, 23:45012–10, 2013.
52. Edoardo Milana, Rongjing Zhang, Maria Rosaria Vetrano, Sam Peerlinck, Michael De Volder, Patrick R Onck, Dominiek Reynaerts, and Benjamin Gorissen. Metachronal patterns in artificial cilia for low reynolds number fluid propulsion. *Science advances*, 6(49):eabd2508, 2020.
53. Edoardo Milana, Bert Van Raemdonck, Andrea Serrano Casla, Michael De Volder, Dominiek Reynaerts, and Benjamin Gorissen. Morphological control of cilia-inspired asymmetric movements using nonlinear soft inflatable actuators. *Frontiers in Robotics and AI*, 8, 2021.

54. Kaitlyn P Becker, Yufeng Chen, Robert J Wood, K P Becker, Y Chen, R J Wood John A Paulson, and R J Wood. Mechanically programmable dip molding of high aspect ratio soft actuator arrays. 2020. .
55. Shigenori Nonaka, Satoko Yoshiba, Daisuke Watanabe, Shingo Ikeuchi, Tomonobu Goto, Wallace F Marshall, and Hiroshi Hamada. De novo formation of left–right asymmetry by posterior tilt of nodal cilia. *PLoS biology*, 3(8):e268, 2005.
56. CE Miller and H Goldfarb. An in vitro investigation of ciliated activity. *Transactions of the Society of Rheology*, 9(1): 135–144, 1965.
57. Tae-Rin Lee, Kieseok Oh, Jae-Hyun Chung, Yoon-Suk Chang, Jae-Boong Choi, Genki Yagawa, and Young-Jin Kim. Resonant behavior and microfluidic manipulation of silicone cilia due to an added mass effect. *Soft Matter*, 7(9):4325, 2011. ISSN 1744-683X. .
58. Christoph Brücker and Armin Keissner. Streaming and mixing induced by a bundle of ciliary vibrating micro-pillars. *Exp. Fluids*, 49(1):57–65, 2010. .
59. Chao Zhang, Pingan Zhu, Yangqiao Lin, Zhongdong Jiao, and Jun Zou. A review of modular soft robotics: Modular units, connection mechanisms, and applications. *Adv. Intell. Syst.*, 2020. .
60. Knut Norstog. Fine structure of the spermatozoid of zamia with special reference to the flagellar apparatus. *American Journal of Botany*, 54(7):831–340, 1967.
61. A. Sleigh, M. *The Biology of cilia and Flagella.* Pergamon Press, 1962.
62. Bing Dai, Siheng Li, Tailin Xu, Yuefeng Wang, Feilong Zhang, Zhen Gu, and Shutao Wang. Artificial asymmetric cilia array of dielectric elastomer for cargo transportation. *ACS Applied Materials & Interfaces*, 10(49):42979–42984, 2018. .
63. Edoardo Milana, Bert Van Raemdonck, Kevin Cornelis, Enrique Dehaerne, Jef De Clerck, Yarno De Groof, Toon De Vil, Benjamin Gorissen, and Dominiek Reynaerts. EELWORM : a bioinspired multimodal amphibious soft robot. 2020.
64. Yu-An Wu, Bivas Panigrahi, Yueh-Hsun Lu, and Chia-Yuan Chen. An Integrated Artificial Cilia Based Microfluidic Device for Micropumping and Micromixing Applications. *Micromachines*, 8(9):260, 2017. .
65. Jacob Belardi, Nicolas Schorr, Oswald Prucker, and Jürgen Rühe. Artificial cilia: Generation of magnetic actuators in microfluidic systems. *Adv. Funct. Mater.*, 21(17):3314–3320, 2011. .
66. Srinivas Hanasoge, Peter J. Hesketh, and Alexander Alexeev. Metachronal actuation of microscale magnetic artificial cilia. *ACS Applied Materials & Interfaces*, 12(41), 2020.
67. Seiji Azukizawa, Hayato Shinoda, Kazuki Tokumaru, and Fujio Tsumori. 3d printing system of magnetic anisotropy for artificial cilia. *Journal of Photopolymer Science and Technology*, 31(1):139–144, 2018. .
68. Hayato Shinoda, Seiji Azukizawa, Kazuki Maeda, and Fujio Tsumori. Bio-mimic motion of 3d-printed gel structures dispersed with magnetic particles. *Journal of The Electrochemical Society*, 166(9), 2019.

Supplementary Materials

Artificial cilia - bridging the gap with nature

Sam Peerlinck*,Edoardo Milana*, Elias De Smet, Michael De Volder, Dominiek Reynaerts, and Benjamin Gorissen

E-mail: benjamin.gorissen@kuleuven.be

This PDF file includes:

Figs. S1 to S6
Tables S1 to S5
References for SI reference citations

S1. Additional information

This sections details the methods used to create the figures in the main text. The raw data that has been used to populate the figures in the main text are tabulated in section S2.

A. Comparison Size versus Swept Area.

Figure S1 is a larger copy of figure 5A in the main text, displaying both cilium length and dimensionless swept area (SA), for different natural and artificial cilia. The numerical values of the data points are provided in table S3. For data points indicated with an asterisk (*) in the table, the dimensionless SA are not directly reported in the manuscripts. For these data points, we estimated the SA based on figures and diagrams in the manuscripts. Figure S2 gives an overview of the specific figures that were used for these estimations. To reduce errors in the estimation, we first tracked the trajectory formed by the cilia tips using image analysis software. This created the boundary of the SA, and the area contained within this boundary is used to calculate the SA. This image-based SA is then nondimensionalized with the cilium length, also derived from the figure, using the following equation:

$$SA_{dimensionless} = \frac{SA_{figure}}{0.5\pi L^2_{figure}}.$$

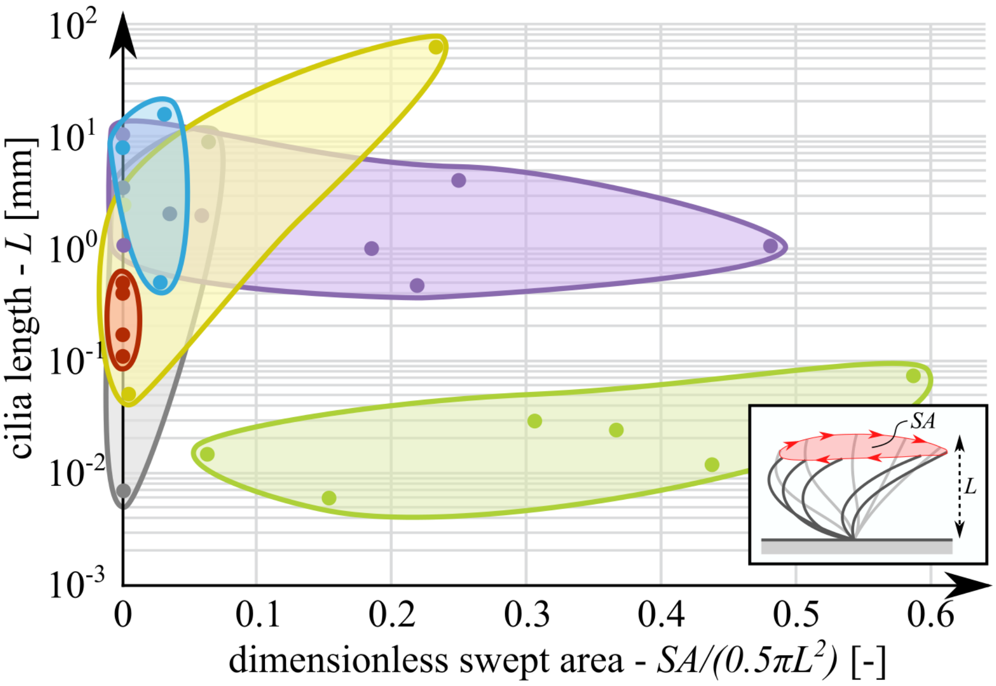

Fig. S1. A comparison between artificial and naturally occurring cilia in terms of size and beat complexity. Here only 2D planar beating motions are considered. Natural cilia beat tends to exhibit larger spatial asymmetry, at smaller size.

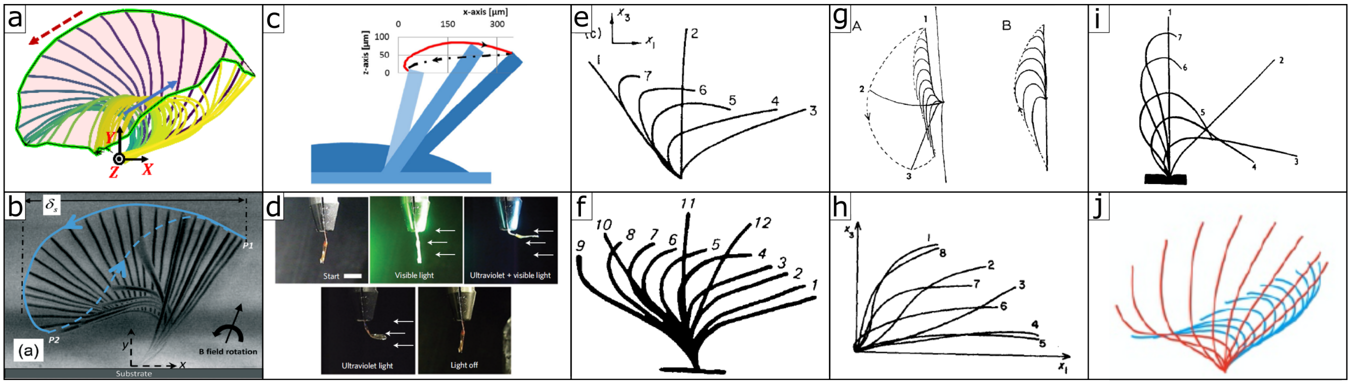

Fig. S2. Figures used for estimation of dimensionless swept area: a(1), b(2), c(3), d(4), e(5), f(6), g(7), h (8), i(9) and j(10).

B. Comparison Sperm number versus proximity.

Figure S3 is a larger copy of figure 5B in the main text displaying the cilia proximity (length divided by interciliary distance) on the logaritmic y-axis and the dimensionless Sperm number on the x-axis. The numerical values of the data points are enumerated in table S4. Although some references report a Sperm number, the same procedure for calculating the Sperm number is used for every data point to be consistent. For reference these are the reported Sperm numbers: Hanasoge (11): 3.2, Milana (12): 1.7, Orbay(13): 1.5 and Eloy(14) for Paramecium: 4.6. For the calculation of the Sperm number, the formulation according to Eloy and Lauga (14) was used:

$$Sp = L\left(\frac{\omega\xi_{\perp}}{B}\right)^{1/4} \qquad [1]$$

with: $\xi_{\perp} = \frac{4\pi\mu}{ln(L/r)}$, $B = EI$, the structure's bending resistance and $\omega = 2\pi f$ the angular frequency. This yields the following expression:

$$Sp = L\left(\frac{8\pi^2\mu f}{ln(L/r)EI}\right)^{1/4}, \qquad [2]$$

where f is a single cilium's beating frequency, μ the dynamic viscosity of the surrounding fluid, E the Young's modulus, I the second moment of inertia, r the radius and L the length of the cilium. These variables are derived from the information in the corresponding references to the best of our ability and displayed in table S4. The bending resistance of the artificial cilia is derived from the material and geometry of the circular or rectangular cross-section of the structures. To enable a fair comparison, the Sperm number of the natural cilia data points is estimated following the same principles as the artificial cilia. The difficulty here is to estimate the passive bending resistance of natural cilia. That is done according to the following reasoning:

All the considered natural cilia are constituted of a 9 + 2 axoneme and the microtubule doublets are the most important factor in the passive bending resistance of the structure (15). By estimating a generalized elasticity modulus (E) for this axoneme microstructure, assuming this remains fairly constant over different cilia sizes and calculating the moment of inertia (I) for the respective cilia cross-sections, the bending stiffness ($B = EI$) of each natural cilium is estimated. Hines and Blum (15) analyzed the kinematics and structure of the sliding filaments inside *Paramecium* cilia, and thus calculated the bending resistance of around 25 $pN\mu m^2$. Using this, we derived the generalized elasticity modulus to be $E = 153500 pN/\mu m^2$, using the reported radius of the *Paramecium* cilium (r = 0.12 µm) to divide the bending resistance by the second moment of inertia (I = $\pi r^4/4$). This generalized elasticity modulus is then used for all the data points representing natural cilia.

Finally, the inter-ciliary distance, or spacing between cilia a is either directly used from the references, or estimated based on images and/or mentioned carpet density. This yields the cilia proximity, a dimensionless metric based on the ratio of the cilium length and this inter-ciliary distance. The higher this ratio, the closer neighbouring cilia are packed together.

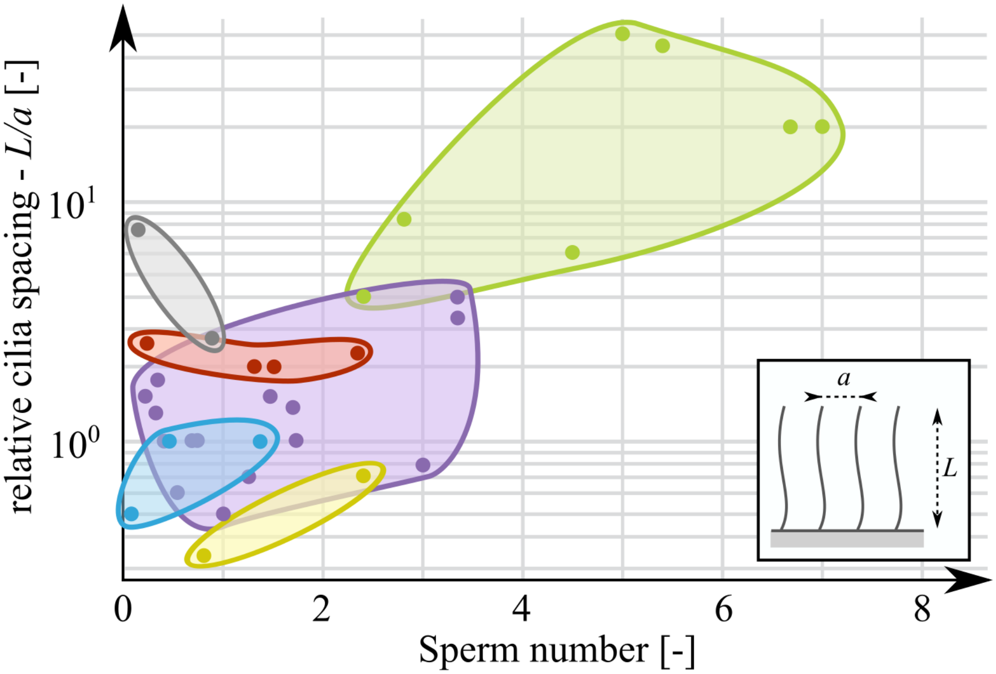

Fig. S3. A comparison between artificial and naturally occurring cilia in terms of Sperm number and cilia proximity. Natural cilia tend to show a higher Sperm number, meaning that the effects of viscous forces are more easily transferred from the fluid onto the cilia structure, and are packed more closely. This indicates that a higher mutual influence through the fluid is to be expected and self-coordinated metachronal asymmetry can emerge.

C. Determination of production technique metrics.

Figures S4, S5 and S6 show the same data as figure 4B in the main text, but are made more legible to facilitate extracting data on specific references. Furthermore, table S5 shows the data points of artificial and natural cilia which were compared in terms of aspect ratio, number of cilia on a carpet and cross sectional area on the aforementioned figures. To determine these three metrics, a distinction was made first between cilia with a rectangular or a circular cross section. For the former a width and thickness has been defined, whereas a diameter has been identified for the latter. The table below gives a summary of the formulas used to determine the aspect ratio and cross sectional area, where L, W, T and D are the length, width, thickness and diameter of cilia, respectively.

	Aspect Ratio	Cross Section
Rectangular	L/W	$W.T$
Circular	L/D	$\pi D^2/4$

Data concerning the number of cilia on the carpets was obtained directly from the text and figures presented in all but five literature resources. It was necessary to estimate the number of cilia produced in these references in order to complete the data. This was done in the following ways:

1. Islam *et al.* (16) present densities of the cilia carpets they produced, but not the total amount of cilia on the carpet. The cilia densities of the carpets that were investigated the most are 10^4 and 10^5 cilia per square centimeter. The publications SI reports a piece of cilia carpet being submerged vertically in an ethanol container with a depth of 500 µm. Based on this, the size of the cilia carpet is assumed here to be at least 500x500 µm or 2.510^7 m^2, which was multiplied by the aforementioned cilia densities to obtain the estimated number of cilia.

2. The amount of cilia on carpets produced by Liu *et al.* (17) was approximated using figure 1(a) and 1(e) of the publication. These figures show close-up side views of the cilia carpets and include a scale bar of 500µm as a reference. The spacing between cilia positioned roughly in line with each other can be observed from these figures. On average, cilia are deemed to be 200µm apart from each other in figure 1(a) and 375 µm in figure 1(e). Assuming the same spacing between cilia occurs in the horizontal direction perpendicular to the observed one, the densities of cilia on the carpet are estimated to be $(1/200)^2$ µm^2 and $(1/375)^2$ µm^2. Additionally, the overall size of the carpet is believed to be 7x2 cm^2, as this value is the size of a PTFE mold, reported in section 4: 'Experimental Section', subsection: 'Characterization'. The total number of cilia on the carpet was again calculated as the product of the carpet size and the cilia density.

3. Sun *et al.* (18) report cilia densities of 660 and 730 cilia per square centimeter and mention using a 35mm wide paper beaker during production of the cilia carpet. The carpet size was calculated as the surface of circle with a diameter of 35mm and the total number of cilia on the carpet was obtained by multiplying this value by the reported cilia densities.

4. Jaakko *et al.* (19) construct their cilia carpet on a 35 mm wide substrate plate, which was assumed to be circular for deriving its surface. Figure 5 of the publication shows a close-up of a small patch of cilia with a density estimated here to be nine per square millimeter. The total number of cilia was obtained analogous to the previous cases.

5. Wang *et al.* (20) fabricated their cilia on 10mm wide circular cover slips and observed a surface coverage of 1.5% (up to 2.9%), counting the area covered by a single bead each time. Therefore, the total area covered by the beads is taken here to be 1.5% of the surface of the cover slips. Dividing this area by the area a single bead takes up results in the total number of cilia on the carpet, since the cilia in this publication are pillars of single beads stacked on top of each other. Wang *et al.* reported the beads to be spherical with a diameter of 2.7µm, which was used as an input to calculate the circular surface they take up on the cover slips.

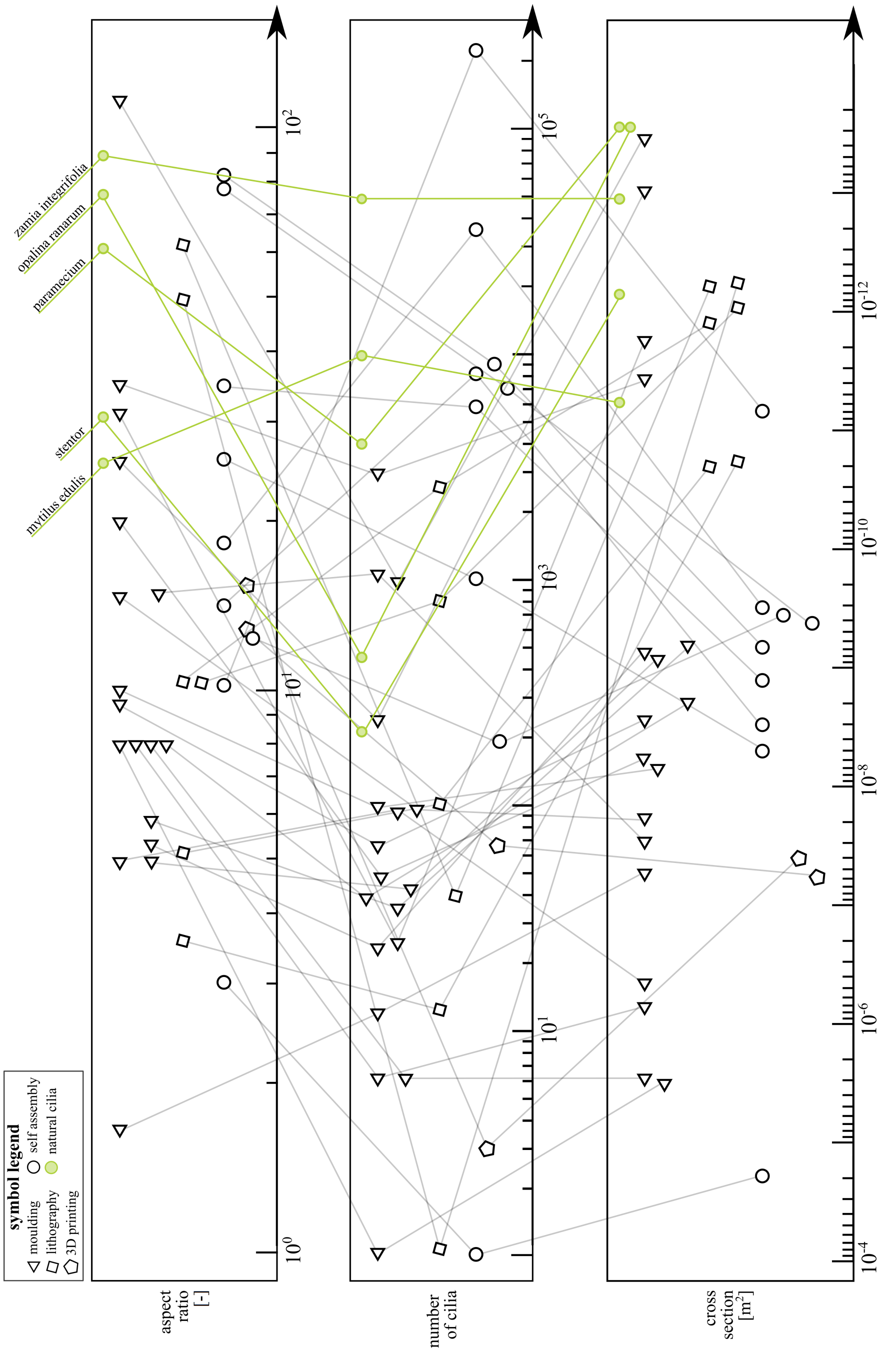

Fig. S4. Production techniques comparison, all data points

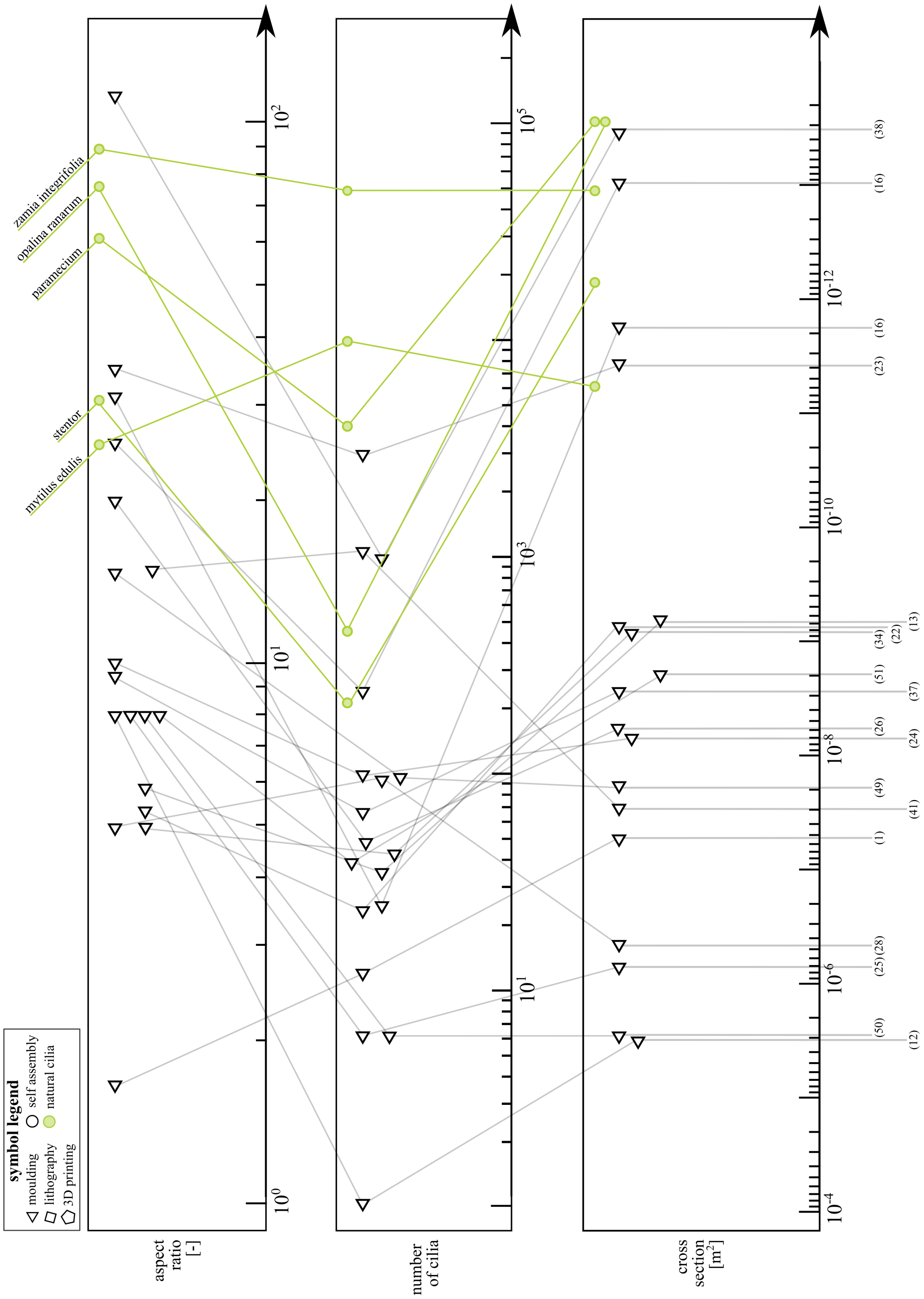

Fig. S5. Production techniques comparison, all data points

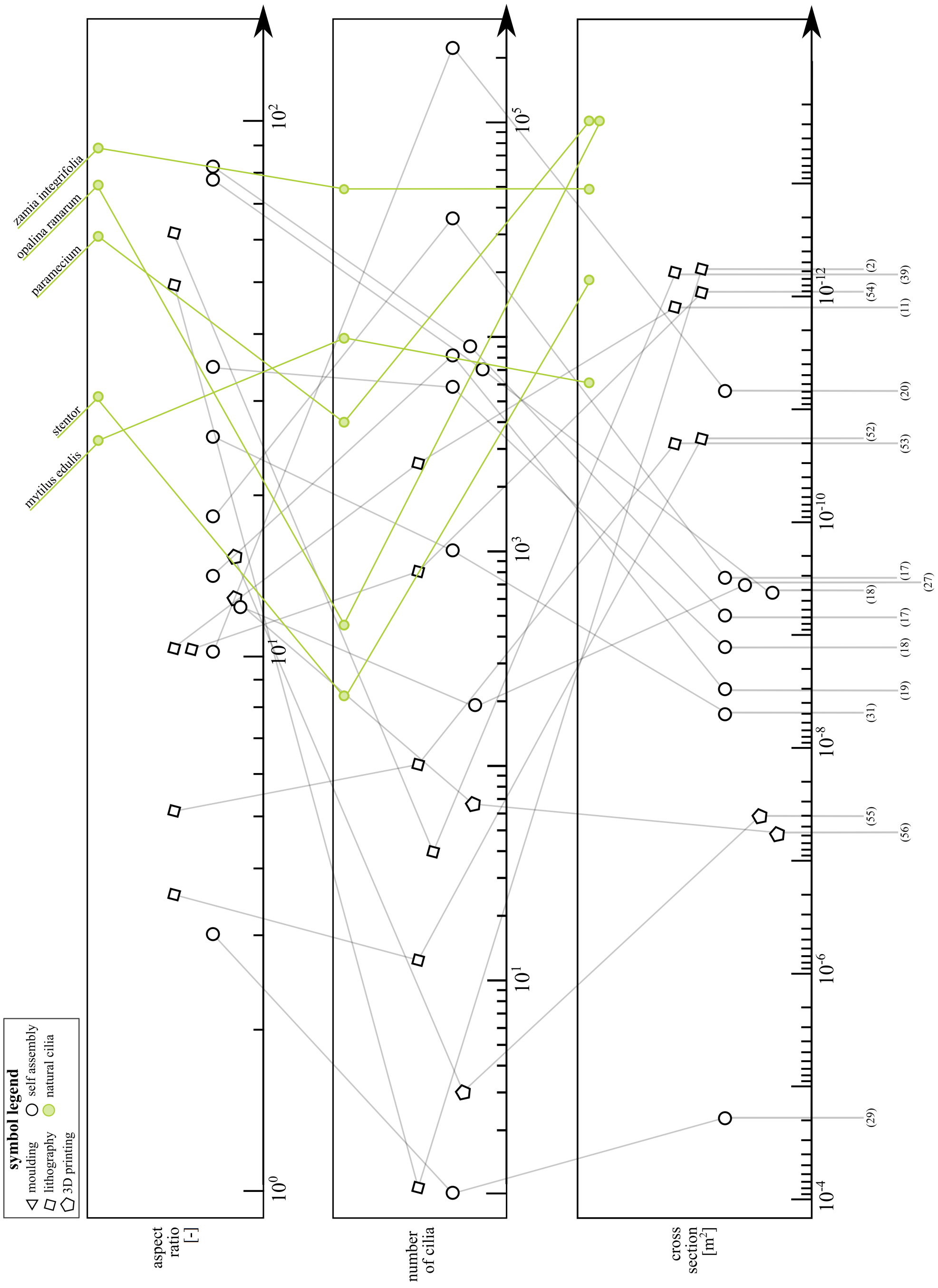

Fig. S6. Production techniques comparison, all data points

S2. Data used for analysis

This section tabulates the data points used to compose the figures in the main text and in SI.

Table S1. Datapoints of the plot displayed in Fig. 3 of the main text. Artificial cilia are classified according to the publication year, cilia length (mm) and Reynolds number. For publication where no fluid propulsion experiments are reported the Reynolds number is not available (n/a).

Author	Year of Publication	Cilia Length (mm)	Reynolds Number
den Toonder (21)	2008	0.1	1
Oh (22)	2009	0.4	68
van Oosten (4)	2009	10	n/a
Shields (23)	2010	0.025	0.025
Hussong (24)	2011	0.070	0.14
Keissner (25)	2012	1	0.040
Sareh (10)	2013	64	410
Gorissen (26)	2015	10	3480
Tsumori (27)	2016	2	n/a
Wang (28)	2016	0.3	6
Hanasoge (2)	2016	0.2	0.12
Rockenbach (3)	2017	0.5	5
Gu (29)	2020	4	0.002
Milana (12)	2020	14	0.04
Dong (1)	2020	1	0.03
Sugioka (30)	2021	16-30	n/a
Panigrahi (31)	2021	10	∼560
Demiroers (32)	2021	0.6-2	∼0.003
Dillinger (33)	2021	0.1	31
van Raak (34)	2021	0.01	n/a
Li (35)	2022	0.15	n/a
Wang (36)	2022	0.05	0.002
Milana (37)	2022	0.45	n/a
Deng (38)	2022	9	60

Table S2. Overview of actuation technologies per reference, indicating presence and type of spatial and metachronal asymmetry, and type of coordination and tethering.

Actuation	Author	Year	Spatial	Metachronal	Coordination	Tethering
Electrical	Den Toonder (39)	2008	-	variable	local	flexible
Electrical	Sareh (10)	2012	yes	-	local	flexible
Electrical	Sugioka (30)	2021	-	fixed	local	flexible
Electrical	Wang (36)	2022	yes	variable	local	flexible
Electrical	Ren (40)	2022	-	variable	local	flexible
Optical	Van Oosten (4)	2009	yes	-	global	contactless
Optical	van Raak (34)	2022	-	-	global	contactless
Optical	Li (35)	2022	planar	emerging	self	contactless
Optical	Deng (38)	2022	planar	emerging	self	contactless
Optical	Gelebart (41)	2016	conical	-	global	contactless
Optical	Liu (17)	2020	conical	-	global	contactless
Magnetic	Evans (42)	2007	conical	-	global	contactless
Magnetic	Shields (23)	2010	conical	-	global	contactless
Magnetic	Vilfan (43)	2010	conical	-	global	contactless
Magnetic	Wang (20)	2013	conical	-	global	contactless
Magnetic	Wang (44)	2014	conical	-	global	contactless
Magnetic	Wang (28)	2016	conical	-	global	contactless
Magnetic	Zhang (45)	2018	conical	-	global	contactless
Magnetic	Hussong (24)	2011	planar	-	global	contactless
Magnetic	Hanasoge (46)	2018	planar	-	global	contactless
Magnetic	Hanasoge (11)	2018	planar	fixed	global	contactless
Magnetic	Tsumori (27)	2016	planar	-	global	contactless
Magnetic	Shinoda (47)	2020	planar	fixed	global	contactless
Magnetic	Gu (29)	2020	planar	fixed	global	contactless
Magnetic	Dong (1)	2020	planar	fixed	global	contactless
Magnetic	Zhang (48)	2020	conical	fixed	global	contactless
Magnetic	Demirors (49)	2020	-	fixed	global	contactless
Magnetic	Panigrahi (31)	2021	planar	fixed	global	contactless
Magnetic	Miao (50)	2022	planar	-	global	contactless
Pressure	Rockenbach (3)	2015	planar	variable	local	elastic
Pressure	Gorissen (51)	2013	-	-	local	elastic
Pressure	Gorissen (26)	2015	-	variable	local	elastic
Pressure	Milana (37)	2022	-	-	local	elastic
Pressure	Milana (12)	2019	planar	-	local	elastic
Pressure	Milana (52)	2020	planar	variable	local	elastic
Pressure	Milana (53)	2021	planar	fixed	global	elastic
Pressure	Becker (54)	2020	-	fixed	local	elastic
Mechanical	Nonaka (55)	2005	conical	variable	local	rigid
Mechanical	Miller (56)	1965	planar	-	local	rigid
Mechanical	Keissner (25)	2012	conical	variable	local	rigid
Inertial	Oh (22)	2009	-	-	global	rigid
Inertial	Lee (57)	2011	-	-	global	rigid
Inertial	Brucker (58)	2010	-	-	global	rigid
Inertial	Orbay (13)	2018	-	-	global	rigid
Inertial	Dillinger (33)	2021	-	-	global	contactless

Table S3. Datapoints for comparison cilium length and nondimensional planar swept area, used to populate figure 5A in the main text.

Actuation	Author	Length (µm)	Swept area absolute (µm²)	Swept area nondimensional
Electric field	Den Toonder (21)	100	0	0%
Electric field	Sareh (10)	64,000	1.5 10^9	23%
Electric field	Wang (36)	50	39	1%
Electric field	Ren (40)	1500	0	0%
Magnetic field	Dong (1)	1,000	7.5 10^5	47%*
Magnetic field	Hanasoge (2)	480	7.9 10^4	22%*
Magnetic field	Tsumori (27)	2,000	3.7 10^5	6%
Magnetic field	Panigrahi (31)	10,000	0	0%
Magnetic field	Miao (50)	3000	3.6 10^6	25%
Pressure	Gorissen (26)	8,000	0	0%
Pressure	Milana (12)	16,000	1.2 10^7	3%
Pressure	Rockenbach (3)	500	1.05 10^4	3%*
Inertial	Brucker (58)	500	0	0%
Inertial	Oh (22)	400	0	0%
Inertial	Orbay (13)	170	0	0%
Inertial	Dillinger (33)	100	0	0%
Light	Van Oosten (4)	10,000	6.3 10^6	4%*
Light	Van Raak (34)	50	0	0%
Light	Deng (38)	9000	8.6 10^6	7%
Natural	Paramecium (5)	12	99	44%*
Natural	Rabbit trachea (6)	6	8.6	15%*
Natural	Mytilus Edulis (7)	75	5.2 10^3	59%*
Natural	Opalina Ranarum (8)	15	22	6%*
Natural	Stentor (9)	30	4.3 10^2	31%*
Natural	Volvox (10)	25	3.6 10^2	37%*

*Swept area not clearly reported in reference but calculated from figures as explained in text.

Table S4. Data points for comparison cilia proximity and Sperm number, used to populate figure 5B in the main text.

Actuation	Author	Length (L) (µm)	Radius (r) (µm)	Frequency (Hz)	Viscosity (mPa.s)	Youngs Modulus	Moment of Inertia (m^4)	Bending stiffness (Nm^2)	Spacing (a) (µm)	Proximity (L/a)	Sperm Number
Electric field	Den Toonder (21)	100	0.5	200	9.3	4 GPa	1.67 10^{-24}	6.67 10^{-15}	300	0.3	0.8
Electric field	Sareh (10)	64000	250	0.5	0.89	180 MPa	5.21 10^{-14}	9.38 10^{-6}	single	single	0.3
Electric field	Wang (36)	50	0.005	40	1	150 GPa	4.17 10^{-31}	6.25 10^{-20}	0	0.7	2.4
Magnetic field	Dong (1)	1000	50	2.5	876	0,144 MPa	4.58 10^{-17}	6.6E 10^{-12}	1000	1.0	137
Magnetic field	Evans (42)	22.5	0.125	15	1	2.6 MPa	1.92 10^{-28}	4.99 10^{-22}	7	3.2	3.3
Magnetic field	Gu (29)	4000	400	0.083	1150	0.185 MPa	2.01 10^{-14}	3.72 10^{-9}	4000	1.0	0.7
Magnetic field	Hanasoge (2)	480	0.03	24	4	200 GPa	1.8 10^{-28}	3.6 10^{-17}	single	single	5.8
Magnetic field	Hanasoge (11)	200	0.03	24	1	200 GPa	3.6 10^{-28}	7.2 10^{-17}	single	single	1.5
Magnetic field	Hanasoge (46)	600	0.03	4	1	200 GPa	1.8 10^{-28}	3.6 10^{-17}	150	4.0	3.3
Magnetic field	Hussong (24)	70	0.45	20	1	2.5 MPa	1.22 10^{-24}	3.0 10^{-18}	100	0.7	1.3
Magnetic field	Shields (23)	25	0.35	34	1	2.5 MPa	1.18 10^{-26}	2.9 10^{-20}	18	1.4	1.7
Magnetic field	Shinoda (47)	3000	100	0.5	970	0.144 MPa	1.33 10^{-15}	1,9 10^{-10}	2113	1,4	1,5
Magnetic field	Tsumori (27)	2000	150	20	1	2.5 MPa	3.98 10^{-16}	9.9 10^{-10}	1100	1.8	0.3
Magnetic field	Vilfan (43)	45	2.2	1	1	2.5 MPa	1.84 10^{-23}	4.6 10^{-17}	30	1.5	0.2
Magnetic field	Wang (20)	30	1.5	10	1	10 MPa	3.98 10^{-24}	4.0 10^{-17}	23	1.3	0.3
Magnetic field	Wang (44)	300	15	15	2.5	2.5 MPa	3.98 10^{-20}	9.9 10^{-14}	500	0.6	0.5
Magnetic field	Wang (28)	250	10	20	10	2.5 MPa	7.85 10^{-21}	2.0 10^{-14}	550	0.5	1.0
Magnetic field	Zhang (45)	350	25	40	0.89	2.5 MPa	3.07 10^{-19}	7.67 10^{-13}	350	1.0	0.4
Magnetic field	Zhang (59)	350	25	100	1400	2.5 MPa	3.07 10^{-19}	7.67 10^{-13}	450	0.8	3.0
Magnetic field	Panigrahi (31)	10000	130	1	1	2.5 MPa	3.26 10^{-16}	8.1 10^{-10}	10000	1.0	0.7
Contact	Keissner (25)	1000	50	3	11.1	2.5 MPa	4.91 10^{-18}	1.2 10^{-7}	500	2.0	0.5
Pressure	Gorissen (26)	8000	500	35	1	2.5 MPa	4.91 10^{-14}	1.2 10^{-7}	8000	1.0	0.4
Pressure	Milana (12)	16000	1000	0.5	1000	2.5 MPa	1.1 10^{-13}	2.75 10^{-7}	single	single	1.4
Pressure	Milana (52)	16000	1000	0.5	1000	2.5 MPa	1.1 10^{-13}	2.75 10^{-7}	16000	1.0	1.4
Pressure	Rockenbach (3)	500	50	9.8	1	2.5 MPa	2.08 10^{-16}	5.2 10^{-10}	1000	0.5	0.1
Inertial	Brucker (58)	500	25	50	10	1.6 MPa	3.07 10^{-19}	4.9 10^{-13}	250	2.0	1.1
Inertial	Oh (22)	400	5	65	1	1 MPa	6.25 10^{-21}	6.25 10^{-15}	200	2.0	1.5
Inertial	Orbay (13)	170	15	4600	1	0.1 MPa	3.98 10^{-20}	4.0 10^{-15}	75	2.3	2.4
Inertial	Dillinger (33)	100	20	100	1	1 MPa	1.13 10^{-19}	1.13 10^{-13}	40	2.5	0.3
Light	Van Oosten (4)	2000	100	1	1	1 GPa	1.33 10^{-18}	1.33 10^{-9}	300	6.7	0.1
Light	Deng (38)	9000	50	2.7	1	4.9 MPa	8.33 10^{-17}	4.08 10^{-10}	5000	1.8	0.9
Natural	Paramecium (5)	12	0.12	31.8	0.89			2.5 10^{-23}	2	6.0	4.5
Natural	Rabbit Trachea (6)	6	0.2	16	1000	0.15 MPa	1.26 10^{-27}	1.9 10^{-22}	0.3	20.0	7.1
Natural	Opalina Ranarum (8)	15	0.1	10	1	0.15 MPa	7.85 10^{-29}	1.2 10^{-23}	0.3	50.0	5.1
Natural	Stentor (9)	30	0.5	33	1	0.15 MPa	4.91 10^{-26}	7.54 10^{-21}	3.5	8.6	2.9
Natural	Mytilu Edulis (7)	80	1.5	25	1	0.15 MPa	3.98 10^{-24}	6.1 10^{-19}	20	4.0	2.4
Natural	Zamia Integrifolia (60, 61)	35	0.1	30	0.0181	0.15 MPa	7.85 10^{-29}	1.2 10^{-23}	0.8	43.8	5.5
Natural	Volvox (10)	25	0.15	25	0.89	0.15 MPa	3.98 10^{-28}	6.1 10^{-23}	1.3	20.0	6.8

Table S5. Data points for comparing aspect ratio, number of cilia, and cross section; used to populated figure 4B in the main text.

Author	Length (m)	Width (m)	Thickness (m)	Diameter (m)	Aspect Ratio	Number of Cilia	Cross Section (m²)
Artificial cilia							
Molding							
Brücker (58)	5.70 10^{-4}			6.0 10^{-5}	9.500 10^{0}	6.7 10^{1}	2.827 10^{-9}
Dai 2018 (62)	2.35 10^{-3}			1.6 10^{-4}	1.469 10^{1}	1.0 10^{2}	2.011 10^{-8}
Dong (1)	1.00 10^{-3}	6.0 10^{-4}	1.0 10^{-4}		1.667 10^{0}	1.2 10^{1}	6.000 10^{-8}
Evans (42)	2.25 10^{-5}			2.0 10^{-7}	1.125 10^{2}	1.0 10^{3}	3.142 10^{-14}
Gorissen (26)	8.00 10^{-3}			1.0 10^{-3}	8.000 10^{0}	6.0 10^{0}	7.854 10^{-7}
Gu (29)	4.00 10^{-3}			8.0 10^{-4}	5.000 10^{0}	1.0 10^{2}	5.026 10^{-7}
Islam (16)	4.70 10^{-5}			1.5 10^{-6}	3.133 10^{1}	2.5 10^{1}	1.767 10^{-12}
Islam (16)	9.00 10^{-6}			3.5 10^{-7}	2.571 10^{1}	2.5 10^{2}	9.621 10^{-14}
Keissner (25)	1.00 10^{-3}			1.0 10^{-4}	1.000 10^{1}	1.0 10^{2}	7.854 10^{-9}
Li (35)	1.50 10^{-4}	3.0 10^{-5}	3.0 10^{-5}		5.000 10^{0}	4.4 10^{1}	9.000 10^{-10}
Milana (12)	1.60 10^{-2}			2.0 10^{-3}	8.000 10^{0}	1.0 10^{0}	3.142 10^{-6}
Milana (63)	1.60 10^{-2}			2.0 10^{-3}	8.000 10^{0}	6.0 10^{0}	3.142 10^{-6}
Oh (22)	4.00 10^{-4}	7.5 10^{-5}	1.0 10^{-5}		5.333 10^{0}	2.4 10^{1}	7.500 10^{-10}
Orbay (13)	1.70 10^{-4}			3.0 10^{-5}	5.667 10^{0}	3.2 10^{1}	7.068 10^{-10}
Shields (23)	2.50 10^{-5}			7.0 10^{-7}	3.571 10^{1}	3.0 10^{3}	3.848 10^{-13}
Shinoda (47)	3.00 10^{-3}			2.0 10^{-4}	1.500 10^{1}	1.2 10^{3}	3.142 10^{-8}
Tsumori (27)	2.00 10^{-3}			1.0 10^{-4}	2.000 10^{1}	4.8 10^{1}	7.854 10^{-9}
Wu (64)	4.00 10^{-4}			5.0 10^{-5}	8.000 10^{0}	4.0 10^{1}	1.963 10^{-9}
Lithography							
Belardi (65)	7.00 10^{-5}	2.0 10^{-5}	9.0 10^{-7}		3.500 10^{0}	1.2 10^{1}	1.800 10^{-11}
Den Toonder (39)	1.00 10^{-4}	2.0 10^{-5}	1.0 10^{-6}		5.000 10^{0}	1.0 10^{2}	2.040 10^{-11}
Hanasoge (2)	4.80 10^{-4}	1.0 10^{-5}	5.6 10^{-8}		4.800 10^{1}	1.0 10^{0}	5.600 10^{-13}
Hanasoge (11)	2.00 10^{-4}	2.0 10^{-5}	6.0 10^{-8}		1.000 10^{1}	2.6 10^{3}	1.200 10^{-12}
Hanasoge (46)	6.00 10^{-4}	1.0 10^{-5}	6.0 10^{-8}		6.000 10^{1}	3.8 10^{1}	6.000 10^{-13}
Hanasoge (66)	1.50 10^{-4}	1.5 10^{-5}	6.0 10^{-8}		1.000 10^{1}	8.0 10^{2}	9.000 10^{-13}
Self assembly							
Demirörs (32)	2.00 10^{-3}			8.0 10^{-5}	2.500 10^{1}	1.0 10^{3}	5.026 10^{-9}
Jaakko (19)	7.81 10^{-4}			5.5 10^{-5}	1.420 10^{1}	8.7 10^{3}	2.376 10^{-9}
Liu (17)	3.75 10^{-4}			2.0 10^{-5}	1.875 10^{1}	3.5 10^{4}	3.142 10^{-10}
Liu (17)	2.50 10^{-3}			3.0 10^{-5}	8.333 10^{1}	1.0 10^{4}	7.068 10^{-10}
Sugioka (30)	1.50 10^{-2}			5.0 10^{-3}	3.000 10^{0}	1.0 10^{0}	1.963 10^{-5}
Sun (18)	1.73 10^{-3}			2.2 10^{-5}	7.864 10^{1}	7.0 10^{3}	3.801 10^{-10}
Sun (18)	1.34 10^{-3}			3.9 10^{-5}	3.436 10^{1}	5.8 10^{3}	1.195 10^{-9}
Wang (20)	3.27 10^{-5}			3.0 10^{-6}	1.090 10^{1}	2.1 10^{5}	7.068 10^{-12}
Wang (28)	2.50 10^{-4}			2.0 10^{-5}	1.250 10^{1}	1.9 10^{2}	3.142 10^{-10}
3D printing							
Azukizawa (67)	3.00 10^{-3}	2.0 10^{-4}	2.0 10^{-4}		1.500 10^{1}	3.0 10^{0}	4.000 10^{-8}
Shinoda (68)	3.00 10^{-3}	2.4 10^{-4}	2.4 10^{-4}		1.250 10^{1}	6.4 10^{1}	5.760 10^{-8}
Natural cilia							
Mytilus Edulis (7)	7.50 10^{-5}			3.0 10^{-6}	2.500 10^{1}	1.0 10^{4}	7.068 10^{-12}
Opalina Ranarum (8)	1.50 10^{-5}			2.0 10^{-7}	7.500 10^{1}	4.5 10^{2}	3.142 10^{-14}
Paramecium (5)	1.20 10^{-5}			2.0 10^{-7}	6.000 10^{1}	4.0 10^{3}	3.142 10^{-14}
Stentor (9)	3.00 10^{-5}			1.0 10^{-6}	3.000 10^{1}	2.1 10^{2}	7.854 10^{-13}
Zamia Integrifolia (60)	3.50 10^{-5}			4.0 10^{-7}	8.750 10^{1}	5.0 10^{4}	1.257 10^{-13}

References

1. Xiaoguang Dong, Guo Zhan Lum, Wenqi Hu, Rongjing Zhang, Ziyu Ren, Patrick R Onck, and Metin Sitti. Bioinspired cilia arrays with programmable nonreciprocal motion and metachronal coordination. *Science advances*, 6(45):eabc9323, 2020.
2. Srinivas Hanasoge, Matthew Ballard, Peter J Hesketh, and Alexander Alexeev. Asymmetric motion of magnetically actuated artificial cilia. *Lab Chip*, 17, 2017. .
3. A Rockenbach, V Mikulich, Ch Br, U Schnakenberg, Ch Brücker, and U Schnakenberg. Fluid transport via pneumatically actuated waves on a ciliated wall. *J. Micromechanics Microengineering*, 25(12):125009, dec 2015.
4. Casper L van Oosten, Cees W M Bastiaansen, and Dirk J Broer. Printed artificial cilia from liquid-crystal network actuators modularly driven by light. *Nat. Mater.*, 8(8):677–682, 2009. .
5. John Blake. Hydrodynamic calculations on the movements of cilia and flagella. i. paramecium. *Journal of theoretical Biology*, 45:183–203, 1974.
6. J. Sanderson, M. and A. Sleigh, M. Ciliary activity of cultured rabbit tracheal epithelium: Beat pattern and metachrony. *Journal of Cell Science*, 47:331–347, 1981.
7. Edward Aiello and MichaelA. Sleigh. The metachronal wave of lateral cilia of mytilu edulis. *The Journal of Cell Biology*.
8. John Blake. Hydrodynamic calculations on the movements of cilia and flagella. ii. opalina. *Journal of theoretical Biology*, 52:67–82, 1975.
9. M. A. Sleigh. The form of beat in cilia of stentor and opalina. *Experimental Biology*, 37(1), 1960.
10. Sina Sareh, Jonathan Rossiter, Andrew Conn, Knut Drescher, and Raymond E Goldstein. Swimming like algae: biomimetic soft artificial cilia. *J. R. Soc. Interface*, 10(78):20120666–, 2012. .
11. Srinivas Hanasoge, Peter J. Hesketh, and Alexander Alexeev. Metachronal motion of artificial magnetic cilia. *Soft Matter*, 14(19):3689–3693, may 2018. .
12. Edoardo Milana, Benjamin Gorissen, Sam Peerlinck, Michael De Volder, and Dominiek Reynaerts. Artificial Soft Cilia with Asymmetric Beating Patterns for Biomimetic Low-Reynolds-Number Fluid Propulsion. *Adv. Funct. Mater.*, 1900462: 1–8, 2019.
13. Sinem Orbay, Adem Ozcelik, Hunter Bachman, and Tony Jun Huang. Acoustic actuation of in situ fabricated artificial cilia. *J. Micromechanics Microengineering*, 28(2):025012, 2018. .
14. Christophe Eloy and Eric Lauga. Kinematics of the most efficient cilium. *Phys. Rev. Lett.*, 109(3), 2012. .
15. M. Hines and J. Blum, J. Thee-dimensional mechanics of eukaryotic flagella. *Biophysical Journal*, 41:67–79, 1983.
16. Tanveer ul Islam, Yves Bellouard, and Jaap M. J. den Toonder. Highly motile nanoscale magnetic artificial cilia. *Proceedings of the National Academy of Sciences*, 118(35), 2021. .
17. Li Liu, Marc del Pozo, Fateme Mohseninejad, Michael G. Debije, Dirk J. Broer, and Albert P.H.J. Schenning. Light tracking and light buiding fiber arrays by adjusting the location of photoresponsive azobenzene in liquid crystal networks. *Advanced Optical Materials*, 8(18), 2020.
18. Wenjie Sun, Huiming Wang, and Jinxiong Zhou. Actuation and instability of interconnected dielectric elastomer balloons. *Appl. Phys. A Mater. Sci. Process.*, 119(2):443–449, may 2015. .
19. Jaakko V. I. Timonen, Christoffer Johans, Kyösti Kontturi, Andreas Walther, Olli Ikkala, and Robin H. A. Ras. A facile template-free approach to magnetodriven, multifunctional artificial cilia. *ACS Applied Materials & Interfaces*, 2(8): 2226–2230, 2010.
20. Ye Wang, Yang Gao, Hans Wyss, Patrick Anderson, and Jaap den Toonder. Out of the cleanroom, self-assembled magnetic artificial cilia. *Lab Chip*, 13(17):3360–6, 2013. .
21. Jaap den Toonder, Femke Bos, Dick Broer, Laura Filippini, Murray Gillies, Judith de Goede, Titie Mol, Mireille Reijme, Wim Talen, Hans Wilderbeek, Vinayak Khatavkar, and Patrick Anderson. Artificial cilia for active micro-fluidic mixing. *Lab Chip*, 8(4):533–41, 2008. .
22. Kieseok Oh, Jae-Hyun Chung, Santosh Devasia, and James J. Riley. Bio-mimetic silicone cilia for microfluidic manipulation. *Lab Chip*, 9(11):1561, 2009. .
23. a R Shields, B L Fiser, B a Evans, M R Falvo, S Washburn, and R Superfine. Biomimetic cilia arrays generate simultaneous pumping and mixing regimes. *Proc. Natl. Acad. Sci. U. S. A.*, 107(36):15670–15675, 2010. .
24. J. Hussong, N. Schorr, J. Belardi, O. Prucker, J. Rühe, and J. Westerweel. Experimental investigation of the flow induced by artificial cilia. *Lab Chip*, 11(12):2017–2022, 2011. .
25. Armin Keißner and Christoph Brücker. Directional fluid transport along artificial ciliary surfaces with base-layer actuation of counter-rotating orbital beating patterns. *Soft Matter*, 8(19):5342, 2012. .
26. Benjamin Gorissen, Michaël de Volder, and Dominiek Reynaerts. Pneumatically-actuated artificial cilia array for biomimetic fluid propulsion. *Lab Chip*, 15(22):4348–4355, 2015.
27. Fujio Tsumori, Ryuma Marume, Akinori Saijou, Kentaro Kudo, Toshiko Osada, and Hideshi Miura. Metachronal wave of artificial cilia array actuated by applied magnetic field. In *Jpn. J. Appl. Phys.*, volume 55, 2016. .
28. Ye Wang, Jaap den Toonder, Ruth Cardinaels, and Patrick Anderson. A continuous roll-pulling approach for the fabrication of magnetic artificial cilia with microfluidic pumping capability. *Lab Chip*, 16(12):2277–2286, 2016. .
29. Hongri Gu, Quentin Boehler, Haoyang Cui, Eleonora Secchi, Giovanni Savorana, Carmela De Marco, Simone Gervasoni, Quentin Peyron, Tian Yun Huang, Salvador Pane, Ann M. Hirt, Daniel Ahmed, and Bradley J. Nelson. Magnetic cilia carpets with programmable metachronal waves. *Nat. Commun.*, 11(1):1–10, 2020. .

30. Hideyuki Sugioka and Hiroki Yoshijima. Metachronal motion of artificial cilia using induced charge electro-osmosis. *Colloids and Surfaces A: Physicochemical and Engineering Aspects*, 626:127023, 2021.
31. Bivas Panigrahi, Vignesh Sahadevan, and Chia-Yuan Chen. Shape-programmable artificial cilia for microfluidics. *iScience*, 24(12):103367, 2021.
32. Ahmet F Demirörs, Sümeyye Aykut, Sophia Ganzeboom, Yuki A Meier, Robert Hardeman, Joost de Graaf, Arnold JTM Mathijssen, Erik Poloni, Julia A Carpenter, Caner Ünlü, et al. Amphibious transport of fluids and solids by soft magnetic carpets. *Advanced Science*, 8(21):2102510, 2021.
33. Cornel Dillinger, Nitesh Nama, and Daniel Ahmed. Ultrasound-activated ciliary bands for microrobotic systems inspired by starfish. *Nature communications*, 12(1):1–11, 2021.
34. Roel J. H. van Raak, Simon J. A. Houben, Albertus P. H. J. Schenning, and Dirk J. Broer. Patterned and collective motion of densely packed tapered multiresponsive liquid crystal cilia. *Advanced Materials Technologies*, page 2101619, 2022.
35. Shucong Li, Michael M Lerch, James T Waters, Bolei Deng, Reese S Martens, Yuxing Yao, Do Yoon Kim, Katia Bertoldi, Alison Grinthal, Anna C Balazs, et al. Self-regulated non-reciprocal motions in single-material microstructures. *Nature*, 605(7908):76–83, 2022.
36. Wei Wang, Qingkun Liu, Ivan Tanasijevic, Michael F Reynolds, Alejandro J Cortese, Marc Z Miskin, Michael C Cao, David A Muller, Alyosha C Molnar, Eric Lauga, et al. Cilia metasurfaces for electronically programmable microfluidic manipulation. *Nature*, 605(7911):681–686, 2022.
37. Edoardo Milana, Benjamin Gorissen, Eline De Borre, Frederik Ceyssens, Dominiek Reynaerts, and Michael De Volder. Out-of-plane soft lithography for soft pneumatic microactuator arrays. *Soft Robotics*, 0(0), 2022. .
38. Zixuan Deng, Hang Zhang, Arri Priimagi, and Hao Zeng. Light-fueled nonreciprocal self-oscillators for fluidic transportation and coupling. *Advanced Materials*, 2022.
39. Jaap den Toonder, Femke Bos, Dick Broer, Laura Filippini, Murray Gillies, Judith de Goede, Titie Mol, Mireille Reijme, Wim Talen, Hans Wilderbeek, Vinayak Khatavkar, and Patrick Anderson. Artificial cilia for active micro-fluidic mixing. *Lab Chip*, 8:533–541, 2008. .
40. Ziyu Ren, Mingchao Zhang, Shanyuan Song, Zemin Liu, Chong Hong, Tianlu Wang, Xiaoguang Dong, Wenqi Hu, and Metin Sitti. Soft-robotic ciliated epidermis for reconfigurable coordinated fluid manipulation. *Science Advances*, 8(34), 2022.
41. Anne Helene Gelebart, Matthew Mc Bride, Albertus P. H..J. Schenning, Christopher N. Bowman, and Dirk J. Broer. Photoresponsive fiber array: Toward mimicking the collective motion of cilia for transport applications. *Advanced Functional Materials*, 26(29):5322–5327, 2016.
42. B. A. Evans, A. R. Shields, R. Lloyd Carroll, S. Washburn, M. R. Falvo, R. Superfine, Chapel Hill, Chapel Hill, North Carolina, West Virginia, V Uni, West Virginia, Chapel Hill, Chapel Hill, and North Carolina. Magnetically Actuated Nanorod Arrays as Biomimetic Cilia. *Nano Lett.*, 7(5):1428–1434, 2007. .
43. Mojca Vilfan, Anton Potocnik, Blaz Kavcic, Natan Osterman, Igor Poberaj, Andrej Vilfan, and Dusan Babic. Self-assembled artificial cilia. *Proc. Natl. Acad. Sci. U. S. A.*, 107(5):1844–1847, feb 2010. .
44. Aihui Wang, Mingcong Deng, Shuichi Wakimoto, and Toshihiro Kawashima. Characteristics analysis and modeling of a miniature pneumatic curling rubber actuator. *Int. J. Innov. Comput. Inf. Control*, 10(3):1029–1039, 2014.
45. Shuaizhong Zhang, Ye Wang, Reinoud Lavrijsen, Patrick R. Onck, and Jaap M.J. den Toonder. Versatile microfluidic flow generated by moulded magnetic artificial cilia. *Sensors Actuators, B Chem.*, 263:614–624, jun 2018. .
46. Srinivas Hanasoge, Peter J. Hesketh, and Alexander Alexeev. Microfluidic pumping using artificial magnetic cilia. *Microsystems Nanoeng.*, 4(1):11, dec 2018. .
47. Hayato Shinoda and Fujio Tsumori. Development of Micro Pump Using Magnetic Artificial Cilia with Metachronal Wave. *Proc. IEEE Int. Conf. Micro Electro Mech. Syst.*, 2020-Janua:497–500, 2020. .
48. Shuaizhong Zhang, Zhiwei Cui, Ye Wang, and Jaap M. J. den Toonder. Metachronal actuation of microscopic magnetic artificial cilia generates strong microfluidic pumping. *Lab Chip*, 20:3569–3581, 2020. .
49. Ahmet F. Demirors, Sumeyye Aykut, Sophia Ganzeboom, Yuki A. Meier, and Erik Poloni. Programmable droplet manipulation and wetting with soft magnetic carpets. *Proceedings of the National Academy of Sciences of the United States of America*, 118, 11 2021. ISSN 10916490. .
50. Jiaqi Miao, Siqi Sun, Tieshan Zhang, Gen Li, Hao Ren, and Yajing Shen. Natural cilia and pine needles combinedly inspired asymmetric pillar actuators for all-space liquid transport and self-regulated robotic locomotion. *ACS Applied Materials Interfaces*, 14(44):50296–50307, 2022.
51. Benjamin Gorissen, Wannes Vincentie, Farid Al-Bender, Dominiek Reynaerts, and Michaël De Volder. Modeling and bonding-free fabrication of flexible fluidic microactuators with a bending motion. *J. Micromech. Microeng*, 23:45012–10, 2013.
52. Edoardo Milana, Rongjing Zhang, Maria Rosaria Vetrano, Sam Peerlinck, Michael De Volder, Patrick R Onck, Dominiek Reynaerts, and Benjamin Gorissen. Metachronal patterns in artificial cilia for low reynolds number fluid propulsion. *Science advances*, 6(49):eabd2508, 2020.
53. Edoardo Milana, Bert Van Raemdonck, Andrea Serrano Casla, Michael De Volder, Dominiek Reynaerts, and Benjamin Gorissen. Morphological control of cilia-inspired asymmetric movements using nonlinear soft inflatable actuators. *Frontiers in Robotics and AI*, 8, 2021.

54. Kaitlyn P Becker, Yufeng Chen, Robert J Wood, K P Becker, Y Chen, R J Wood John A Paulson, and R J Wood. Mechanically programmable dip molding of high aspect ratio soft actuator arrays. 2020. .
55. Shigenori Nonaka, Satoko Yoshiba, Daisuke Watanabe, Shingo Ikeuchi, Tomonobu Goto, Wallace F Marshall, and Hiroshi Hamada. De novo formation of left–right asymmetry by posterior tilt of nodal cilia. *PLoS biology*, 3(8):e268, 2005.
56. CE Miller and H Goldfarb. An in vitro investigation of ciliated activity. *Transactions of the Society of Rheology*, 9(1): 135–144, 1965.
57. Tae-Rin Lee, Kieseok Oh, Jae-Hyun Chung, Yoon-Suk Chang, Jae-Boong Choi, Genki Yagawa, and Young-Jin Kim. Resonant behavior and microfluidic manipulation of silicone cilia due to an added mass effect. *Soft Matter*, 7(9):4325, 2011. ISSN 1744-683X. .
58. Christoph Brücker and Armin Keissner. Streaming and mixing induced by a bundle of ciliary vibrating micro-pillars. *Exp. Fluids*, 49(1):57–65, 2010. .
59. Chao Zhang, Pingan Zhu, Yangqiao Lin, Zhongdong Jiao, and Jun Zou. A review of modular soft robotics: Modular units, connection mechanisms, and applications. *Adv. Intell. Syst.*, 2020. .
60. Knut Norstog. Fine structure of the spermatozoid of zamia with special reference to the flagellar apparatus. *American Journal of Botany*, 54(7):831–340, 1967.
61. A. Sleigh, M. *The Biology of cilia and Flagella.* Pergamon Press, 1962.
62. Bing Dai, Siheng Li, Tailin Xu, Yuefeng Wang, Feilong Zhang, Zhen Gu, and Shutao Wang. Artificial asymmetric cilia array of dielectric elastomer for cargo transportation. *ACS Applied Materials & Interfaces*, 10(49):42979–42984, 2018. .
63. Edoardo Milana, Bert Van Raemdonck, Kevin Cornelis, Enrique Dehaerne, Jef De Clerck, Yarno De Groof, Toon De Vil, Benjamin Gorissen, and Dominiek Reynaerts. EELWORM : a bioinspired multimodal amphibious soft robot. 2020.
64. Yu-An Wu, Bivas Panigrahi, Yueh-Hsun Lu, and Chia-Yuan Chen. An Integrated Artificial Cilia Based Microfluidic Device for Micropumping and Micromixing Applications. *Micromachines*, 8(9):260, 2017. .
65. Jacob Belardi, Nicolas Schorr, Oswald Prucker, and Jürgen Rühe. Artificial cilia: Generation of magnetic actuators in microfluidic systems. *Adv. Funct. Mater.*, 21(17):3314–3320, 2011. .
66. Srinivas Hanasoge, Peter J. Hesketh, and Alexander Alexeev. Metachronal actuation of microscale magnetic artificial cilia. *ACS Applied Materials & Interfaces*, 12(41), 2020.
67. Seiji Azukizawa, Hayato Shinoda, Kazuki Tokumaru, and Fujio Tsumori. 3d printing system of magnetic anisotropy for artificial cilia. *Journal of Photopolymer Science and Technology*, 31(1):139–144, 2018. .
68. Hayato Shinoda, Seiji Azukizawa, Kazuki Maeda, and Fujio Tsumori. Bio-mimic motion of 3d-printed gel structures dispersed with magnetic particles. *Journal of The Electrochemical Society*, 166(9), 2019.